Towards an underdamped thermodynamic uncertainty relation

Von der Fakultät Mathematik und Physik der Universität Stuttgart zur Erlangung der Würde eines Doktors der Naturwissenschaften (Dr. rer. nat.) genehmigte Abhandlung

Vorgelegt von:

Lukas P. Fischer

aus Stuttgart

Hauptberichter:	Prof. Dr. Udo Seifert
Mitberichter:	Prof. Dr. Eric Lutz
Vorsitzender:	Prof. Dr. Sebastian Loth

Tag der Einreichung: 04.09.2020
Tag der mündliche Prüfung: 23.11.2020

II. Institut für Theoretische Physik der Universität Stuttgart

2020

Ehrenwörtliche Erklärung

Ich erkläre, dass ich diese Arbeit selbstständig verfasst und keine anderen als die angegebenen Quellen und Hilfsmittel verwendet habe.

Lukas P. FISCHER

Stuttgart, 04. September 2020

> *A good means to discovery is to take away certain parts of a system to find out how the rest behaves.*
>
> Georg Christoph Lichtenberg

UNIVERSITÄT STUTTGART

Abstract

Fakultät 8
-

Dr. rer. nat.

Towards an underdamped thermodynamic uncertainty relation

by Lukas P. FISCHER

A recent result of stochastic thermodynamics is the so-called thermodynamic uncertainty relation (TUR). This relation, appearing in the form of an inequality, bounds the precision of fluctuating currents by the entropic costs that are required to drive the non-vanishing mean of the observable. As a consequence, the relation enables the access to parameters that are not accessible in an experimental setting via the precision of a experimentally accessible observable. For instance, it was possible to bound the efficiency of molecular machines by means of their measurable moments of motion. Albeit being generalized and modified to more general terms and dynamics, the putative generalization of the thermodynamic uncertainty relation to underdamped dynamics where the inertia is not negligible remains a puzzling problem. Although there are convincing indications for the overdamped TUR being valid for underdamped dynamics as well in some systems, a straightforward application can also lead to violations of the bound.

This thesis summarizes the efforts towards an underdamped generalization of the thermodynamic uncertainty relation and shows challenges and chances that come along by generalization of the TUR. To this end, the intriguing limitations of the TUR in the underdamped domain are explored and discussed. For instance, the TUR is inherently broken for finite times where the evolution is governed by ballistic dynamics due to the inertia being present. Furthermore, it is possible to improve the precision beyond the overdamped bound in presence of velocity dependent forces such as the Lorentz force induced by a magnetic field.

Beyond the limitations of the TUR in the underdamped regime, this thesis gives a thorough analysis of the proof that leads to the TUR in the overdamped regime and discusses the obstacles which have to be overcome to find the sought-after proof that is valid for underdamped dynamics. The method is illustrated by deriving thermodynamic bounds that are, however, not as transparent and often not as tight as the original TUR.

Finally, a conjecture for a generalized TUR is presented which is based on the precision of free diffusion and holds for all times. The corresponding bound converges to the overdamped TUR in the appropriate limit and tightly bounds the precision, even in the ballistic regime. Being based on free diffusion this conjecture also puts the interpretation of the original TUR in a different perspective.

Summary by chapters:

Chapter 1: Motivation

In this chapter the thermodynamic uncertainty relation is embedded in the context of stochastic motion and its current status for the underdamped regime is outlined. To this end, the history of stochastic motion is briefly summarized before its relevance for biology is described. In this biological context, the thermodynamic uncertainty relation is outlined.

Chapter 2: Underdamped dynamics and stochastic thermodynamics

In this chapter the theoretical foundation for a description of random motion is laid out. To this end, a mathematical description for underdamped stochastic motion, the so-called Langevin equation, is motivated from deterministic dynamics. This approach highlights assumptions and restrictions entering in the Langevin description. Although the Langevin equation is presented as a differential equation, there is an ambiguity in its interpretation. This issue of stochastic integration is discussed briefly before the limit of vanishing inertia, the overdamped limit, is presented and its different characteristic under time-reversal with respect to the underdamped regime is discussed. In addition, the Fokker-Planck equation is introduced. In contrast to the microscopic Langevin equation it describes the statistics observed for infinitely many realizations. Finally, the chapter focuses on the notion of stochastic thermodynamics and how it can be used to transfer the definition of thermodynamic quantities in stochastic systems.

Chapter 3: Fluctuations in the steady state

In this chapter the conceptual framework that is necessary for defining and proving the thermodynamic uncertainty relation is presented. To this end different methods are introduced which can be used to characterize and quantify the strength of fluctuations. The cumulants are defined as a measure of how fluctuations shape the vicinity of the most probable value. In principle it is possible to reconstruct the complete probability distribution from these cumulants. A more microscopic perspective off the description of fluctuations is presented in the way of the path integral formalism which allows to assess the probability of specific trajectories. The formalism is set into practice by deriving not only fluctuation theorems, an intriguing result from the stochastic thermodynamic framework, but also the large-deviations functional. The path integrals can be included in a hierarchy of large deviation functions in which each level can be contracted from the respective higher level function. At the bottom stands the level 1 large deviation function which, in turn, can be linked to the cumulants. This rather abstract concept of large deviations

is particularly relevant for the scope of this thesis as it is at the heart of the proof for the overdamped TUR which is outlined at the end of this chapter. This proof can, however, not be generalized to the underdamped regime straightforwardly as discussed in the remainder of the chapter.

Chapter 4: An underdamped finite time TUR?

In this chapter a putative underdamped finite-time thermodynamic uncertainty relation is discussed on base of model systems and by means of example calculations. Differences to the overdamped case are highlighted which in turn have a major effect on the validity of the TUR in the underdamped regime. It is important to point out that observables in the underdamped regime do not necessarily have a clear behavior when the trajectory is traversed in reverse. While the overdamped TUR holds naturally only for currents that by construction change their sign when the trajectory is reversed, this constraint must be introduced explicitly in an underdamped generalization. For the case of even observables, these are observables that result in the same outcome for the original and a reversed trajectory, it is shown that the precision is not bound by means of the TUR. Furthermore, it is shown that the TUR does not hold for finite-times. The short-time regime is governed by the inertia of the particle and the precision can be improved beyond the boundaries set by the TUR. This is illustrated by calculations for the arguably simplest model: free diffusion with drift. The consequences on the validity of the putative underdamped generalization of the TUR and appropriate restrictions are finally considered.

Chapter 5: The underdamped LDF in one dimension

In this chapter the concept of large deviations that led to the proof of the overdamped thermodynamic uncertainty relation is reviewed from an underdamped point of view. To this end, a method to numerically calculate the large deviation function is derived for a particle in a one-dimensional periodic potential. The resulting functions and their features are discussed from both an applied and a general point of view to allow for a more intuitive interpretation of the rather abstract large deviation functions. On top of the theoretic foundations established in Chapter 3, bounds on said functions are then derived. These bounds serve both a practical and a pedagogical purpose. On the one hand, the bounds provide further intuition regarding the course of the large deviation function and establish a link to the overdamped analogous. On the other, hand they illustrate how bounds can be inferred from the higher level large deviation functions. Finally, numerical data which indicate the validity of a parabolic bound on the large deviation function are presented. This is especially interesting as this bounding

parabola has also been proven in the overdamped regime. In this regime the uncertainty relation is a direct consequence of the bound.

Chapter 6: Thermodynamic bounds for underdamped motion

In this chapter possibilities to proof the thermodynamic uncertainty relation and other bounds on thermodynamic quantities using the previously introduced methods are discussed. As illustrated in Chapter 5, bounds follow easily from the hierarchy of large deviation functions by developing suited ansatzes for some of the involved functions. Thermodynamic quantities are typically averages that capture likely events and it is important to develop ansatzes in the vicinity of the typical trajectories. Two different concepts, each motivated from an overdamped perspective, are introduced. First, an ansatz which employs rescaling of time. Second, an ansatz that amplifies the irreversible contributions to the motion. Unfortunately, neither of the resulting bounds have the transparent form of the overdamped uncertainty relation thereby limiting their significance in practice. The bounds are benchmarked by using free diffusion and numerical results. This also allows to asses the quality of an estimate of thermodynamic quantities that is based on the bound, as relevant in experiments. While the time-scale bound is not particularly tight, the bound based on rescaling the irreversible contribution allows for a quite precise estimation of the precision with regimes where the bound outperforms the putative thermodynamic uncertainty relation regarding its tightness. However, this comes with the cost of involving the dependency of the averaged observables with respect to a changed friction. Since it is not possible to freely control all parameters in an experimental setting, this would require a more complex setup. Finally, a bound in one dimension which is based on free diffusion is conjectured based on numerical results. By design the bound becomes tight for free diffusion similar to the overdamped analogous and can be applied for all times and for different (odd) velocity dependencies of the measured observables. In addition, it has a similar transparent form and converges to the overdamped TUR in the appropriate limit and for large times. A way of generalizing the conjectured bound to higher dimensions is pointed out by considering two-dimensional systems. Moreover, properties of a potential proof for the conjectured bound are discussed.

Chapter 7: Beating the overdamped TUR limit

In this chapter the effect of velocity-dependent forces on the thermodynamic uncertainty relation are explored. As pointed out in the previous chapters, it is possible to improve the precision beyond the limits of the TUR for even observables and for finite times. This can, however, also be realized for generalized forces with a velocity-dependent contribution. The breakdown of an

uncertainty relation is not particularly surprising for feedback mechanisms which can be implemented by using such forces, for instance, by slowing down and accelerating the particle dependent on the current velocity. Intriguingly, a breakdown of the TUR can also be observed in the presence of a magnetic field. This collapse is first described in the analytically solvable Brownian gyrator model. Here, the precision of a charged particle driven in a two-dimensional harmonic potential can be improved beyond the limit of the overdamped TUR even in the long-time limit when a Lorentz force acts on the particle. In this model numerical results for different winding number currents also indicate that the breakdown of the thermodynamic uncertainty relation crucially depends on the chosen observable. To get additional insight on how a magnetic field can decrease the uncertainty, a stripped down model is introduced which allows to compute different observables analytically. In accordance with the observations made considering the Brownian gyrator, the sole existence of a magnetic field is not sufficient to improve the precision, but, in addition, the weight of the observable has to be chosen adequately. In an interplay of the magnetic force deflecting faster trajectories, thereby coupling the velocity with the spatial position, and a weight that increases when the trajectories are deflected further, the precision can be improved significantly. In this sense, the magnetic force implements a feedback mechanism that increases the weight of the parts of trajectories that are faster.

Chapter 8: Concluding Perspective

In this chapter, the results from this thesis are concluded and set into perspective of current research. Results presented in the previous chapters suggest that a thermodynamic uncertainty relation holds for underdamped dynamics as well at least for odd observables and for large times. As discussed in this chapter, a proof is still pending. Since it is not possible to straightforwardly adapt any of the proofs presented for overdamped dynamics, properties of the putative proof which arose in the course of this thesis are summarized. Such a proof is particularly desirable, as it could identify the physical mechanism behind the thermodynamic uncertainty relation and help to develop a unified picture of the numerous thermodynamic inequalities which were introduced in the spirit of the original thermodynamic uncertainty relation. Furthermore, open questions and new impulses for future research that were identified in this thesis are listed and suggested.

Publications

Parts of this thesis have been published in:

Lukas P. Fischer, Patrick Pietzonka, and Udo Seifert,
"Large deviation function for a driven underdamped particle in a periodic potential"
Phys. Rev. E **97**, 022143 (2018)

 Chapter 5 and parts of Chapter 6 are based on this publication.

Hyun-Myung Chun, Lukas P. Fischer, and Udo Seifert,
"Effect of a magnetic field on the thermodynamic uncertainty relation"
Phys. Rev. E **99**, 042128 (2019)

 Chapter 7 is partially based on this publication.

Lukas P. Fischer, Hyun-Myung Chun, Udo Seifert,
"Free diffusion bounds the precision of currents in underdamped dynamics"
Phys. Rev. E **102**, 012120 (2020)

 Chapter 4 and parts of Chapter 6 are based on this publication.

Contents

Zusammenfassung in deutscher Sprache

Die Thermodynamische Unschärferelation (TUR) ist ein recht neues Resultat der Stochastischen Thermodynamik. Diese, in Form einer Ungleichung auftauchende Relation bildet eine Schranke auf die Präzision eines fluktuierenden Stroms über die entropischen Kosten, die für die Erzeugung eines nicht-verschwindenden durchschnittlichen Stroms benötigt werden. Damit erlaubt die TUR auch den indirekten Zugang zu Größen, die experimentell nicht zugänglich sind, indem die Präzision einer messbaren Observablen gemessen wird. Die Relation wurde zum Beispiel genutzt, um die Effizienz von molekularen Maschinen durch die messbaren Momente der Bewegung zu beschränken und damit abzuschätzen. Obgleich die ursprüngliche Formulierung der TUR verallgemeinert und modifiziert wurde, so dass diese auch unter allgemeineren Voraussetzungen und in allgemeinerer Dynamik anwendbar ist, bleibt die mutmaßliche Generalisierung der TUR auf unterdämpfte Dynamik, also stochastische Bewegung in welcher der Impuls nicht vernachlässigbar ist, ein ungelöstes und rege diskutiertes Problem. Obgleich es überzeugende Indizien für die Gültigkeit der Schranke auch im unterdämpften Regime gibt, kann die direkte Anwendung unter bestimmten Bedingungen zu einer Verletzung der Schranke führen.

Diese Abhandlung fasst die Bemühungen um einer generalisierten thermodynamische Unschärferelation für unterdämpfte Systeme zusammen und stellt dar, welche Herausforderungen und Chancen die Verallgemeinerung der TUR mit sich bringt. Hierzu werden die Einschränkungen der Relation im Bereich unterdämpfter Bewegung untersucht und diskutiert. So ist die TUR, zum Beispiel, für endliche Zeiten grundsätzlich verletzt, da die Bewegung von ballistische Effekte beherrscht wird. Darüber hinaus ist es möglich die Präzision jenseits der durch die überdämpfte Relation gesetzte Schranke zu verbessern, wenn Kräfte wirken, die von der Geschwindigkeit abhängen wie zum Beispiel die durch magnetische Felder induzierte Lorentz Kraft.

Über die Einschränkungen der TUR im unterdämpften Regime hinaus liefert diese Abhandlung eine gründliche Analyse des Beweises, der für die

TUR im überdämpften Regime geführt wurde und diskutiert die Hindernisse die überwunden werden müssen, um den begehrten Beweis in unterdämpfter Dynamik zu finden. Die Methodik wird durch den Beweis thermodynamischer Schranken veranschaulicht. Diese gewähren allerdings weniger Einblick in physikalische Prinzipien und stellen oftmals eine schlechtere Schranke als die originale TUR dar.

Schlussendlich wird auf Basis numerischer Simulationen die vermutete Form einer generalisierten Unschärferelation präsentiert. Diese beruht auf der Präzision von freier Diffusion und ist für alle Zeiten gültig. Die zugehörige Schranke konvergiert im entsprechenden Limes zur überdämpften TUR und liefert auch im ballistischen Regime eine enge Schranke. Da die Vermutung auf freier Diffusion aufbaut, eröffnet sie zugleich eine neue und anschauliche Perspektive auf die Interpretationen der TUR für überdämpften Bewegung.

Kapitel 1: Motivation

In diesem Kapitel wird die thermodynamische Unschärferelation in den Kontext stochastischer Bewegung eingebettet und der aktuelle Status der Forschung bezüglich einer unterdämpften Verallgemeinerung umrissen. Dazu wird die Historie stochastischer Bewegung zusammengefasst und nachfolgend die besondere Bedeutung für die Biologie herausgestellt.

Kapitel 2: Underdamped dynamics and stochastic thermodynamics

In diesem Kapitel wird die theoretische Grundlage für die Beschreibung zufälliger Bewegung geschaffen. Ausgehend von einer rein deterministischen Dynamik wird die Modellierung von zufälliger Bewegung durch die Langevin-Gleichung motiviert. Dieses Vorgehen erlaubt es, die Annahmen und Beschränkungen hervorzuheben, die in die Beschreibung eingehen. Obgleich die Langevin-Gleichung dabei als Differentialgleichung präsentiert wird, gibt es eine Mehrdeutigkeit in der Interpretation derselben. Diese, als Problem der stochastischen Integration bezeichnete Mehrdeutigkeit, wird kurz thematisiert. Anschließend wird der Bereich zu vernachlässigenden Impulses, der überdämpfte Bereich, beschrieben und im Hinblick auf das zur unterdämpften Dynamik unterschiedliche Verhalten unter Zeitumkehr diskutiert. Zusätzlich wird die Fokker-Planck Gleichung eingeführt welche es erlaubt, die Statistik unendlicher vieler zufälliger Realisationen zu beschreiben. Zuletzt wird das Konzept der stochastischen Thermodynamik beschrieben, im Besonderen wie dieses genutzt werden kann, um Größen der klassischen Thermodynamik in zufälligen Systemen zu definieren.

Kapitel 3: Fluctuations in the steady state

In diesem Kapitel wird das konzeptionelle Grundgerüst eingeführt, welches benötigt wird, um die thermodynamische Unschärferelation zu definieren und zu beweisen. Dazu werden zuerst unterschiedliche Methoden zur Charakterisierung und Quantifizierung der Stärke von Fluktuationen vorgestellt. Als ein Maß, das angibt wie Fluktuationen die Umgebung des wahrscheinlichsten Ereignisses formen, werden die Kumulanten definiert. Aus diesen Kumulanten kann im Prinzip die komplette Wahrscheinlichkeitsverteilung rekonstruiert werde. Eine mikroskopische Perspektive für die Beschreibung von Fluktuationen nimmt der Pfadintegral Formalismus ein. Dieser erlaubt es die Wahrscheinlichkeit unterschiedlicher Trajektorien abzuschätzen. In diesem Kapitel wird der Formalismus genutzt um nicht nur Fluktuationstheoreme, und damit ein weiteres faszinierendes Resultat der stochastischen Thermodynamik, zu beweisen, sondern auch um die sogenannten Large--Deviation Funktionale herzuleiten. Die Pfadintegrale können dabei in eine Hierarchie von Large- Deviation Funktionen eingebettet werden, in welcher jedes Level jeweils aus der hierarchisch nächsthöherer Funktion kontraktiert werden kann. Am Ende steht die Level 1 Large-Deviation Funktion, welche wiederum auf direkter Art mit den Kumulanten gekoppelt ist. Das eher abstrakte Konzept der großen Abweichungen ist im Bereich dieser Abhandlung im Besonderen relevant, da es die Basis des Beweises der überdämpften TUR bildet. Am Ende dieses Kapitels wird der Beweis skizziert. Der Beweis kann jedoch nicht direkt für das unterdämpfte Regime verallgemeinert werden, was ebenfalls diskutiert wird.

Kapitel 4: An underdamped finite time TUR?

In diesem Kapitel wird eine mutmaßliche thermodynamische Unschärferelation für endliche Zeiten auf Basis von repräsentativen Modellsystemen und Beispielsrechnungen diskutiert. Unterschiede zum überdämpften Fall mit wesentlichen Auswirkungen auf die Gültigkeit der TUR im unterdämpften Bereich werden hervorgehoben. So weisen Observablen im unterdämpften Regime nicht notwendigerweise ein eindeutiges Verhalten unter Zeitumkehr auf. Während die überdämpfte TUR natürlicherweise nur für die Klasse der ungeraden Observablen gilt, das sind jene die ihr Vorzeichen wechseln wenn die Trajektorie umgekehrt wird, muss diese Beschränkung explizit in eine unterdämpfte Generalisierung eingeführt werden. Für gerade Observablen, also Observablen die invariabel unter Änderung der Richtung der Trajektorie sind, wird gezeigt, dass die Präzision nicht über die TUR beschränkt werden kann. Darüber hinaus wird belegt, dass die TUR nicht für endliche Zeiten gilt. Da die Bewegung auf kurzen Zeitskalen vom Impuls der Teilchen dominiert wird, kann die Präzision auch über die Schranke der TUR hinweg optimiert werden. Dies wird an einem einfachen Modell veranschaulicht:

Freier Diffusion mit konstantem Drift. Die Konsequenzen für die Gültigkeit einer mutmaßlichen unterdämpften TUR und entsprechende Einschränkungen werden zuletzt klar benannt.

Kapitel 5: The underdamped LDF in one dimension

In diesem Kapitel wird das Konzept der großen Abweichungen, welches zum Beweis der TUR im überdämpften Regime führte, für den unterdämpften Bereich diskutiert. Hierfür wird eine Methode zur numerischen Berechnung der Large-Deviation Funktion für ein unterdämpftes Teilchen in einem eindimensionalen Potential hergeleitet. Um einen intuitiven Zugang zu den eher abstrakten Large-Deviation Funktionen zu eröffnen, können die auf diese Weise berechneten Funktionen und deren Eigenschaften damit sowohl aus einer angewandten als auch aus einer theoretischen Perspektive betrachtet werden. Auf Basis der theoretischen Grundlagen, die im vorangegangen Kapitel 3 etabliert wurden, werden daraufhin Schranken an diese Funktionen bewiesen. Diese Schranken haben sowohl einen praktischen als auch einen pädagogischen Nutzen. Auf der einen Seite sorgen sie für weitere Einblicke in die Form der Large-Deviation Funktionen und stellen eine Verbindung zum überdämpften Analgon her. Auf der anderen Seite illustrieren sie, wie solche Schranken aus den Large-Deviation Funktionen höherer Ordnung abgeleitet werden können. Zuletzt werden numerische Indizien präsentiert, welche die Existenz einer parabolischen Schranke an die Large-Deviation Funktion andeuten. Dies ist von besonderer Bedeutung, da eine parabolische Schranke gleicher Form bereits für den überdämpften Bereich bewiesen wurde. In diesem Bereich ist die thermodynamische Unschärferelation eine direkte Konsequenz der Schranke.

Kapitel 6: Thermodynamic bounds for underdamped motion

In diesem Kapitel wird die Möglichkeit eines Beweises der thermodynamischen Unschärferelation und anderer Schranken an thermodynamische Größen über die bereits eingeführten Methoden diskutiert. Da solche Größen üblicherweise aus Mittelwerten bestehen, die wahrscheinliche Ereignisse charakterisieren, ist es unabdingbar Ansätze zu entwickeln, welche die Umgebung der typischen Trajektorien modellieren. Zwei unterschiedliche Ansätze, jeweils aus einer überdämpften Perspektive motiviert, werden eingeführt: Ein Ansatz, der auf Variation der Zeitskala basiert, sowie einer der irreversible Anteile der Bewegung verstärkt. Jedoch resultiert keiner der beiden Ansätze in einer Schranke, die eine ähnlich transparente Form hat wie die überdämpfte TUR. Daher sind die hergeleiteten Schranken für die Praxis nicht besonders signifikant. Durch Beispielrechnungen für freie Diffusion sowie numerischen Simulationen werden die Schranken beurteilt und die Qualität der daraus resultierenden Abschätzung der Unschärfe bemessen.

Während die Zeitskalen-Schranke keine enge Schranke darstellt, erlaubt die Schranke, die auf Reskalierung der irreversiblen Anteile beruht, eine recht präzise Abschätzung der Präzision und kann in diesem Aspekt sogar die mutmaßliche TUR übertreffen. Jedoch enthält die Schranke die Abhängigkeit der Observable von der Reibung. Diese ist in einem experimentellen Kontext nur schwer zu bestimmen. Zuletzt wird, basierend auf numerischen Daten, eine vermutete, auf freier Diffusion basierende Schranke für Bewegung in einer Dimension präsentiert. Der Grundlage folgend wird die Schranke, wie die überdämpfte TUR, für freie Diffusion gesättigt und ist für alle Zeiten sowie für unterschiedliche (ungerade) Geschwindigkeitsabhängigkeiten der gemessenen Observablen gültig. Darüber hinaus hat die vermutete Schranke eine ähnlich durchsichtige Form und konvergiert im entsprechenden Limes und für große Zeiten gegen die überdämpfte TUR. Durch Betrachtung zweidimensionaler Modelle wird auch ein Weg zur Generalisierung der Schranke für höhere Dimension skizziert. Darüber hinaus werden auch die Eigenschaften eines potentiellen Beweises diskutiert.

Kapitel 7: Beating the overdamped TUR limit

In diesem Kapitel werden die Effekte einer geschwindigkeitsabhängigen Kraft auf die thermodynamische Unschärferelation beleuchtet. In den vorangegangen Kapiteln wurde bereits betont, dass die Präzision auch jenseits der Grenzen der TUR verbessert werden kann, wenn die Observablen gerade sind oder endliche Zeiten betrachtet werden. Dies ist jedoch auch dann möglich, wenn generalisierte Kräfte wirken, die einen geschwindigkeitsabhängigen Anteil besitzen. Für Feedback Mechanismen, die über solche Kräfte implementiert werden können, ist das nicht besonders überraschend. Je nach aktueller Geschwindigkeit können diese das Teilchen abbremsen oder beschleunigen und damit die Präzision der Bewegung aktiv erhöhen. Interessanterweise kann der Zusammenbruch der Unschärferelation jedoch auch dann beobachtet werden, wenn lediglich eine durch magnetische Felder induzierte Lorentzkraft wirkt. Die Verletzung der mutmaßlichen TUR wird zuerst im analytisch lösbaren Modell eines Brownschen Gyrators beschrieben. Numerische Resultate für unterschiedliche Umdrehungsmaße lassen in diesem Modell bereits vermuten, dass die Gültigkeit der thermodynamischen Unschärferelation von den Eigenschaften der betrachteten Variable abhängen. Um weitere Einblicke darin zu ermöglichen, wie magnetische Felder die Unsicherheit verringern können, wird ein minimalistisches Modell eingeführt. In diesem Modell können Observablen unterschiedlichen Charakters analytisch ausgewertet werden. In Übereinstimmung mit den Ergebnissen für den Brownschen Gyrator ist die bloße Existenz eines magnetischen Feldes nicht hinreichend, um die mutmaßliche TUR zu veretzen und, denn auch die Observable muss entsprechend gewählt werden. In einem Zusammenspiel der magnetischen Kraft, welche schnellere Trajektorien ablenkt, und

einer Observablen die solche, nun räumlich sortierte, Trajektorien höher gewichtet kann, wird die Präzision deutlich gesteigert. In diesem Sinne hat die wirkende Lorentzkraft einen ähnlich Effekt wie Feedback Mechanismus indem die Teile der Trajektorien welche eine hohe Präzision aufweisen stärker gewichtet werden.

Kapitel 8: Concluding Perspective

In diesem Kapitel werden die Resultate der Abhandlung zusammengefasst und im Kontext des aktuellen Stands der Forschung diskutiert. Die Ergebnisse der vorangegangenen Kapitel erhärten den Verdacht, dass eine thermodynamische Unschärferelation auch für unterdämpfte Dynamik gilt, zumindest für ungerade Observablen und große Zeiten. Ein Beweis steht jedoch noch aus. Da es nicht möglich ist die bisher präsentierten Methoden für den Beweis einer überdämpften TUR zu generalisieren, werden die Konsequenzen dieser Arbeit auf einen potentiellen Beweis herausgearbeitet. Ein solcher Beweis könnte dazu beitragen, den bisher nicht komplett verstandenen physikalischen Mechanismus hinter der TUR zu identifizieren und zudem helfen ein einheitliches Bild für die vielen thermodynamischen Ungleichungen zu entwickeln, die im Stil der ursprünglichen TUR entstanden sind. Darüber hinaus werden auch offene Fragen und neue Impulse für die zukünftige Forschung benannt, die durch diese Abhandlung aufkamen.

Chapter 1

Motivation

When *Robert Brown* first described Brownian motion in 1828 [1] he was not fully aware of the endeavor that would follow. He ascribed the effect of random motion of small particles to an active component being present in the particles itself. It took almost 80 years to identify the solvent itself as source of the random motion culminating in the (Sutherland)-Einstein-Smoluchowski-equation [2, 3]. This result did not only give credence to the, at that time, still debated discrete nature of fluids but also was the first representative of flucutation-dissipation theorems relating fluctuations (the random) with dissipation of energy. Shortly after, *Paul Langevin* implemented this random character in a Newtonian description and thus allowed for a microscopic description of Brownian motion [4][1].

An early application of the framework was the analysis of diffusion processes over energetic barriers by *Hendrik Anthony Kramers* [6]. By defining the rate at that chemical reactions take place, it is at the heart of chemical rate equations. A notable and arguably outstanding experiment is that of *Eugen Kappler*. He used obtainable statistics from a small mirror on a metal rod to experimentally infer the Avogadro number. The surprising connection is made by statistical physics via the Ornstein-Uhlenbeck process that describes the diffusion in a harmonic potential [7]. With this approach he exploited statistics as a mean of inferring underlying quantities.

The rational behind this work was in a sense visionary for modern bio- and statistical physics. Driven by advances in experimental methods, studying and manipulating small systems and micromachines became more and more feasible. Such systems are, literally, vital as they assume important tasks in biology [8] such as cargo transport inside the cell, production of Adenosine triphosphate (ATP) and muscle motion. While it is often not possible to track all involved components, statistical properties are easily accessible.

When the considered systems, however, become smaller, they cannot be described by classical thermodynamics anymore. The notions of thermodynamics, like work or heat, that are elementary for discussing macroscopic

[1] A translation of the french article can be found in [5].

machines do not generalize to systems small in number and size as thermal fluctuations become more and more pronounced. Rather than the averaged quantities that govern classical thermodynamics, each realization is different due to the influence of the fluctuating surrounding. Nevertheless, the definitions and concepts that were that by prominent names as *Maxwell*, *Boltzmann* and *Gibbs* can be transferred to single realizations of such systems using the framework of stochastic thermodynamics [9, 10].

Such a mapping does not only allow for a formal analysis of microscopic machines, it also brings order in the random by characterizing its details. Most notably, fluctuation theorems [11] succeed in relating the probabilities of certain realizations with those of opposing outcome. While this is trivial in equilibrium, where the probability of a trajectory is symmetric under time-reversal, it becomes highly relevant for exploring systems that are driven out of equilibrium and are characterized by an overall energy turnover.

A more recent result of stochastic thermodynamics is the thermodynamic uncertainty relation [12] (TUR). The relation bounds the precision of time asymmetric observables by the entropic costs to drive the system out of equilibrium. It implements the intuitive picture that higher precision comes at an energetic cost. From a theoretical perspective the inequality gives a valuable insight in the dynamics of small machines and reaction networks. From a more applied point of view it also proved useful for deriving bounds on the efficiency of microscopic machines [13] or, more generally, to infer the entropy production from the statistics of an observable [14]. This is of particular relevance for chemically driven systems, such as biological systems, where measuring the entropy production would require the virtually impossible task of tracking all molecules that contribute energy to the system.

Several generalizations of the TUR have been reported, but they are tied to an regime where the inertia does not play a role. The rationale behind this assumption is that the frictional forces on the typical length-scales are much larger compared to the masses. In other words, any motion is quickly dampened down, hence dubbed the overdamped regime. As a consequence of the high damping, the velocities in the system quickly relax and can thus be marginalized. This leads to a description with only the spatial dimensions of freedom remaining in the dynamics.

While this approximation is justified in a broad class of systems, there is a renewed interest in the contrary underdamped regime. First, the underdamped regime is much closer to a Hamiltonian description and can describe effects that do not carry over to the overdamped limit [15, 16]. Further, the underdamped approach correctly captures thermodynamic quantities that are misrepresented in a purely overdamped approach [17]. Second, with the advances of nanotechnology underdamped systems shift in the experimental focus [18, 19]. Last, a class of self propelled particles, namely the active Ornstein-Uhlenbeck particles, are described by an underdamped Langevin

equation [20, 21]. The precision of such active particles is of particular interest for the design of micromachines and their application to biomedicine.

So far attempts to generalize the uncertainty relation to underdamped systems have been made without a conclusive proof. Alternative thermodynamic bounds that have been derived are less tight, less transparent or even both. Although there is no doubt that a relation similar in spirit to the TUR holds for such dynamics as well, the precision can be improved beyond the restrictions of the TUR under more general terms.

Taken these aspects into account, there is an additional reason that longs for a proof of the generalized underdamped TUR: Understanding the physical mechanism that guarantees the validity of the bounds. The proofs presented for the overdamped case are rather abstract [22, 23, 24] and can neither directly nor in spirit be transfered to the underdamped case. A physical mechanism that provides the basis for the TUR has not been established, yet.

In this thesis, we explore the proofs and analyze possibilities to use them in the underdamped case. To this end, we give an introduction to large deviation theory which is the foundation for the overdamped proof. By deriving new bounds, we demonstrate how to apply the framework. We then discuss the additional restrictions that prevent a straightforward application of the overdamped proof.

Apart from this path, we discuss a putative underdamped TUR more generally. We show that a traditional TUR only holds in the long-time limit and for the class of observables that the overdamped TUR applies to, namely current-like observables that are odd under time-reversal.

To include the finite-time behavior that is dominated by the inertia of the particle, we conjecture an inequality that is based on free diffusion. This inequality coincides with the overdamped TUR in the long-time limit, but has a different behavior for short times. In stark contrast with other bounds that have been derived so far, it can be saturated for all times. With the bound being based on free diffusion, it also gives a new direction in assessing the physical nature of the TUR. Lastly, we discuss how velocity-dependent forces can improve the precision, before we conclude with an perspective on the TUR and its putative proof for underdamped dynamics.

Chapter 2

Underdamped dynamics and stochastic thermodynamics

Before we discuss fluctuations and how they can be bound using thermodynamic uncertainty relations, we establish the foundations that are needed for modeling and discussing underdamped systems. To this end, we first recapitulate the basics of underdamped stochastic systems and how to treat such systems mathematically. As a second step, we briefly introduce the necessary features of stochastic thermodynamics.

2.1 Describing the random

With the work by Einstein and Smoluchowski [2, 3] it became clear that the nature of Brownian motion are random collisions of the smaller fluid particles with the larger Brownian particle. If one considers all particles in the system, including the fluid particles[1], the system is perfectly deterministic. In the following we will use the deterministic foundation of the (apparent) random Brownian motion to motivate the stochastic dynamics of an underdamped Brownian particle. We then establish the foundation that is needed for describing such stochastic systems both microscopically and statistically. Finally, we discuss how the velocity effects the dynamics and compare the underdamped regime with its overdamped analogous.

2.1.1 The Langevin equation

The first microscopic description of Brownian motion has been presented by Paul Langevin, the so-called *Langevin equation* [4, 5]. Essentially, this is a Newtonian equation that accounts for random noise imparted by the environment. In the following, we will motivate these stochastic equations of motion heuristically following Ref. [25]. The Langevin equation can also be rigorously derived from the more general *Mori-Zwanzig formalism* [26, 27]

[1] As a reference, the number of particles in 18 ml water is one Mole or $6.022 \cdot 10^{23}$ particles.

where, ultimately, the same assumptions enter that are presented below. For the objective of motivating the Langevin equation, we restrict ourselves to one-dimensional diffusion and generalize it to multiple dimensions at the end.

We start with an isolated Brownian particle in one spatial dimension x. Lets assume its position and velocity is described by x and v, respectively, then its motion is described by the Newtonian equation

$$\dot{x} = v \qquad m\dot{v} = F(x) = -\partial_x V(x) + f \tag{2.1}$$

with some force that stems from a conservative potential potential $V(x)$, an external driving f and the mass of the Brownian particle m.

The Brownian particle is surrounded by much smaller fluid particles. Due to the difference in size and mass, the timescales of the Brownian particle and of the fluid particles are separated. On an intermediate timescale $\Delta\tau$ in between the characteristic times of the Brownian particle and the fluid, the former is almost at rest whereas the fluid molecules move rapidly. Consequently, there are many collisions between the Brownian particle and the fluid molecules. We collect these interactions in a force $\xi^{\text{tot}}(t)$.

By the central limit theorem, the overall force of collisions accumulated during the nth timestep

$$\Xi_n^{\text{tot}} \equiv \int_0^{\Delta\tau} dt\, \xi_{\text{tot}}(t + n\Delta\tau) \tag{2.2}$$

can be described by a Gaussian distribution of some width D. This is due to the fast relaxation of the fluid that prohibits a memory effect between two timesteps. As a result, the accumulated collisions are not correlated for different timesteps

$$\langle \Xi_n \Xi_m \rangle = 2D\delta_{n,m}. \tag{2.3}$$

Here, $\delta_{n,m}$ is the Kronecker delta which is one if $n = m$ and 0 otherwise, $\langle \cdot \rangle$ denotes the average over the ensemble of all possible realizations, and D is a constant that we leave undetermined for the moment.

If the particle is at rest, we assume that there is no prefered direction and thus the collisions balance out on average. If the particle, however, moves, collisions at the front (against the direction of travel) are more likely than on its back. Consequently, the motion of the particle is slowed down. As the Brownian particle is very slow on the characteristic timescale of the fluid, we model this asymmetry as being proportional to the velocity

$$\left\langle \Xi_n^{\text{tot}} \right\rangle = -\gamma v_n \Delta\tau \tag{2.4}$$

with the coefficient γ and the velocity v_n at time $n\Delta\tau$. This biased part of the collision term acts against persistent motion and has the form of a frictional drag. Consistently, γ can be identified as the *friction coefficient*.

Subtracting the non-symmetric part of the fluctuating force ξ_{tot}

$$\Xi_n \equiv \Xi_n^{\text{tot}} + \gamma v_n \Delta\tau. \tag{2.5}$$

yields a fluctuating force with the same variance as before, but zero mean. Due to its character, this unbiased collision force is dubbed *fluctuating force* or simply *noise*.

By discretizing the Newtonian equation, Eq. (2.1), and adding the effect of the collisions Ξ_n^{tot}, the overall update during one timestep yields

$$x_n = x_{n-1} + v_n \Delta\tau \qquad m v_n = m v_{n-1} + F(x_n)\Delta\tau - \gamma v_n \Delta\tau + \Xi_n. \tag{2.6}$$

This discretized equation of motion can also be written as a differential equation that describes the dynamics on the timescale of the Brownian particle. Furthermore, it can be straightforwardly generalized to higher dimensions ultimately leading to

$$\begin{aligned} \dot{\boldsymbol{x}}(t) &= \boldsymbol{v}(t) \\ m\dot{\boldsymbol{v}}(t) &= \boldsymbol{F}\left(\boldsymbol{x}(t)\right) - \gamma \boldsymbol{v}(t) + \boldsymbol{\xi}(t) \end{aligned} \tag{2.7}$$

with the vectors $\boldsymbol{x} = (x_1, x_2, ...)^\intercal$ and $\boldsymbol{v} = (v_1, v_2, ...)^\intercal$. Now, $\boldsymbol{\xi}$ is a vector containing zero-mean Gaussian white noise with covariances $\langle \xi_i(t)\xi_j(t')\rangle = 2D_{ij}\delta(t-t')$ and a symmetric covariance matrix $\boldsymbol{D}$ by definition. It is worth noting that the fluctuating force has a fractal self-similarity. This means that its structure is similar noisy irrespective of the chosen timescale. As before, we can split the force in a conservative and non-conservative contribution $\boldsymbol{F}(\boldsymbol{x}) \equiv \boldsymbol{f} + \nabla_x V(\boldsymbol{x})$ where ∇_x is the gradient with respect to $\boldsymbol{x}$.

So far, the correlations $\boldsymbol{D}$ are still undetermined. In the next section we will connect this matrix to thermodynamic quantities and, thereby, give the Langevin equation a physical meaning.

2.1.2 Fokker-Planck equation

The Langevin equation (2.7) describes the microscopic motion of a Brownian particle. Often, however, one is not interested in the exact fluctuating motion of the particle but rather its distribution after time t

$$p(\boldsymbol{x}, \boldsymbol{v}, t) \equiv \langle \delta\left(\boldsymbol{x} - \boldsymbol{x}(t)\right) \delta\left(\boldsymbol{v} - \boldsymbol{v}(t)\right)\rangle_t \,\Big|_{p(\boldsymbol{x},\boldsymbol{v},0)}. \tag{2.8}$$

The average in this expression is taken over an ensemble of all realizations at time t that start from some initial distribution $p(\boldsymbol{x}, \boldsymbol{v}, 0)$. Instead of evaluating the Langevin equation multiple times to calculate the above average, this distribution can also be obtained directly using the so-called *Fokker-Planck equation* [28].

The Fokker-Planck equation governs the evolution of the probability density function (PDF) $p(\boldsymbol{x}, \boldsymbol{v}, t)$ and is given by

$$\partial_t p = \left\{ -\nabla_{\boldsymbol{x}} \cdot \boldsymbol{v} + \nabla_{\boldsymbol{v}} \cdot \frac{1}{m} \left(\gamma \boldsymbol{v} - \boldsymbol{F}(\boldsymbol{x}) \right) + \nabla_{\boldsymbol{v}}^{\intercal} \cdot \boldsymbol{D}' \cdot \nabla_{\boldsymbol{v}} \right\} p \equiv \mathcal{L} p \tag{2.9}$$

where the arguments are dropped for brevity and $\boldsymbol{D}' \equiv \boldsymbol{D}/m^2$. The operator $\mathcal{L}$ is called the *Fokker-Planck operator*. The Fokker-Planck equation can be interpreted as a probability flow equation where all terms with single derivatives define the drift in a specific direction, whereas those with partial derivatives in second order specify how the probability broadens. This interpretation also manifests by writing it as the continuity equation

$$\partial_t p(\boldsymbol{x}, \boldsymbol{v}, t) + \nabla \cdot \boldsymbol{j}(\boldsymbol{x}, \boldsymbol{v}, t) = 0 \tag{2.10}$$

with the microscopic current

$$\boldsymbol{j}(\boldsymbol{x}, \boldsymbol{v}, t) = \begin{pmatrix} \boldsymbol{j}_{\boldsymbol{x}}(\boldsymbol{x}, \boldsymbol{v}, t) \\ \boldsymbol{j}_{\boldsymbol{v}}(\boldsymbol{x}, \boldsymbol{v}, t) \end{pmatrix} \equiv \begin{pmatrix} \boldsymbol{v} p(\boldsymbol{x}, \boldsymbol{v}, t) \\ -\left((\gamma \boldsymbol{v}/m - \boldsymbol{F}(\boldsymbol{x}))/m + \boldsymbol{D}' \cdot \nabla_{\boldsymbol{v}} \right) p(\boldsymbol{x}, \boldsymbol{v}, t) \end{pmatrix} \tag{2.11}$$

which describes in which direction the probability flows at each given point in phase space and time.

Since the noise in the Langevin equation only affects the time evolution of the velocity $\boldsymbol{v}$, no derivatives appear in the current $\boldsymbol{j}_{\boldsymbol{x}}$. As a result, the probability flow in spatial directions only consists of a drift that points in the direction of the velocity.

In the long-time limit the PDF often approaches a stationary state in which it becomes time independent. Consistently, the left hand side of the Fokker-Planck equation vanishes and the differential equation reduces to

$$0 = \mathcal{L} p^{\mathrm{ss}}(\boldsymbol{x}, \boldsymbol{v}) \tag{2.12}$$

where p^{ss} is the *steady state distribution*. One further can distinguish between equilibrium and non-equilibrium steady states. In the former, the arrow of time vanishes, meaning that if one takes a movie of a trajectory and plays it in reverse, it is impossible to distinguish it from the original one. In the latter, in contrast, one can distinguish them as one seems more likely then the other. For instance a particle consistently moving up a potential slope seems impropable compared to the particle rolling down said slope.

Normally, this duality of the steady state is translated in microscopic currents vanishing in equilibrium and being non-zero otherwise. For underdamped motion, the microscopic current in x-direction $\boldsymbol{j}_{\boldsymbol{x}}$ does, however, never vanish. Strictly, an absence of any net currents also known as equilibrium state can never be observed. We will, nevertheless, refer to a system

as being *in equilibrium* if the microscopic current in v-direction is zero everywhere, i.e. $\boldsymbol{j}_v = 0$. States in which the steady-state condition, Eq. (2.12), is met although $\boldsymbol{j}_v$ does not vanish are called non-equilibrium steady states (NESS).

In the absence of an external driving $\boldsymbol{f} = 0$ the PDF is known to be the equilibrium Maxwell-Boltzmann distribution

$$p^{\mathrm{eq}}(\boldsymbol{v}) \propto \exp\left[-\frac{m}{2k_{\mathrm{B}}T}\boldsymbol{v}^2 - \frac{1}{k_{\mathrm{B}}T}V(\boldsymbol{x})\right] \tag{2.13}$$

with the Boltzmann constant k_{B}. In the following, we set the Boltzmann constant to unity, $k_{\mathrm{B}} = 1$. Plugging this distribution into the Fokker-Planck equation (2.9) yields a fluctuation-dissipation relation

$$D_{ij} \overset{!}{=} T\gamma \tag{2.14}$$

also known as *Einstein-Smoluchowski-relation* [2, 3] [2]. By connecting the yet undetermined noise intensity D to the Boltzmann-distribution, this relation gives the Langevin equation a physical meaning and ensures that the correct equilibrium distribution is attained in the corresponding limit.

In the following we drop the prime on D' for brevity and include the mass directly in the diffusion coefficient

$$D_{ii} \equiv \frac{T\gamma}{m^2}. \tag{2.15}$$

2.1.3 The Problem of stochastic integration

Although the Langevin equation has been presented in the form of the differential equation (2.7), integrating it is ambiguous due to the fluctuating noise $\boldsymbol{\xi}$ which is not differentiable. Of course, it is possible to evaluate the differential equation in the discretized image, see for instance Eq. (2.6), and perform the continuum limes. In contrast to regular differential equations, however, the outcome does depend on the underlying discretization scheme which is a consequence of the fractal character of the noise.

The discretization scheme assumed previously for the Langevin equation, Eq. (2.6), is known as Itô convention. In general, the integral of a function $\boldsymbol{g}(\boldsymbol{q})$ along a fluctuating trajectory $\boldsymbol{q}(t) \equiv (\boldsymbol{x}(t), \boldsymbol{v}(t))^{\intercal}$ is interpreted as

$$\int_0^{\mathcal{T}} \boldsymbol{g}(\boldsymbol{q}(t)) \cdot d\boldsymbol{q}(t) \equiv \lim_{\Delta t \to 0} \sum_{n=0}^{\lfloor \mathcal{T}/\Delta t \rfloor} \boldsymbol{g}(\boldsymbol{q}_n) \cdot [\boldsymbol{q}_{n+1} - \boldsymbol{q}_n] \tag{2.16}$$

[2] One year prior to Einstein, the relation was also presented on a conference by Australien physicist William Sutherland [29]. Consistently, the relation is sometimes dubbed the Sutherland-Einstein-Smoluchowksi-relation.

in the Itô sense with the floor function $\lfloor \cdot \rfloor$ that gives the largest integer that is less or equal than the argument. This convention corresponds to the left Riemann sum, where $\boldsymbol{g}$ is evaluated on the start point of every discretized time-interval of lenght Δt.

Another common convention is known as Stratonovich integration. Its use is typically indicated by the symbol $\circ$

$$\int_0^{\mathcal{T}} \boldsymbol{g}(\boldsymbol{q}(t)) \circ d\boldsymbol{q}(t) \equiv \lim_{\Delta t \to 0} \sum_{n=0}^{\lfloor \mathcal{T}/\Delta t \rfloor} \frac{1}{2} \left[\boldsymbol{g}(\boldsymbol{q}_n) + \boldsymbol{g}(\boldsymbol{q}_{n+1})\right] \cdot \left[\boldsymbol{q}_{n+1} - \boldsymbol{q}_n\right]. \quad (2.17)$$

In contrast to the Itô convention, the function is evaluated at both the start and end point of the interval and corresponds to a trapezoidal Riemann sum. As a consequence, the integral on the left hand side of Eq. (2.17) obeys the conventional chain rule for derivation and can be integrated like a regular integral.

The two conventions can be converted using the rule [30]

$$\int_0^{\mathcal{T}} \boldsymbol{g}(\boldsymbol{q}(t)) \circ d\boldsymbol{q}(t) = \int_0^{\mathcal{T}} \boldsymbol{g}(\boldsymbol{q}(t)) \cdot d\boldsymbol{q}(t) + \int_0^{T} \nabla_{\boldsymbol{v}} \boldsymbol{D} \boldsymbol{g}_{\boldsymbol{v}}(\boldsymbol{q}(t))\, dt \quad (2.18)$$

where $\boldsymbol{g}_{\boldsymbol{v}}$ is the part of the current that is multiplied with $d\boldsymbol{v}$ in the integral.

For the part of the weight function that is integrated with respect to $d\boldsymbol{x}$, namely $\boldsymbol{g}_{\boldsymbol{x}}$, the Riemann integral exists and both conventions are equivalent. This is due to the absence of noise in the deterministic $\boldsymbol{x}$-part of the Langevin equation. Consequently, the stochastic integral can be rewritten in the regular form

$$\int_0^{\mathcal{T}} \boldsymbol{g}_{\boldsymbol{x}}(\boldsymbol{q}(t)) \circ d\boldsymbol{x}(t) = \int_0^{\mathcal{T}} \boldsymbol{g}_{\boldsymbol{x}}(\boldsymbol{q}(t)) \cdot d\boldsymbol{q}(t) = \int_0^{\mathcal{T}} \boldsymbol{g}_{\boldsymbol{x}}(\boldsymbol{q}(t)) \cdot \boldsymbol{v}\, dt. \quad (2.19)$$

Based on this distinction between stochastic and regular integrals, we can define a general class of *time-integrated observables*

$$X(\mathcal{T}) = \int_0^{\mathcal{T}} w(\boldsymbol{x}(t), \boldsymbol{v}(t))\, dt + \int_0^{\mathcal{T}} \boldsymbol{g}_{\boldsymbol{v}}(\boldsymbol{x}(t), \boldsymbol{v}(t)) \circ d\boldsymbol{v}(t) \quad (2.20)$$

where the function w incorporates both a weighted mean and the stochastic integration with respect to $\circ d\boldsymbol{x}$ according to Eq. (2.19). Since each realization is different, the observable is subject to fluctuations that have consequences on the statistics of the observable.

2.1.4 The overdamped limit

A common assumption for microscopic systems is that the effect of friction affects the particle much stronger than the inertia. In other words, the mass

of the particle is so small that it is immediately slowed down by friction. Mathematically, this condition is expressed as the limit $\gamma/m \gg 1$ and fittingly dubbed the *overdamped limit*. The Langevin and Fokker-Plancl equation follows in the respective limit from the previously established expressions. Since we will focus on the truely underdamped case, we will only give the results for completeness and discuss some distinct properties in the following.

The overdamped Langevin equation involves only the spatial degrees of freedom

$$\dot{\boldsymbol{x}} = \frac{1}{\gamma}\boldsymbol{F}(\boldsymbol{x}) + \boldsymbol{\xi}(t) \tag{2.21}$$

with correlations $\langle \boldsymbol{\xi}(t)\boldsymbol{\xi}(t')\rangle = \frac{T}{\gamma}\delta(t-t')$. This is due to the fact that the velocity distribution becomes infinitely broad due to the small mass of the Brownian particle. As a consequence, there is an additional time-scale separation between the change of the position and the change of the velocity. With the velocity relaxing much faster, the dynamics can be marginalized with respect to $\boldsymbol{x}$.

The same holds for the Fokker-Planck equation

$$\partial_t p(\boldsymbol{x},t) = -\frac{1}{\gamma}\nabla \boldsymbol{F}(\boldsymbol{x})p(\boldsymbol{x},t) + \nabla \boldsymbol{D}\nabla p(\boldsymbol{x},t) \tag{2.22}$$

that reduces to a differential equation in the spatial coordinates $\boldsymbol{x}$ and time t and $D_{ij} = T/\gamma$.

2.1.5 Effect of time-reversal

A distinct feature of underdamped motion, in comparison with its overdamped counterpart, is the presence of degrees of freedom with different characteristics when the time is reversed. By this we mean that a trajectory $\Gamma_{\mathcal{T}} \equiv (\boldsymbol{x}(t), \boldsymbol{v}(t))_{\mathcal{T}}$ of lenght $\mathcal{T}$ is traversed in the opposite direction

$$\Gamma_{\mathcal{T}}^{\mathsf{T}} = (\boldsymbol{x}^{\mathsf{T}}(t), \boldsymbol{v}^{\mathsf{T}}(t))_{\mathcal{T}} \equiv (\boldsymbol{x}(\mathcal{T}-t), -\boldsymbol{v}(\mathcal{T}-t))_{\mathcal{T}}. \tag{2.23}$$

The different nature of the degrees of freedom becomes apparent when the original trajectory is compared with the time-reversed trajectory, Eq. (2.23). Whereas the sign of an the position $\boldsymbol{x}$ does not change under time-reversal, it must be flipped for the velocity $\boldsymbol{v}$. This behavior is dubbed even and odd under time-reversal, respectively. Put more generally, we consider a function or observable even (odd) under time-reversal if its sign does not change (does change) if all degrees of freedom are time-reversed.

The microscopic current $\boldsymbol{j}_v$, Eq. (2.11), has an ambigious behaviour under time-reversal for underdamped dynamics. If the microscopic current is evaluated for an ensemble of time-reversed trajectories it cannot be related to the

original current straightforwardly. It can, however, be split in an odd part

$$j_v^{\text{irr}}(\boldsymbol{x},\boldsymbol{v},t) \equiv \frac{1}{2}\left(\boldsymbol{j}_v(\boldsymbol{x},\boldsymbol{v},t) - \boldsymbol{j}_v(\boldsymbol{x},-\boldsymbol{v},t)\right) = -\left(\gamma\boldsymbol{v} + \boldsymbol{D}\cdot\nabla_v\right)p(\boldsymbol{x},\boldsymbol{v},t) \quad (2.24)$$

and an even part

$$j_v^{\text{rev}}(\boldsymbol{x},\boldsymbol{v},t) \equiv \frac{1}{2}\left(\boldsymbol{j}_v(\boldsymbol{x},\boldsymbol{v},t) + \boldsymbol{j}_v(\boldsymbol{x},-\boldsymbol{v},t)\right) = \boldsymbol{F}(\boldsymbol{x})p(\boldsymbol{x},\boldsymbol{v},t). \quad (2.25)$$

Here, the even part includes the parts that can be reversed, e.g. the energy put in this motion can be regained by reversing the trajectory. In contrast, the irreversible, odd part describes dissipation which cannot be reverted. In this case, the dissipation along the time-reversed trajectory is the same as for the original one.

2.2 Stochastic thermodynamics along single trajectories

Now that the we have outlined the dynamical description of a Brownian particle, we consider its energetics in the framework of stochastic thermodynamics. The overarching notion of stochastic thermodynamics is, to map the laws of classical thermodynamics on the single trajectory of stochastic systems. This way one can analyze microscopical processes just like its macroscopic counterparts and discuss, for instance, work and heat turnover. Since the trajectories are subject to noise, these quantities, however, fluctuate.

In this section, we touch on the topic of stochastic thermodynamics and fix the notations needed throughout this thesis. A broader review of the framework can be found in Ref. [11].

2.2.1 First law of thermodynamics

Along the stochastic trajectories of the particle, the first law of (stochastic) thermodynamics represents energy conservation. The rate of change of the internal energy $U = 1/2m\boldsymbol{v}^2 + V(\boldsymbol{x})$ of the particle is given by [9]

$$\dot{U}(t) = m\boldsymbol{v}(t)\circ\dot{\boldsymbol{v}}(t) + \nabla_x V(\boldsymbol{x}(t))\cdot\boldsymbol{v}(t) = \dot{Q}(t) + \dot{W}(t) \quad (2.26)$$

where one can identify the heat exchanged with the medium during an infinitesimal time interval dt as

$$đ\dot{Q}(t) = m\boldsymbol{v}(t)\circ d\boldsymbol{v} - \boldsymbol{F}(\boldsymbol{x})\cdot\boldsymbol{v}dt \quad (2.27)$$

and the rate of work done on the particle against the non-conservative force $\boldsymbol{f}$

$$\dot{W}(t) = \boldsymbol{f}\cdot\boldsymbol{v}(t). \quad (2.28)$$

Using these rates, we can express the respective quantities along single trajectories of finite length as time-integrated observables of the form (2.20). The heat $\Delta Q[\Gamma_{\mathcal{T}}]$ dissipated along a path $\Gamma_{\mathcal{T}} \equiv (\boldsymbol{x}(t), \boldsymbol{v}(t))_{\mathcal{T}}$ can be calculated by integrating Eq. (2.27)

$$\Delta Q[\Gamma_{\mathcal{T}}] \equiv \int_0^{\mathcal{T}} \left(m\boldsymbol{v}(t) \circ d\boldsymbol{v} - \boldsymbol{F}(\boldsymbol{x}) \cdot \boldsymbol{v} dt \right). \tag{2.29}$$

Analogeously, the functional for the work against an external force

$$\Delta W[\Gamma_{\mathcal{T}}] \equiv \int_0^{\mathcal{T}} \boldsymbol{f} \cdot \boldsymbol{v}(t) dt \tag{2.30}$$

follows from integrating Eq. (2.28).

2.2.2 The second law of thermodynamics

Defining the first law of thermodynamics along an individual trajectory naturally raises the question how to formulate the second law of thermodynamics. To this end, we need to identify a stochastic entropy production.

The entropy production has two contributions [10]: The entropy produced in the medium by dissipated heat

$$\Delta S^{\mathrm{m}}[\Gamma_T] \equiv -\frac{1}{T} \Delta Q[\Gamma_T] \tag{2.31}$$

and a stochastic contribution

$$\Delta S^{\mathrm{s}}[\Gamma_T] \equiv -\ln \frac{p^{\mathrm{ss}}(\boldsymbol{x}(\mathcal{T}), \boldsymbol{v}(\mathcal{T})}{p^{\mathrm{ss}}(\boldsymbol{x}(0), \boldsymbol{v}(0))} \tag{2.32}$$

that captures the informational entropy produced in the system, e.g., when the system is prepared in a state that is not the steady state. Adding up both contributions gives the total entropy produced along the trajectory Γ as

$$\Delta S^{\mathrm{tot}}[\Gamma_T] \equiv \Delta S^{\mathrm{m}}[\Gamma_T] + \Delta S^{\mathrm{s}}[\Gamma_T]. \tag{2.33}$$

On first sight, this entropy production seems to violate the second law of thermodynamics as the entropy can also decrease. For instance a particle can traverse against an external force, powered by random fluctuations. On average, however, the mean rate of entropy production in the steady state can be expressed as an integral over the dissipative part of the microscopic steady-state current $\boldsymbol{j}_v^{\mathrm{irr,ss}}$, Eq. (2.24) in the form

$$\langle \dot{S}^{\mathrm{tot}} \rangle \equiv \sigma = \int d\boldsymbol{x} \int d\boldsymbol{v} \; \frac{\boldsymbol{j}_v^{\mathrm{irr,\,ss}}(\boldsymbol{x}, \boldsymbol{v}) \cdot \boldsymbol{D}^{-1} \cdot \boldsymbol{j}_v^{\mathrm{irr,\,ss}}(\boldsymbol{x}, \boldsymbol{v})}{p(\boldsymbol{x}, \boldsymbol{v})} \tag{2.34}$$

which, in accordance with the second law of thermodynamics, is strictly positive. In particular, for one-dimensional diffusion the mean entropy production rate is given by the positive expression

$$\sigma = \frac{m^2}{\gamma T} \int dx \int dv \; \frac{j_v^{\text{irr, ss}}(\boldsymbol{x}, \boldsymbol{v})^2}{p(\boldsymbol{x}, \boldsymbol{v})}. \tag{2.35}$$

Applied to the example above, the positive average of the entropy production means that one might observe examples of a decreasing entropy. For long observation times or many realizations, however, the expected validity of the second law is restored.

The mean entropy production rate in the steady state can equivalently be extracted from the first law, Eq. (2.26)

$$\sigma = -\frac{1}{T}\langle \dot{Q} \rangle = \frac{1}{T}\langle \boldsymbol{f} \cdot \boldsymbol{v} \rangle \tag{2.36}$$

where we use that in the steady state the internal energy becomes constant on average and the stochastic contribution ΔS^{s} vanishes.

Although the definitions for thermodynamic quantities introduced here can also be formulated for the overdamped regime, is is not guaranteed that the underdamped results converge appropriately. For instance when a system is driven out of equilibrium by an inhomogeneous temperature. Such a temperature profile can be handled in the underdamped formulation straightforwardly. One can also show that the correct steady-state distribution can be obtained from an overdamped perspective as well by modifying the Fokker-Planck equation. However, the exchanged heat and thus the entropy production is misrepresented in an a priori overdamped approach when compared to the respective quantities from an underdamped approach where the overdamped limit is performed explicitly [17]. This is due to the fact that heat is transported from regions of high temperature to regions where it is lower by means of a spatially varied velocity distribution which can not be tracked in overdamped dynamics.

Chapter 3

Fluctuations in the steady state

So far, we have mainly discussed typical values in the form of ensemble averages. Due to the random noise that affects the dynamics, however, every realization is different and the fluctuations of an observed quantity result in a not necessarily trivial probability distribution.

These fluctuations can be bound by means of the thermodynamic uncertainty relation. Before introducing the TUR properly at the end of the Chapter, we introduce methods that can be used to characterize and quantify the strength of fluctuations. As a measure of how fluctuations shape the vicinity of the most probable value, we first define the cumulants. By introducing the cumulant generating function, we show that the cumulants can, in principle, reconstruct the complete distribution. We then highlight the more microscopic path integral formalism that associates a probability measure to each possible trajectory. We put this formalism into practice by deriving fluctuation theorems that relate the relative probability of realizations with opposing signs.

As a central point of this chapter we introduce the large-deviations framework that illuminates how the probability distribution of an observable collapses onto the typical value in an appropriate limit. This framework is particularly relevant for the scope of this thesis as it is at the heart of the proof for the overdamped TUR that we outline at the end of this chapter. We wrap up by discussing why this proof can not be straightforwardly applied to the underdamped regime.

3.1 Cumulants: Fluctuations around the average

First we explore the fluctuations in the direct vicinity of the typical values. These are realizations that are quite probable and directly shape observations.

3.1.1 Characterizing typical fluctuations

The most direct way of characterizing fluctuations is to analyze the cumulants of an observable X

$$K_n(\mathcal{T}) \equiv \partial_\lambda^n \alpha(\lambda, \mathcal{T}) \tag{3.1}$$

with the *finite-time scaled cumulant generating function* or short cumulant generating function (CGF)

$$\alpha(\lambda, \mathcal{T}) \equiv \ln \left\langle e^{\lambda X} \right\rangle_{\mathcal{T}} \tag{3.2}$$

where the subscript $\mathcal{T}$ indicates that the ensemble average is taken after an observation time $\mathcal{T}$. It is worth mentioning that the CGF is the logarithm of the moment generating function. Prominently, the first two cumulants

$$K_1(\mathcal{T}) = \langle X \rangle_{\mathcal{T}} \qquad \text{and} \qquad K_2 = \mathrm{Var}[X]_{\mathcal{T}} \equiv \left\langle X^2 \right\rangle_{\mathcal{T}} - \langle X \rangle_{\mathcal{T}}^2 \tag{3.3}$$

are the mean value and the variance after an observation time $\mathcal{T}$, respectively.

The variance is the quadratic deviation of the observable around its typical value. For a Gaussian distribution it simply relates to the width of the distribution.

3.1.2 The generating function

As the name indicates, all cumulants are generated by the cumulant generating function. The latter, in a sense, contains all information of the complete distribution of the observable. However, computing the CGF from Eq. (3.2) in practice is challenging. When the distribution is not known analytically but inferred numerically, the CGF is heavily weighted towards rare, barely sampled events for $|\lambda| \gg 0$.

In the long-time limit the CGF can also be computed on a different, more controlled path. For long times, the CGF is dominated by the largest eigenvalue of the differential equation governing the time evolution of the average $\left\langle e^{\lambda X} \right\rangle$ over a steady state ensemble. To keep the notation slim we denote the time-independent long-time limit of the CGF as $\alpha(\lambda)$ without time dependence.

For the class of observables considered here, Eq. (2.20), the so-called *tilted operator* governing the dynamics of the CGF is [31]

$$\begin{aligned} \mathcal{L}(\lambda) \equiv & -\nabla_{\boldsymbol{x}} \cdot \boldsymbol{v} + \lambda f - (\nabla_{\boldsymbol{v}} - \lambda \boldsymbol{g}_{\boldsymbol{v}}) \cdot (\gamma \boldsymbol{v} - \boldsymbol{F}(\boldsymbol{x})) \\ & - (\nabla_{\boldsymbol{v}} - \lambda \boldsymbol{g}_{\boldsymbol{v}})^{\mathsf{T}} \cdot \boldsymbol{D} \cdot (\nabla_{\boldsymbol{v}} - \lambda \boldsymbol{g}_{\boldsymbol{v}}) \end{aligned} \tag{3.4}$$

which reduces to the Fokker-Planck operator $\mathcal{L}$, Eq. (2.9), for $\lambda = 0$. When the probability distribution is expanded in a suited basis, the problem of calculating the CGF can thus be translated to a numerically well controlled eigenvalue problem. The continuous generalization of the Perron-Frobenius theorem guarantees that the largest eigenvalue is real as long as the spectrum remains gapped [31]. Since all other eigenvalues have a negative real part, the largest eigenvalue corresponds to the CGF $\alpha(\lambda)$ for large observation times.

Moreover, the left and right eigenfunction allow to construct the density of the ensemble that becomes typical for a given tilting λ. Let $H_r(\boldsymbol{x}, \boldsymbol{v}, \lambda)$ denote the right eigenfunction corresponding to the largest eigenvalue of Eq. (3.4)

$$\mathcal{L}(\lambda) H_r(\lambda) = \alpha(\lambda) H_r(\lambda). \tag{3.5}$$

This eigenfunction is also dubbed the dominant eigenfunction. Equivalently H_l is the corresponding eigenfunction of the adjoint operator $\mathcal{L}^\dagger$

$$\mathcal{L}^\dagger(\lambda) H_l(\lambda) = \alpha(\lambda) H_l(\lambda) \tag{3.6}$$

for some tilting λ. The *typical density* then is the product at each point [32]

$$\rho_{\text{typ}}(\boldsymbol{x}, \boldsymbol{v}, \lambda) = H_r(\boldsymbol{x}, \boldsymbol{v}, \lambda) H_l(\boldsymbol{x}, \boldsymbol{v}, \lambda) / \mathcal{N} \tag{3.7}$$

with appropriate normalization $\mathcal{N}$. Most notably, for $\lambda = 0$ the right eigenfunction is the stationary distribution p^{ss} and the left eigenfunction is 1 due to probability conservation. Consistently, the typical density for vanishing tilting is $\rho_{\text{typ}}(\boldsymbol{x}, \boldsymbol{v}, 0) = p^{\text{ss}}(\boldsymbol{x}, \boldsymbol{v})$.

3.2 Path integrals: Fluctuating trajectories

The cumulant generating function is a suited tool to characterize fluctuations of an observable. Given that calculating the CGF can be mapped to a numerically well controllable eigenvalue problem it does not only allow to efficiently calculate the cumulants of a distribution but also to illustrate the ensemble that generates specific fluctuations by means of the typical densities.

The approach is, however, limited to ensembles of trajectories. To assess the probabilities of specific fluctuations or even individual trajectories one can employ so-called path integrals. We demonstrate the relevance of such a description as a follow-up by deriving fluctuation theorems.

3.2.1 Assessing the probability of certain trajectories

The probabilistic weight of a specific trajectory conditioned on a starting point $(\boldsymbol{x}(0), \boldsymbol{v}(0))$ can be expressed in form of the path weight functional [33]

$$\mathcal{P}\left[\Gamma_{\mathcal{T}}\right] \equiv \frac{1}{\mathcal{Z}} \exp\left[-\int_0^{\mathcal{T}} \mathcal{S}(\boldsymbol{x}(t), \boldsymbol{v}(t)) dt\right] p^{\text{ss}}\left(\boldsymbol{x}(0), \boldsymbol{v}(0)\right) \tag{3.8}$$

with the so-called action

$$\mathcal{S}(\boldsymbol{x},\boldsymbol{v}) \equiv -\log[\delta(\dot{\boldsymbol{x}}-\boldsymbol{v})] \tag{3.9}$$
$$+\left\{ \left[\dot{\boldsymbol{v}}-\left(\boldsymbol{F}(\boldsymbol{x})-\gamma\boldsymbol{v}\right)/m\right]\boldsymbol{D}^{-1}\left[\dot{\boldsymbol{v}}-\left(\boldsymbol{F}(\boldsymbol{x})-\gamma\boldsymbol{v}\right)/m\right]-\nabla_{\boldsymbol{v}}\gamma\boldsymbol{v}\right\}.$$

which must be interpreted in the Stratonovich sense. For the Itô interpretation, the last term must be omitted. Unique for underdamped motion, is the delta function that reflects the deterministic equation of motion for the spatial variables $\boldsymbol{x}$. As a result, the weight for trajectories with inconsistent change in the position, i.e., a particle moving faster than its current velocity, is zero.

The path weight can be used to evaluate averages over any functional observable. For instance, for the observable $X[\Gamma_{\mathcal{T}}]$ after time $\mathcal{T}$, see Eq. (2.20), the mean can be expressed as the integral

$$\langle X[\Gamma_{\mathcal{T}}]\rangle_{\mathcal{T}} = \int_{\mathcal{T}}[\mathcal{D}\Gamma]\ X[\Gamma]\ \mathcal{P}[\Gamma], \tag{3.10}$$

where $\int_{\mathcal{T}}[\mathcal{D}\Gamma]$ denotes an integral over the space of trajectories of length $\mathcal{T}$. Analogously, the probability of a specific value $\tilde{X}$ of the observable is given by

$$P(\tilde{X},\mathcal{T}) = \int_{\mathcal{T}}[\mathcal{D}\Gamma]\ \delta\left(X[\Gamma]-\tilde{X}\right)\ \mathcal{P}[\Gamma]. \tag{3.11}$$

3.2.2 Entropy as a measure of irreversibility

After having introduced the path integral formalism, we can use it to rewrite the stochastic entropy production, Eq. (2.33), in a compact form

$$S^{\text{tot}}[\Gamma_{\mathcal{T}}] = \ln\left[\frac{\mathcal{P}[\Gamma_{\mathcal{T}}]}{\mathcal{P}^{\mathsf{T}}[\Gamma^{\mathsf{T}}_{\mathcal{T}}]}\right] \tag{3.12}$$

with the time-reversed path $\Gamma^{\mathsf{T}}_{\mathcal{T}}$, Eq. (2.23), and the complement path weight [34]

$$\mathcal{P}^{\mathsf{T}}[\Gamma^{\mathsf{T}}_{\mathcal{T}}] \equiv \mathcal{P}[\Gamma^{\mathsf{T}}_{\mathcal{T}}|(\boldsymbol{x}^{\mathsf{T}}(0),\boldsymbol{v}^{\mathsf{T}}(0))]\ \ p^{\text{ss}}\left(\boldsymbol{x}^{\mathsf{T}}(0),-\boldsymbol{v}^{\mathsf{T}}(0)\right) \tag{3.13}$$
$$= \mathcal{P}[\Gamma^{\mathsf{T}}_{\mathcal{T}}|(\boldsymbol{x}(\mathcal{T}),-\boldsymbol{v}(-\mathcal{T}))]\ \ p^{\text{ss}}\left(\boldsymbol{x}(\mathcal{T}),\boldsymbol{v}(\mathcal{T})\right) \tag{3.14}$$

which is the original path weight but the initial probability of the complementary weight is given by the final distribution $p^{\text{ss}}\left(\boldsymbol{x}(\mathcal{T}),\boldsymbol{v}(\mathcal{T})\right)$ of the original process. In the ratio of path weights, Eq. (3.12) the initial probability and conditioned path weight form the system and medium contribution of the entropy along a trajectory, Eq. (2.33), respectively.

By relating the probability of the two opposing trajectories, this definition of the entropy, Eq. (3.12), directly embodies the interpretation as a measure

of irreversibility. When the system is in equilibrium one would not be able to distinguish a trajectory from its time-reversed counterpart since both are equally probable. In this case the entropy production (3.12) vanishes. In non-equilibrium situations there is, however, a difference between the probabilities. The trajectory has an irreversible contribution that is captured by the entropy production.

3.3 Fluctuation theorems: Characterizing fluctuations

While introducing the path weight gives a theoretical way of studying fluctuations, they are hard to evaluate in practice. However, they allow to derive a class of relations known as fluctuation theorems [11] that relate the probabilities of certain fluctuations. In this section, we derive a detailed fluctuation theorem that specifies the relative probability of measuring a negative medium entropy production $-\Delta S^{\mathrm{m}}$, Eq. (2.31).

Before we discuss the underdamped case, we introduce the fluctuation theorem for the entropy production in overdamped dynamics. Here, all degrees of freedom are even under time-reversal and the entropy production along a trajectory can be calculated as the logarithmic ratio of the path weight of the original trajectory and its time-reversed counterpart without adjusting the initial probability as was necessary in Eq. (3.12) for the velocity. By this definition one can straightforwardly derive the so-called steady-state detailed fluctuation theorem (DFT) [10] that has the form

$$P(-S) = P(S)e^{-S} \tag{3.15}$$

where S is the overdamped entropy production and $P(S)$ is the probability to observe a specific value. This is true for all times. As a consequence of the DFT, the probability of negative fluctuations is dampened by the entropy production for large times.

By integrating both sides the integral fluctuation theorem (IFT)

$$\left\langle e^{-S} \right\rangle = 1 \tag{3.16}$$

follows. By applying Jensen's inequality it follows $\langle S \rangle \geq 0$. Since this is exactly the statement of the second law of thermodynamics, the IFT is often interpreted as a refinement of the second law.

In contrast to the overdamped case, a detailed fluctuation theorem holds for the entropy production in the underdamped regime only in the long-time limit [35]. This is due to the different complement path weight that appears in the definition of the entropy production (3.11). In the long-time limit these

boundary terms vanish. Nevertheless, an IFT holds for all times due to the form of the entropy production.

A detailed fluctuation theorem valid for all times can, however, be derived for the different irreversibility measure

$$\Delta\Psi[\Gamma_{\mathcal{T}}] \equiv \ln\left[\frac{\mathcal{P}[\Gamma_{\mathcal{T}}]}{\mathcal{P}[\Gamma^{\dagger}_{\mathcal{T}}]}\right]. \tag{3.17}$$

This functional involves the time-reversed trajectory $\Gamma^{\dagger}_{\mathcal{T}}$ and a complementary path weight that is the same as for the forward process. The functional $\Delta\Psi$ coincides with the entropy production in the long-time limit, where the boundary terms from the system entropy production become irrelevant. Plug-gin this measure in Eq. (3.11) and changing the integration to an integration over the time-reversed trajectory yields the detailed fluctuation theorem

$$\begin{aligned} P(\tilde{\Psi},\mathcal{T}) &= \int_{\mathcal{T}}[\mathcal{D}\Gamma]\ \delta\left(\Delta\Psi[\Gamma]-\tilde{\Psi}\right)\ \mathcal{P}[\Gamma] && (3.18)\\ &= \int_{\mathcal{T}}[\mathcal{D}\Gamma]\ \delta\left(\Delta\Psi[\Gamma]-\tilde{\Psi}\right)\ \frac{\mathcal{P}[\Gamma]}{\mathcal{P}[\Gamma^{\dagger}]}\mathcal{P}[\Gamma^{\dagger}] && (3.19)\\ &= \int_{\mathcal{T}}[\mathcal{D}\Gamma^{\dagger}]\ \delta\left(-\Delta\Psi[\Gamma^{\dagger}]-\tilde{\Psi}\right)\ e^{-\Delta\Psi[\Gamma]}\mathcal{P}[\Gamma^{\dagger}] && (3.20)\\ &= e^{\tilde{\Psi}}P(-\tilde{\Psi},\mathcal{T}) && (3.21) \end{aligned}$$

where in the third line we use that $\Delta\Psi$ is odd under time-reversal.

While the irreversibility measure $\Delta\Psi$ itself has no physical interpretation, we can use its convergence in the long-time limit. In this limit, the detailed fluctuation theorem for the irreversibility, Eq. (3.21), can mapped to the entropy production

$$P(\Delta S^{\text{tot}},\mathcal{T}) \approx e^{\Delta S^{\text{tot}}}P(-\Delta S^{\text{tot}},\mathcal{T}) \qquad (\mathcal{T}\gg 1) \tag{3.22}$$

as already discussed in Ref. [35].

3.4 Large deviations theory: Studying rare fluctuations

We have shown that the CGF and the path integral formalism are good tools to characterize fluctuations and even to study specific fluctuations. Since we are interested in the TUR, we introduce a third framework, namely *large deviation theory* [36]. For a pedagogical review see Ref. [37]. After introducing the basics of the framework, we show that its most basic form is tightly tied to the cumulant generating function. However, in a more abstract form it plays an important role in the proof of the TUR in the overdamped regime [38, 39, 22].

3.4.1 The large deviation principle

The basis of the large deviations framework is the question, how a probability distribution collapses for a large parameter N. Although the framework can be employed in a more general context we will restrict ourselves to two cases, namely the long-time limit where the observation time $\mathcal{T}$ is the large parameter, and many copies of the same system where N is the number of copies. As an introduction, we discuss the latter and consider the mean observable $X_N(\mathcal{T}) = 1/N \sum_{i=1}^{N} X_i$ over N copies measured over some time $\mathcal{T}$.

We consider the probability distribution of a possibly path-dependent observable X and rewrite it in the asymptotic form

$$P(\tilde{X}, N) \approx e^{-NI(\tilde{X})+o(N)} \qquad (N \gg 1) \tag{3.23}$$

where

$$I(\tilde{X}) = \lim_{N\to\infty} \frac{1}{N} \ln P(\tilde{X}, N) \tag{3.24}$$

is called the *large deviation function* (LDF) and $o(N)$ denotes the small Landau-o symbole. This function captures the exponential rate of decay of the probability to observe a specific value $\tilde{X} \stackrel{!}{=} X_N(\mathcal{T})$ for large values of the parameter N. If this limit exists, X is said to satisfy a *large deviation principle*.

In the $N \to \infty$ limit the mean observable $X^N(\mathcal{T})$ over a finite number of copies converges to the ensemble average $\langle X \rangle_{\mathcal{T}}$. In this case, the probability must vanish anywhere except for the typical value. As a consequence, the LDF is 0 only for the typical value and strictly positive elsewhere. All fluctuations around this stationary value become exponentially less likely for the increasing large-deviation parameter N.

Analogously, one can consider the mean rate recorded along a finite-length trajectory $J_{\mathcal{T}} \equiv X(\mathcal{T})/\mathcal{T}$ with the large-deviation parameter $\mathcal{T}$. For large times, the observed velocity converges to the steady state value $\langle J \rangle$ meaning that $\lim_{\mathcal{T}\to\infty} P(\langle J \rangle, \mathcal{T}) = 1$. As a consequence, the LDF is zero only at the steady-state value.

To distinguish between the two conceptually slightly different LDFs, we use a superscript $\mathcal{T}$ to denote the long-time LDF in the following.

3.4.2 Relation to the cumulants

While the concept of large deviations seems rather abstract at first, the LDF can be tightly connected to the previously introduced and ostensible more applicable scaled cumulant in the long-time limit. This link is established by the *Gärtner-Ellis theorem* stating that the LDF can be derived from the generating function by means of a Legendre-Fenchel transformation

$$I^{\mathcal{T}}(J) = \sup_{\lambda} [\lambda J - \alpha(\lambda)] \tag{3.25}$$

where $\alpha(\lambda)$ is the CGF in the long-time limit and J is the mean rate $X(\mathcal{T})/\mathcal{T}$. Using this relation, the LDF can be calculated from the CGF which in turn can be calculated by solving the eigenvalue problem of the tilted operator, Eq. (3.4).

This tight connection to the cumulants can be made for finite times as well. If we consider the N copies version of the LDF, then the direct vicinity of the typical value is characterized by the central limit theorem. For a large number of copies N, the distribution of the sum over the observable is approximately described by a Gaussian centered around the typical value with the variance being a multiple of the variance of a single copy

$$P^N(\tilde{X},\mathcal{T}) \approx \mathcal{N} \exp\left[-\frac{1}{N\mathrm{Var}[X]_{\mathcal{T}}}\left(\tilde{X}-\langle X\rangle_{\mathcal{T}}\right)^2\right] \qquad (N \gg 1, \tilde{X} \approx \langle X\rangle) \tag{3.26}$$

where $\mathcal{N}$ is a suited normalization and $\mathrm{Var}[X]_{\mathcal{T}}$ is the variance of the observable at time $\mathcal{T}$. As a result, the LDF becomes parabolic in the vicinity of the typical value with curvature

$$I''(\langle X\rangle, \mathcal{T}) = \frac{1}{\mathrm{Var}[X]_{\mathcal{T}}}. \tag{3.27}$$

3.4.3 Functional large deviation functions - high level LDFs

The large deviations framework is not limited to scalar observables. It can be generalized to functional observables as well. The large deviation function then measures the exponential rate of decay for the probability to observe a specific function, e.g. a specific probability density. In this section, we derive the functional LDF for the probability density following Ref. [40]. This functional form has also be considered in Ref. [41] from a more mathematically point of view.

We consider N identically prepared copies of the system that evolve according to the same Langevin dynamics. The probability distribution observed for N systems evolving in parallel along trajectories Γ_i is given by

$$\rho^N(\tilde{\boldsymbol{x}},\tilde{\boldsymbol{v}})[\{\Gamma_i\},\mathcal{T}] \equiv \frac{1}{N\mathcal{T}}\sum_{n=1}^{N}\int_0^{\mathcal{T}} dt\ \delta(\boldsymbol{x}_i(t)-\tilde{\boldsymbol{x}})\delta(\boldsymbol{v}_i(t)-\tilde{\boldsymbol{v}}) \tag{3.28}$$

where the copies of the system are labeled by the subscript i. We will refer to this distribution as *empirical distribution*. Analogously, the *empirical current* can be defined as

$$\boldsymbol{\mu}^N(\tilde{\boldsymbol{x}},\tilde{\boldsymbol{v}})[\{\Gamma_i\},\mathcal{T}] \equiv \frac{1}{N\mathcal{T}}\sum_{n=1}^{N}\int_0^{\mathcal{T}} dt\ \delta(\boldsymbol{x}_i(t)-\tilde{\boldsymbol{x}})\delta(\boldsymbol{v}_i(t)-\tilde{\boldsymbol{v}}) \circ d\begin{pmatrix}\boldsymbol{x}(t)\\ \boldsymbol{v}(t)\end{pmatrix} \tag{3.29}$$

where in the following we denote the spatial current with $\boldsymbol{\mu}_x^N$ and the velocity part with $\boldsymbol{\mu}_v^N$.

In the limit $N \to \infty$, the ensemble average is recovered and the empirical distribution and current converge to the solution of the Fokker-Planck equation with appropriate boundary conditions

$$p(\boldsymbol{x}, \boldsymbol{v}, t) = \lim_{N\to\infty} \rho^N(\boldsymbol{x}, \boldsymbol{v}, t) \tag{3.30}$$

and the corresponding microscopic current, Eq. (2.11)

$$\boldsymbol{j}(\boldsymbol{x}, \boldsymbol{v}, t) = \lim_{N\to\infty} \boldsymbol{\mu}^N(\boldsymbol{x}, \boldsymbol{v}, t), \tag{3.31}$$

respectively.

To calculate the LDF for observing these quantities, we first need to calculate the probability to observe a specific value for the empirical distribution and current. Using the path integral, Eq. (3.11), this probability can be written as

$$P^N[\tilde{\rho}, \tilde{\boldsymbol{\mu}}, \mathcal{T}] = \int_{\mathcal{T}} \prod_{i=1}^{N} (\mathcal{D}\Gamma_i) \mathcal{P}_{\mathcal{T}}[\Gamma_i] \;\; \delta\left(\rho[\{\Gamma_i\}, \mathcal{T}] - \tilde{\rho}\right) \delta\left(\boldsymbol{\mu}[\{\Gamma_i\}, \mathcal{T}] - \tilde{\boldsymbol{\mu}}\right) \tag{3.32}$$

where $\rho[\{\Gamma_i\}, \mathcal{T}]$ and $\boldsymbol{\mu}[\{\Gamma_i\}, \mathcal{T}]$ are the empirical distribution, Eq. (3.28), and current, Eq. (3.29), evaluated with the N trajectories $\{\Gamma_i\}$ at time $\mathcal{T}$. The path weight $\mathcal{P}_{\mathcal{T}}$ contains a delta condition that guarantees that the path weight vanishes when $\dot{\boldsymbol{x}} \neq \boldsymbol{v}$ for all times. As a consequence, we can rewrite the spatial part of the current as outlined in Sec. 2.1.3 and get

$$\boldsymbol{\mu}_x[\{\Gamma_i\}, \mathcal{T}] = \boldsymbol{v}\rho[\{\Gamma_i\}, \mathcal{T}]. \tag{3.33}$$

This constraints the desired empirical current in x-direction

$$\tilde{\boldsymbol{\mu}}_x(\boldsymbol{x}, \boldsymbol{v}, t) \stackrel{!}{=} \boldsymbol{v}\tilde{\rho}[\{\Gamma_i\}, \mathcal{T}] \tag{3.34}$$

with P^N being zero otherwise. Keeping this in mind, we can drop the condition $\delta(\dot{\boldsymbol{x}} - \boldsymbol{v})$ in the path weight.

We now introduce an alternative driving force $\boldsymbol{G}(\boldsymbol{x}, \boldsymbol{v})$ that makes the desired empirical functions $\tilde{\rho}$ and $\tilde{\boldsymbol{\mu}}$ typical. This is only possible if the continuity equation

$$\partial_t \tilde{\rho}(\boldsymbol{x}, \boldsymbol{v}, t) = -\nabla \boldsymbol{\mu} \tag{3.35}$$

holds. Empirical functions that do not match this continuity equation, are unlikely and their probability rapidly vanish as the number of copies $N \to \infty$ increases. Consistently, the large deviation functional becomes infinity for such functions.

Using this altered force, the integration in Eq. (3.32) can be changed to an integration in the altered dynamics. As a second step, all integrals occuring in the path integration can then be replaced by empirical densitites and currents thus allowing to evaluate the integral. The details of the derivation can be found in the Appendix 3.A. Using the *associated current*, this is the microscopic current, Eq. (2.11), associated with the empirical distribution instead of the probability distribution p,

$$\boldsymbol{j}_v(\boldsymbol{x},\boldsymbol{v})[\rho] \equiv \boldsymbol{A}(\boldsymbol{x},\boldsymbol{v})\rho(\boldsymbol{x},\boldsymbol{v}) + \boldsymbol{D}\cdot\nabla_v\rho(\boldsymbol{x},\boldsymbol{v}) \tag{3.36}$$

the LDF can be written in the obviosuly positive form

$$I[\tilde{\rho},\tilde{\boldsymbol{\mu}},\mathcal{T}] \equiv \mathcal{T}\int d\boldsymbol{x}d\boldsymbol{v}\frac{(\tilde{\boldsymbol{\mu}}_v - \boldsymbol{j}_v[\tilde{\rho}])\cdot\boldsymbol{D}^{-1}\cdot(\tilde{\boldsymbol{\mu}}_v - \boldsymbol{j}_v[\tilde{\rho}])}{4\tilde{\rho}} + K\left(\tilde{\rho}||p^{\mathrm{ss}}\right) \tag{3.37}$$

where the initial change in the LDF for a non-typical distribution $\tilde{\rho}$ is captured by the so-called *Kullback-Leibler divergence*

$$K\left(\tilde{\rho}||p^{\mathrm{ss}}\right) = \int d\boldsymbol{x}d\boldsymbol{v}\;\tilde{\rho}(\boldsymbol{x},\boldsymbol{v})\ln\frac{\tilde{\rho}(\boldsymbol{x},\boldsymbol{v})}{p^{\mathrm{ss}}(\boldsymbol{x},\boldsymbol{v})}. \tag{3.38}$$

As pointed out before, however, the LDF is infinity if either the continuity equation (3.35) is violated or the current in the deterministic degree of freedom $\tilde{\boldsymbol{\mu}}_x$ does not match the current dictated by the empirical distribution according to Eq. (3.34).

Using these two constraints on the LDF, it can be reduced to a functional that depends only on the empirical density. Since $\boldsymbol{\mu}_x = \boldsymbol{v}\rho$, the continuity equation constraints $\boldsymbol{\mu}_v$ as

$$\nabla_v\boldsymbol{\mu}_v = \partial_t\rho(\boldsymbol{x},\boldsymbol{v},t) - \boldsymbol{v}\nabla_x\rho(\boldsymbol{x},\boldsymbol{v},t) \tag{3.39}$$

which defines $\boldsymbol{\mu}_v$ up to a possibly $\boldsymbol{x}$-dependent integration constant. For $\boldsymbol{v}\to\pm\infty$ the current $\boldsymbol{\mu}$ must, however, vanish, so that the integration constant is 0. Hence, the empirical current associated with a given empirical density can be expressed as a functional $\boldsymbol{\mu}_v[\rho]$ and the large deviation functional reduces to

$$I[\tilde{\rho},\mathcal{T}] \equiv I[\tilde{\rho},\boldsymbol{\mu}[\tilde{\rho}],\mathcal{T}] \tag{3.40}$$

without further constraints on the choice of the empirical density.

On first sight, it is surprising that such a constraint holds in underdamped dynamics but not for the overdamped case. However, the overall information that must be provided to the large deviation functional stays the same. Whereas for overdamped dynamics one is free to chose an empirical distribution in $\boldsymbol{x}$ and current $\boldsymbol{\mu}$, one instead can specify a two dimensional empirical distribution $\rho(\boldsymbol{x},\boldsymbol{v})$. Being a function in $\boldsymbol{x}$ and $\boldsymbol{v}$ it can carry the same information as for the overdamped case, in particular one can map two independent

functions in a bijective matter in such a form. For real processes, however, the position and velocity are correlated. This is due to the relaxation of velocity and its coupling the spatial degrees of freedom. For instance, if a particle is locally faster due to an underlying potential, the velocity is overall higher in the vicinity independent of the potential landscape.

It is worth noting that one can also consider the observation time $\mathcal{T}$ as a large parameter. The empirical density and current can then be defined as averaged density and current along a long trajectory. The resulting large deviation functional has the same form as the one derived here, Eq. (3.37), but without the Kullback-Leibler divergence. This is due to the fact that the system becomes decorrelated from its initial distribution in the long-time limit.

3.4.4 The contraction principle and a hierarchy of LDFs

The functional LDF, Eq. (3.37), that was derived in the previous section can be connected with the LDFs for the scalar class of observables defined in Eq. (2.20). Using the definition of the empirical density, the ensemble statistics of an observable that is an average along a trajectory, this is $\boldsymbol{g}_v = 0$, can be expressed by means of the empirical current

$$\frac{1}{N}\sum_{i=1}^{N} X[\Gamma_i] = \sum_{i=1}^{N}\int_0^{\mathcal{T}} dt\; w(\boldsymbol{x}_i(t), \boldsymbol{v}_i(t)) = \int d\boldsymbol{x}d\boldsymbol{v}w(\boldsymbol{x},\boldsymbol{v})\rho^N(\boldsymbol{x},\boldsymbol{v}). \tag{3.41}$$

Similarly, an observable that consists only of an path-integration along a trajectory, i.e. $w = 0$, can be converted

$$\frac{1}{N}\sum_{i=1}^{N} X[\Gamma_i] = \sum_{i=1}^{N}\int_0^{\mathcal{T}} \boldsymbol{g}_v(\boldsymbol{x}_i(t), \boldsymbol{v}_i(t)) \circ d\boldsymbol{v}(t) = \int d\boldsymbol{x}d\boldsymbol{v}\boldsymbol{g}(\boldsymbol{x},\boldsymbol{v})\boldsymbol{\mu}_v^N(\boldsymbol{x},\boldsymbol{v}). \tag{3.42}$$

In general an observable can contain both types of integration and thus we rewrite the observable as functional $X[\rho]$ with $\boldsymbol{\mu}[\rho]$ following through consistency conditions as before. The LDFs associated with such a scalar observable will be referred to as *level 1 LDF*.

When we can express the scalar observables by means of the empirical density and current, it is possible to derive the corresponding level 1 LDF from the functional LDF of the empirical measures via the so-called *contraction principle*. In detail, the level 1 LDF can be derived through the contraction

$$I(\tilde{X}) = \min_{\rho \mid \tilde{X}=X[\rho]} I[\rho] \tag{3.43}$$

which is a minimization over the densities ρ that generate the desired value $\tilde{X}$ of the observable. The rationale behind this contraction is that the probability of $\tilde{X}$ decays as slow as the slowest in the ensemble of empirical density that generates the desired value.

With the level 1 LDF being contractable from the functional LDF it was dubbed the *level 2.5 LDF* in the overdamped context. In this regime, the empirical density and current can be chosen individually and thus the contraction in (3.43) involves both functions as a parameter. Since the functional LDF $I[\rho]$ can in turn be contracted from the level 2.5 LDF by minimizing over the empirical densities only, it was dubbed the *level 2 LDF*. From this intermediate level, the lower level 1 LDF can only be contracted if the observable depends only on the empirical density ρ in a functional sense, i.e. a mean-like observable. In this hierarchy, an LDF on the trajectory level can be regarded as a level 3 LDF and lower level LDFs can be contracted from as we did in the proof in Sec. 3.4.3.

The notion of a level 2.5 does, however, not carry over to underdamped case. Here, the empirical density and current are interlinked by Eq. (**??**) and hence scalar observables are functionals of the empirical density, only. As a consequence, the level 2 functional fulfills the task previously associated with the level 2.5 LDF.

Building upon the connection of the CGF and the LDF, the typical density (3.7) extracted from the left and right eigenvectors of the tilted operator can be shown to minimize the contraction of $I^{\mathcal{T}}[\rho]$ for the realization $\tilde{J} = \alpha'(\lambda)$ [32]. Hence, $\rho_{\text{typ}}(\boldsymbol{x}, \boldsymbol{v}, \lambda)$ can be interpreted as the phase space density associated with the ensemble of trajectories producing a specific fluctuation $J = \alpha'(\lambda)$.

3.5 Bounds on fluctuations: The thermodynamic uncertainty relation

A recent result in stochastic thermodynamics is the *thermodynamic uncertainty relation* (TUR) [12]. It bounds the precision of any current in overdamped dynamics by the mean rate of entropy production σ of the system in the steady state. The bound embodies the intuitive picture that increasing the precision of currents comes with the cost of higher dissipation. The TUR was first proven for continuous-time Markovian dynamics in the long-time limit for discrete states [38] and for overdamped continuous states [39, 42]. First only proven in the long-time limit, the validity of the TUR was extended to finite times $\mathcal{T}$ [43, 22]. In this section, we will give a detailed overview over the TUR and its proof for overdamped dynamics.

3.5.1 The Statement of the TUR

As the name *uncertainty relation* implies, the TUR bounds the uncertainty that is observed in stochastic systems. To quantify the uncertainty, the relation

utilizes the measure

$$\epsilon(\mathcal{T})^2 \equiv \frac{\mathrm{Var}[X(\mathcal{T})]}{\langle X(\mathcal{T})\rangle^2}. \tag{3.44}$$

which puts the variance of some observable X in perspective to its average. From a metrology point of view, the uncertainty can also be interpreted as the inverse signal to noise ratio that quantifies the signal, the mean value, in relation to the spread around this value. In this sense, a high uncertainty means that the mean value can hardly be extracted from an observation that is based on only a few realizations. Consequently, the inverse of this definition is also used as a measure for the precision.

One of the key success factors of the TUR is its compact form and general conditions of validity. Using the *uncertainty product* $\mathcal{Q}$

$$\mathcal{Q}(\mathcal{T}) \equiv \epsilon(\mathcal{T})^2 \sigma \mathcal{T} \tag{3.45}$$

the TUR takes on the form of the inequality

$$\mathcal{Q}(\mathcal{T}) \geq 2. \tag{3.46}$$

and holds for all Stratonovich integrated observables

$$X(\mathcal{T}) = \int_0^{\mathcal{T}} \boldsymbol{g}_x(\boldsymbol{x}) \circ d\boldsymbol{x}(t). \tag{3.47}$$

3.5.2 A proof of the overdamped TUR

Although the TUR can be stated in an arguably simple form, its proof turns out to be more involved. In this section, we scetch the proof for overdamped dynamics to later discuss the challenges in the generalization to the underdamped regime.

The original proof presented for overdamped dynamics [39, 42, 22] exploits the contraction principle of large deviations, as introduced in Sec. (3.4.4). As mentioned before, the level 2.5 LDF

$$I^{\mathrm{ov}}[\rho, \boldsymbol{\mu}] = \begin{cases} \int d\boldsymbol{x} \dfrac{(\boldsymbol{\mu} - \boldsymbol{j}^{\mathrm{ov}}[\rho]) \cdot D^{-1} \cdot (\boldsymbol{\mu} - \boldsymbol{j}^{\mathrm{ov}}[\rho])}{4\rho} + K(\rho || p^{\mathrm{ss}}) & \nabla \boldsymbol{\mu} = 0 \\ \infty & \text{otherwise} \end{cases} \tag{3.48}$$

can be used to contract the level 1 LDF of a Stratonovich current of the form (3.47). In analogy to Eq. (3.36), the associated current $\boldsymbol{j}^{\mathrm{ov}}[\rho]$ is the microscopic probability current

$$\boldsymbol{j}^{\mathrm{ov}}(\boldsymbol{x})[\rho] \equiv \boldsymbol{F}(\boldsymbol{x})\rho(\boldsymbol{x})/\gamma - \boldsymbol{D} \cdot \nabla \rho(\boldsymbol{x}) \tag{3.49}$$

expected for the empirical distribution ρ. The main idea of the proof is, to find a bound on the level 1 LDF for the current X by making a suitable ansatz

to the minimization of the contraction principle. Every non-optimal function that produces the expected current X is an upper bound at that point.

In contrast to underdamped dynamics, this overdamped LDF has two expedient features. First, there is no constraining link between the empirical density and current. As a consequence, they can be chosen independently to get a bound on the level 1 LDF, for instance by using the stationary density and simultaneously rescaling the stationary current, i.e.

$$\tilde{\rho} = p^{\mathrm{ss}} \quad , \quad \tilde{\boldsymbol{\mu}} = c\boldsymbol{j}^{\mathrm{ss}}. \tag{3.50}$$

Since $X[\boldsymbol{\mu}]$ is linear in the current the corresponding observable is simply the rescaled steady state value

$$X[\tilde{\boldsymbol{\mu}}] = cX[\boldsymbol{j}^{\mathrm{ss}}] = c\,\langle X\rangle\,. \tag{3.51}$$

With $c = \tilde{X}/\langle X\rangle$ we can meet the minimization condition in Eq. (3.49) and obtain

$$I(\tilde{X}) = \min_{\rho,\boldsymbol{\mu}\ |\ \tilde{X}=X[\boldsymbol{\mu}]} I^{\mathrm{ov}}[\rho,\boldsymbol{\mu}] \leq I^{\mathrm{ov}}\left[p^{\mathrm{ss}}, \frac{\tilde{X}}{\langle X\rangle}\boldsymbol{j}^{\mathrm{ss}}\right]. \tag{3.52}$$

The second important feature is that there is no reversible contribution to the associated current, Eq. (3.49). Consequently, it reduces to the irreversible current for the stationary distribution

$$\boldsymbol{j}^{\mathrm{ov}}[p^{\mathrm{ss}}](\boldsymbol{x}) = \boldsymbol{j}^{\mathrm{ss}}_{\mathrm{irr}} = \boldsymbol{j}^{\mathrm{ss}}. \tag{3.53}$$

Plugging the ansatz for the empirical density and current in Eq. (3.48) thus yields

$$I(\tilde{X}) \leq \left(1 - \frac{\tilde{X}}{\langle X\rangle}\right)^2 \int d\boldsymbol{x}\, \frac{\boldsymbol{j}^{\mathrm{ss}}\cdot D^{-1}\cdot \boldsymbol{j}^{\mathrm{ss}}}{4p^{\mathrm{ss}}} \tag{3.54}$$

and we can readily identify the entropy production. The bound resulting from the ansatz in Eq. (3.52) thus becomes

$$I(\tilde{X}) \leq \left(1 - \frac{\tilde{X}}{\langle X\rangle}\right)^2 \frac{\sigma\mathcal{T}}{4}. \tag{3.55}$$

Since for the typical observable $\tilde{X} = \langle X\rangle$ the bound becomes 0 and thus is tight at that point, we can directly derive a bound on the variance from the bound on the LDF . To this end, we calculate the second derivative and use that the curvature of the LDF is given by the variance at its minimum, see Eq. (3.27),

$$\mathrm{Var}[X] = I''(\langle X\rangle)^{-1} \geq \frac{2\,\langle X\rangle^2}{\sigma\mathcal{T}}. \tag{3.56}$$

This is exactly the statement of the TUR, Eq. (3.45).

Appendix

3.A Derivation of the functional LDF

The ratio of the path weights of the original dynamics and the altered dynamics $\mathcal{P}^G$ yields the ratio

$$\frac{\mathcal{P}_{\mathcal{T}}[\Gamma_i]}{\mathcal{P}^G_{\mathcal{T}}[\Gamma_i]} = \frac{p^{\mathrm{ss}}(\boldsymbol{x}_i(0), \boldsymbol{v}_i(0))}{\rho(\boldsymbol{x}_i(0), \boldsymbol{v}_i(0), 0)} \exp\left\{ -\int_0^{\mathcal{T}} [\mathbb{A}_i(t)dt + \mathbb{B}_i(t) \circ d\boldsymbol{v}_i] \right\} \tag{3.A.1}$$

with the time integrand

$$\mathbb{A}_i(t) \equiv \frac{1}{4} \left\{ \boldsymbol{A}_i(t)^{\intercal} \boldsymbol{D}^{-1} \boldsymbol{A}_i(t) - \boldsymbol{G}_i(t)^{\intercal} \boldsymbol{D}^{-1} \boldsymbol{G}_i(t) + 2\nabla_v \left(\boldsymbol{A}_i(t) - \boldsymbol{G}_i(t) \right) \right\} \tag{3.A.2}$$

where we write

$$\boldsymbol{A}_i(t) \equiv \boldsymbol{A}(\boldsymbol{x}_i(t), \boldsymbol{v}_i(t)) \equiv \gamma \boldsymbol{v}_i(t) - \boldsymbol{F}(\boldsymbol{x}_i(t)) \quad \text{and} \quad \boldsymbol{G}_i(t) \equiv \boldsymbol{G}(\boldsymbol{x}_i(t), \boldsymbol{v}_i(t)) \tag{3.A.3}$$

for brevity. The Stratonovich integrand is simply given by

$$\mathbb{B}_i(t) \equiv \frac{1}{2} \left(\boldsymbol{A}_i(t) - \boldsymbol{G}_i(t) \right) \tag{3.A.4}$$

The convergence of this path-weight ratio, Eq. (3.A.1), is guaranteed by the Girsanov theorem, see Ref. [44], stating that the probability measures are absolutely continuous under changes in the drift.

Using the ratio of path weights, we can change the integration in Eq. (3.32) to be with respect to the $\boldsymbol{G}$- altered dynamics. The result of this transformation is

$$\begin{aligned} P^N[\tilde{\rho}, \tilde{\boldsymbol{\mu}}, \mathcal{T}] = \int_{\mathcal{T}} \prod_{i=1}^{N} (\mathcal{D}\Gamma_i) \mathcal{P}^G_{\mathcal{T}}[\Gamma_i] \cdot \prod_{i=1}^{N} \frac{\mathcal{P}_{\mathcal{T}}[\Gamma_i]}{\mathcal{P}^G_{\mathcal{T}}[\Gamma_i]} \\ \cdot \delta\left(\rho[\{\Gamma_i\}, \mathcal{T}] - \tilde{\rho}\right) \delta\left(\boldsymbol{\mu}[\{\Gamma_i\}, \mathcal{T}] - \tilde{\boldsymbol{\mu}}\right) \end{aligned} \tag{3.A.5}$$

In the product of the ratio, Eq. (3.A.1), we can now replace the trajectories piece by piece with the empiric counterparts. First, we analyze the logarithm of the initial weight of the path and insert a delta-function to subsequently

identify the empirical density

$$\sum_{i=1}^{N} \ln \frac{p^{\mathrm{ss}}(\boldsymbol{x}_i(0), \boldsymbol{v}_i(0))}{\rho(\boldsymbol{x}_i(0), \boldsymbol{v}_i(0), 0)} = \int d\boldsymbol{x}d\boldsymbol{v} \ln \frac{p^{\mathrm{ss}}(\boldsymbol{x}, \boldsymbol{v})}{\rho(\boldsymbol{x}, \boldsymbol{v}, 0)} \sum_{i=1}^{N} \delta(\boldsymbol{x}_i(0) - \boldsymbol{x})\delta(\boldsymbol{v}_i(0) - \boldsymbol{v})$$
$$= N \int d\boldsymbol{x}d\boldsymbol{v} \ln \frac{p^{\mathrm{ss}}(\boldsymbol{x}, \boldsymbol{v})}{\rho(\boldsymbol{x}, \boldsymbol{v}, 0)} \rho(\boldsymbol{x}, \boldsymbol{v}, 0) = -NK\left(\rho || p^{\mathrm{ss}}\right) \tag{3.A.6}$$

where $K(\cdot||\cdot)$ in the second line is called the Kullback-Leibler divergence. Analogeously, we can transform the dt integration in the exponent of the path weight as

$$\sum_{i=1}^{N} \int_0^{\mathcal{T}} \mathbb{A}_i(t)dt = \frac{N\mathcal{T}}{4} \int d\boldsymbol{x} \int d\boldsymbol{v} \ \left\{ \boldsymbol{A}^{\intercal}\boldsymbol{D}^{-1}\boldsymbol{A} - \boldsymbol{G}\boldsymbol{D}^{-1}\boldsymbol{G} + 2\nabla_{\boldsymbol{v}} \left(\boldsymbol{A} - \boldsymbol{G}\right) \right\} \rho^N \tag{3.A.7}$$

where we skipped the arguments of $\boldsymbol{A}(\boldsymbol{x}, \boldsymbol{v})$ and $\boldsymbol{G}(\boldsymbol{x}, \boldsymbol{v})$. This can be written in a shorter form using the current that is associated with the empirical density in the respective dynamics. This *associated current* is the microscopic current, Eq. (2.11), with the distribution p replaced by the empirical distribution

$$\boldsymbol{j}_{\boldsymbol{v}}(\boldsymbol{x}, \boldsymbol{v})[\rho] \equiv \boldsymbol{A}(\boldsymbol{x}, \boldsymbol{v})\rho(\boldsymbol{x}, \boldsymbol{v}) + \boldsymbol{D} \cdot \nabla_{\boldsymbol{v}}\rho(\boldsymbol{x}, \boldsymbol{v}) \tag{3.A.8}$$

and, for the altered dynamics,

$$\boldsymbol{j}_{\boldsymbol{v}}^{\boldsymbol{G}}(\boldsymbol{x}, \boldsymbol{v})[\rho] \equiv \boldsymbol{G}(\boldsymbol{x}, \boldsymbol{v})\rho(\boldsymbol{x}, \boldsymbol{v}) + \boldsymbol{D} \cdot \nabla_{\boldsymbol{v}}\rho(\boldsymbol{x}, \boldsymbol{v}) \tag{3.A.9}$$

By this definition, Eq. (3.A.7) can be written as

$$\sum_{i=1}^{N} \int_0^{\mathcal{T}} \mathbb{A}_i(t)dt = \frac{N\mathcal{T}}{4} \int d\boldsymbol{x} \int d\boldsymbol{v} \ \left[\frac{\boldsymbol{j}_{\boldsymbol{v}}[\rho]^{\intercal}\boldsymbol{D}^{-1}\boldsymbol{j}_{\boldsymbol{v}}[\rho]}{\rho(\boldsymbol{x}, \boldsymbol{v})} - \frac{\boldsymbol{j}_{\boldsymbol{v}}^{\boldsymbol{G}}[\rho]^{\intercal}\boldsymbol{D}^{-1}\boldsymbol{j}_{\boldsymbol{v}}^{\boldsymbol{G}}[\rho]}{\rho(\boldsymbol{x}, \boldsymbol{v})} \right]. \tag{3.A.10}$$

Finally, we can transform the Stratonovich part of the path weight ratio using the empirical current

$$\sum_{i=1}^{N} \int_0^{\mathcal{T}} \mathbb{B}_i(t) \circ d\boldsymbol{v}(t) = \frac{N\mathcal{T}}{2} \int d\boldsymbol{x} \int d\boldsymbol{v} \ \left(\boldsymbol{A} - \boldsymbol{G}\right) \boldsymbol{D}^{-1}\boldsymbol{\mu}_{\boldsymbol{v}}^{N}. \tag{3.A.11}$$

In the probability, Eq (3.A.5), the delta distributions fix the empirical densities and current to the desired ones. Consequently, all terms that appeared through the ratio of weights, Eq. (3.A.1) and are now only functionals of the empirical functions can be pulled out of the integral. The remaining integral

$$\int_{\mathcal{T}} \prod_{i=1}^{N} (\mathcal{D}\Gamma_i)\mathcal{P}_{\mathcal{T}}^{G}[\Gamma_i] \ \ \delta\left(\rho[\{\Gamma_i\}, \mathcal{T}] - \tilde{\rho}\right) \delta\left(\boldsymbol{\mu}[\{\Gamma_i\}, \mathcal{T}] - \tilde{\boldsymbol{\mu}}\right) = P_{\boldsymbol{G}}^{N}[\tilde{\rho}, \tilde{\boldsymbol{\mu}}, \mathcal{T}] \tag{3.A.12}$$

is the probability to observe $\tilde{\rho}$ and $\tilde{\boldsymbol{\mu}}$ in the altered dynamics. This probability converges to 1 in the large N limit, since we have chosen the altered dynamics in a fashion that makes the desired functions typical.

Iterating the same steps as described in Ref. [40], the LDF of the probability density $P_{\boldsymbol{G}}^{N}[\tilde{\rho}, \tilde{\boldsymbol{\mu}}, \mathcal{T}]$ can be cast in the obviously positive form that is presented in Eq. (3.37) and infinity if either the continuity equation (3.35) is violated or the current in the deterministic degree of freedom $\tilde{\boldsymbol{\mu}}_x$ does not match the current dictated by the empirical distribution according to Eq. (3.34).

Chapter 4

An underdamped finite time TUR?

In the previous chapter, the overdamped formulation of the finite time TUR was presented along with its proof. In this chapter, we make a first step towards the underdamped regime by naively adopting the notations from the overdamped regime, calculating the uncertainty product $\mathcal{Q}$ and exploring its properties. Even though the TUR has not been proven for underdamped dynamics, we from now on call it a "violation of the TUR" if Eq. (3.45) does not hold.

4.1 Underdamped observables

Naively extending the notations from the original, overdamped TUR, we consider time-integrated observables of the form

$$Y^{(\circ)}(\mathcal{T};\tilde{\boldsymbol{w}}(\boldsymbol{x},\boldsymbol{v})) = \int_{t=0}^{\mathcal{T}} \tilde{\boldsymbol{w}}(\boldsymbol{x}(t),\boldsymbol{v}(t)) \circ d\boldsymbol{x}(t) \tag{4.1.1}$$

where we can replace the Stratonovich integration $\circ\, d\boldsymbol{x}(t)$ with the regular Riemann integration $\boldsymbol{v}(t)dt$ and get the integral

$$Y(\mathcal{T};w(\boldsymbol{x},\boldsymbol{v})) \equiv \int_{0}^{\mathcal{T}} w(\boldsymbol{x}(t),\boldsymbol{v}(t))dt \tag{4.1.2}$$

along the trajectory $(\boldsymbol{x}(t),\boldsymbol{v}(t))$ with weight

$$w(\boldsymbol{x},\boldsymbol{v}) \equiv \tilde{\boldsymbol{w}}(\boldsymbol{x},\boldsymbol{v}) \cdot \boldsymbol{v}. \tag{4.1.3}$$

In analogy to the overdamped results, we for now allow the weight function to depend on all degrees of freedom, especially the velocity. An example for such an observable is the integrated work up to time $\mathcal{T}$, Eq. (2.28), with $w(\boldsymbol{x},\boldsymbol{v}) = \boldsymbol{f}\cdot\boldsymbol{v}$.

For this observable, Eq. (4.1.2), the uncertainty product

$$\mathcal{Q}(\mathcal{T};w(\boldsymbol{x},\boldsymbol{v})) \equiv \frac{\mathrm{Var}[Y(\mathcal{T};w(\boldsymbol{x},\boldsymbol{v}))]}{\langle Y(\mathcal{T};w(\boldsymbol{x},\boldsymbol{v}))\rangle^2}\sigma\mathcal{T} \tag{4.1.4}$$

depends on the weight function as well. It is worth noting that a constant factor in the weight cancels and does, thus, not change the uncertainty product.

4.1.1 Even observables

At this level, there already is a grave difference to the overdamped case. While the observable for which the TUR is proven in the overdamped regime, Eq. (3.47), is guaranteed to be odd under time-reversal, the underdamped analogous Eq. (4.1.2) does not have a clear signature under time-reversal. Depending on the weight function w, the observable can have even, odd and even an inconclusive behavior under time-reversal.

For an observables that is even under time-reversal the TUR is not expected to hold as discussed in Ref. [45]. For such an observable, the time reversed trajectory $(x(\mathcal{T}-t), -v(\mathcal{T}-t))$ of any realization yields the same value as for the original trajectory. As a consequence, the mean $\langle Y \rangle$ does typically not vanish. Even in the equilibrium limit $f \to 0$ the uncertainty ϵ^2 is expected to stay finite while at the same time the entropy production becomes 0. As a result, the uncertainty product $\mathcal{Q}$ approaches 0 for small driving forces. In contrast, for an odd observable the time reversed trajectory contributes the negative value and thus the original and time reversed trajectory cancel in the calculation of the mean when they are equally probable. As a result, the uncertainty diverges in the equilibrium limit for odd observables.

The conceptual difference between time symmetric and antisymmetric observables is not unique to underdamped dynamics. For Markovian jump dynamics the TUR only holds for odd, current-like observables. In such dynamics the precision of even observables, dubbed "traffic" or "frenesy", is not bounded by the entropy production but by the so-called time-symmetric dynamical activity [46]. The fact that the uncertainty approaches 0 for even observables suggest that the same distinction is necessary for underdamped dynamics as well. A TUR in its original form with the uncertainty being solely bound by the entropy production cannot hold for such observables.

This strengthens the presumption that there is a universal physical concept behind the TUR that applies only to observables that are odd under time-reversal. The same might hold for even observables but with a bound that reflects the activity instead of the irreversibility in the spirit of the bounds from Refs. [46, 47].

4.2 Calculating the cumulants for a general observable

With the definition of a generalized observable, Eq. (4.1.2), in the previous section, we can now compute the time evolution of the uncertainty product. To this end, the first and second cumulant are required. While the first cumulant can be calculated from the steady state distribution directly, calculating the second cumulant is more involved. To this end we first calculate the second moment.

The time evolution of the second moment follows the ordinary differential equation

$$\frac{d}{d\mathcal{T}}\langle Y^2\rangle_{\mathcal{T}} = 2\,\langle Y\,w\rangle_{\mathcal{T}}\,. \tag{4.2.1}$$

Here and in the following, the arguments of Y and w are dropped for better readability. The time evolution of the average on the right hand side can, in turn, be calculated using Itô's Lemma. After inserting the Langevin equation (2.7) and using that ensemble averages containing the fluctuating force in first order vanish, we arrive at

$$\begin{aligned}\frac{d}{d\mathcal{T}}\langle Y\,w\rangle_{\mathcal{T}} &= \left\langle w^2\right\rangle_{\mathcal{T}} + \langle Y\,\left(\nabla_x w\right)\boldsymbol{v}\rangle_{\mathcal{T}} \\ &\quad + \frac{1}{m}\,\langle Y\,\left(\nabla_v w\right)\left(\boldsymbol{F}(\boldsymbol{x}) - \gamma\boldsymbol{v}\right)\rangle_{\mathcal{T}} + \frac{T\gamma}{m^2}\,\langle Y\,\Delta_v w\rangle_{\mathcal{T}}\end{aligned} \tag{4.2.2}$$

where $\Delta_v \equiv \sum_i \partial^2/\partial v_i^2$ is the Laplace-operator with respect to the velocity.

4.2.1 Short-time behavior

Although the expression Eq. (4.2.1) seems rather intransparent, it nicely illustrates the impact of inertia. In contrast to overdamped motion where the second moment is constant for all times, the inertia introduces a non-linear time-dependence in the variance of Y for small times. This can be shown by taking the time derivative on both sides of Eq. (4.2.1) and, subsequently, plugging in Eq. (4.2.2). Since Y vanishes for $\mathcal{T} = 0$ by definition, all ensemble averages involving Y vanish as well. Consequently, the variance simplifies to

$$\mathrm{Var}\left[Y(\mathcal{T}; w(\boldsymbol{x},\boldsymbol{v}))\right]_{\mathcal{T}} = \mathrm{Var}\left[w\right]_{\mathcal{T}=0}\mathcal{T}^2 + \mathcal{O}(\mathcal{T}^3) \tag{4.2.3}$$

where the variance on the right hand side can be calculated using the initial PDF. The quadratic dependence on the observation time $\mathcal{T}$ is a result of the deterministic equation of motion for $\boldsymbol{x}$ which results in a ballistic regime for short times. For longer times, the noise gains importance and the velocity decorrelates thus giving rise to the expected linear behavior of the variance.

The ballistic regime in the variance of Y also changes the characteristics of the uncertainty ϵ^2, Eq. (3.44). While in the overdamped limit the uncertainty

scales with $\mathcal{T}^{-1}$ for all times, for underdamped dynamics it is of order one in the ballistic regime. As a result, the uncertainty product generally becomes linear in this regime

$$\mathcal{Q}(\mathcal{T}; w(\boldsymbol{x}, \boldsymbol{v})) = \frac{\mathrm{Var}[w]}{\langle w \rangle^2} \sigma \mathcal{T} + \mathcal{O}(\mathcal{T}^2) \tag{4.2.4}$$

thus violating the overdamped TUR and even approaching 0 in the limit $\mathcal{T} \to 0$. The reported violations of the overdamped TUR for the (odd) particle current in Ref. [45] can be attributed to this ballistic effect.

4.2.2 A bound based on the detailed fluctuation theorem

On first sight, the linear order of $\mathcal{Q}$ in time in the ballistic regime, Eq. (4.2.4) seems to contradict a proof of the overdamped TUR for small times that is solely based on the detailed fluctuation theorem for entropy production [43]. This proof can, however, not be generalized to underdamped motion as the total entropy production does not follow a detailed fluctuation theorem in a non-equilibrium steady state (NESS).

As introduced in Sec. 3.2.2, the entropy production of a certain trajectory $\Gamma_{\mathcal{T}} = \{(\boldsymbol{x}(t), \boldsymbol{v}(t)) | t \in [0, \mathcal{T}]\}$ can be written as

$$\Delta S[\Gamma_{\mathcal{T}}] = \ln \frac{\mathcal{P}[\Gamma_{\mathcal{T}}]}{\mathcal{P}^\dagger[\Gamma^\dagger_{\mathcal{T}}]} \tag{4.2.5}$$

with the time-reversed trajectory $\Gamma^\dagger_{\mathcal{T}} = \{(\boldsymbol{x}(\mathcal{T} - t), -\boldsymbol{v}(\mathcal{T} - t)) | t \in [0, \mathcal{T}]\}$, Eq. (3.13). Since $\mathcal{P}^\dagger \neq \mathcal{P}$ due to the different initial probabilities, a detailed fluctuation theorem follows only for the irreversibility measure $\Delta\Psi[\Gamma_T]$, Eq. (3.17).

In the same way as described in Ref. [43], we can proof a bound on the uncertainty that follows from the DFT for said irreversibility measure. Iterating the same steps results in the following bound on the precision

$$\frac{\mathrm{Var}[Y(\mathcal{T})]}{\langle Y(\mathcal{T}) \rangle^2} \geq \frac{2 - \langle \Delta\Psi(\mathcal{T}) \rangle}{\langle \Delta\Psi(\mathcal{T}) \rangle}. \tag{4.2.6}$$

This bound is valid for non-equilibrium steady states and for all times $\mathcal{T}$. Noteworthy, a similar bound for overdamped diffusion involving the entropy production proofs the TUR for small times and thus raises the question if something similar is possible in the underdamped regime.

The functional $\Delta\Psi$ coincides with the entropy production in the long-time limit where the boundary terms become irrelevant and form the asymptotic DFT, Eq. (3.22). In the short-time limit, however, this irreversibilty measure converges to the finite value

$$\lim_{\mathcal{T} \to 0} \Delta\Psi[\Gamma_{\mathcal{T}}] = \ln \frac{p(\boldsymbol{x}(0), \boldsymbol{v}(0))}{p(\boldsymbol{x}(0), -\boldsymbol{v}(0))} \tag{4.2.7}$$

that involves only the initial distribution.

The different convergence of the irreversibility measure renders the result trivial in both the long-time and the short-time limit. As heat is constantly dissipated in the medium in a NESS, the irreversibility measure $\langle \Delta\Psi(\mathcal{T})\rangle$ grows with time so that the right hand side of Eq. (4.2.6) eventually becomes negative. For large times, the bound thus reduces to a trivial statement. For small times, the mean irreversibility can be calculated by taking the average of Eq. (4.2.7) which can be identified as the Kullback-Leibler divergence between the initial distribution and its v-reflected counterpart. In a NESS, where currents do not vanish, the distribution of v for fixed x becomes asymmetric. As a result, the Kullback-Leibler divergence can grow beyond any value when the driving increases and the right hand side becomes negative, which also renders this bound trivial. Only for small times and near equilibrium the expression on the right hand side of Eq. (4.2.6) becomes non-negative.

Due to the different behavior for small times, the irreversibility bound does not proof that the uncertainty product saturates the TUR for small times. Thus, the observed linear behavior of the uncertainty product for small times does not contradict the bound, Eq. (4.2.6). Apart from that, no universal insight can be gained from the this bound.

4.3 The simplest model: Free diffusion with drift

Although the expression for the time evolution of the second moment, Eq. (4.2.2), in principle allows to derive the TUR for arbitrary dynamics, solving the differential equation is not feasible in a general setting. To gain further insight on the validity of the TUR in underdamped dynamics, we thus consider the arguably simplest underdamped model: one-dimensional free diffusion with drift. That is diffusion described by the Langevin equation dimension

$$\dot{x} = v \qquad m\dot{v} = -\gamma v + f + \xi(t) \tag{4.3.1}$$

with constant force $F(x) = f$. We project the motion in x on a ring with perimeter 2π to get a unique steady state. As before, the initial conditions are sampled from the steady state distribution

$$p^{\mathrm{ss}}(x,v) = \frac{1}{2\pi}\sqrt{\frac{m}{2\pi T}}\exp\left[-\frac{m}{2T}\left(v-\frac{f}{\gamma}\right)^2\right]. \tag{4.3.2}$$

To further simplify we restrict ourselves to the class of observables

$$Y_n(\mathcal{T}; w(x)) \equiv Y(\mathcal{T}; w(x)v^n) = \int_0^{\mathcal{T}} w(x)v^n dt \tag{4.3.3}$$

with an unambiguous symmetry under time-reversal that is defined by the v-order $n \in \mathbb{N}$ of the observable. The subscript n on the uncertainty product

$$\mathcal{Q}_n(\mathcal{T}; w(x)) \equiv \mathcal{Q}(\mathcal{T}; w(x)v^n). \tag{4.3.4}$$

indicates the v-order of the corresponding observable. Since we want to discuss the dependence on the external force, we write $\mathcal{Q}_n^f$ in the following with a superscript f that indicates this parametric dependence.

4.3.1 Evolution of the uncertainty product

By choosing $w(x) = 1$, all moments occurring in the uncertainty product $\mathcal{Q}_n^f(\mathcal{T}; 1)$, Eq. (4.3.4), can be calculated analytically. The first moment of Y_n is simply given by $\langle Y_n(\mathcal{T}; 1)\rangle = \langle v^n\rangle \mathcal{T}$ where the ensemble average can be evaluated using the steady state distribution (4.3.2). The second moment is defined by Eqs. (4.2.1) and (4.2.2). After inserting the corresponding weight $w(x, v) = v^n$, we obtain the time evolution of the second moment as

$$\frac{d}{d\mathcal{T}}\left\langle Y_n^2\right\rangle = 2\left\langle Y_n v^n\right\rangle \tag{4.3.5}$$

$$\begin{aligned}\frac{d}{d\mathcal{T}}\left\langle Y_n v^j\right\rangle &= \left\langle v^{n+j}\right\rangle - \frac{j}{m}\left(\gamma\left\langle Y_n v^j\right\rangle - F_{\text{ext}}\left\langle Y_n v^{j-1}\right\rangle\right) \\ &\quad + j(j-1)\frac{T\gamma}{m^2}\left\langle Y_n v^{j-2}\right\rangle \quad \text{for } 1 \le j \le n\end{aligned} \tag{4.3.6}$$

where we dropped the arguments of Y_n as well as the subscript $\mathcal{T}$ of the ensemble averages for brevity.

This recurrent set of ordinary differential equations can be solved for any power n, beginning with the lowest order $j = 1$, i.e. the correlation $\langle Y_n(\mathcal{T}; 1)v\rangle$. The corresponding integration constants are fixed by the condition that for $\mathcal{T} = 0$ all correlations $\langle Y_n v^j\rangle$ vanish.

We start the analysis with the lowest v-order $n = 1$. In this case, the observable $Y_1(\mathcal{T}; 1)$ corresponds to the distance travelled in time $\mathcal{T}$. The solution of the uncertainty product for free diffusion according to Eqs. (4.3.5) and (4.3.6) takes the form

$$\mathcal{Q}_1^f(\mathcal{T}; 1) = \mathcal{Q}_1^0(\mathcal{T}; 1) = \frac{2}{\tau}(\tau - 1 + \exp[-\tau]) \approx \begin{cases}\tau & \tau \ll 1 \\ 2 & \tau \to \infty\end{cases} \tag{4.3.7}$$

with dimensionless time $\tau \equiv \gamma\mathcal{T}/m$. Interestingly, the uncertainty product does not depend on the force f.

As mentioned in Sec. 4.2.1, the uncertainty product for free diffusion (4.3.7) is linear for small times which is a consequence of the ballistic evolution. For long times it asymptotically approaches 2 from below. Consequently, the

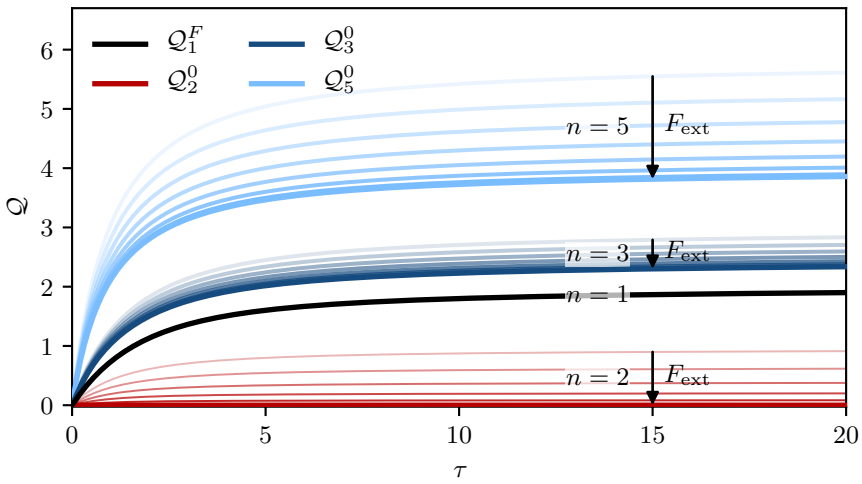

FIGURE 4.3.1: Uncertainty product of free diffusion $\mathcal{Q}_n^f(\mathcal{T};1)$ as defined in equation (4.3.4) for observables of the form $Y_n(\mathcal{T};1)$ (see Eq. (4.3.3)) with $n \in \{1,2,3,5\}$ plotted against dimensionless time $\tau = \gamma\mathcal{T}/m$. The solid lines are the results for different forces f while the colors encode the v-order n. The thick black line is the exact result for $n = 1$ which is independent from the applied force, see Eq. (4.3.7). The thick lines in the $n = 3$ set and $n = 5$ set correspond to the minimized uncertainty product, Eq. (4.3.8) and (4.3.10), respectively. The thick line in the $n = 2$ set corresponds to the limit $f \to 0$ where $\mathcal{Q}_2^0$ is zero for all τ.

overdamped TUR is violated for all finite times. However, if we consider the overdamped limit of (4.3.7) where $\gamma/m \gg 1$ we indeed recover the expected behavior for overdamped free diffusion with the uncertainty product reaching 2 for times $\tau \gg m/\gamma$.

For a higher v-order, the uncertainty product for free diffusion depends on the driving force f with a striking difference for odd and even observables. First, we discuss the odd case. As shown in Fig. 4.3.1, $\mathcal{Q}_3^f$ decreases for $f \to 0$ and eventually converges to a finite limit given by

$$\mathcal{Q}_3^f(\mathcal{T};1) \geq \mathcal{Q}_3^0(\mathcal{T};1) = \frac{2}{\tau}\left(\frac{11}{9}\tau - \frac{29}{27} + e^{-\tau} + \frac{2}{27}e^{-3\tau}\right) \tag{4.3.8}$$

as indicated by the thick line in Fig. 4.3.1.

The minimum of the uncertainty product of free diffusion $\mathcal{Q}_3^0(\mathcal{T};1)$ with an observable of order $n = 3$ has similar properties as the $n = 1$ uncertainty product. In particular, it is linear for small times and converges to a finite

long-time limit

$$\mathcal{Q}_3^0(\mathcal{T};1) \approx \begin{cases} \frac{5}{3}\tau & \tau \ll 1 \\ \frac{22}{9} & \tau \to \infty. \end{cases} \tag{4.3.9}$$

that is, however, larger compared to the $n = 1$ case. The steeper slope for small times and the larger value in the long-time limit compared to $\mathcal{Q}_1^0$ is due to the fact that the higher exponent in the weight increases the contribution of events in the vicinity of the typical value, thus increasing the variance of the observable without influencing its mean as strongly. This effect results in the uncertainty product increasing faster in the ballistic regime and in settling on a higher value in the long-time limit. Consistently, $\mathcal{Q}_3^0$ is larger than $\mathcal{Q}_1^0$ for all times.

The qualitative observations made for the observable scaling with v^3 are valid for the observable $Y_5(\mathcal{T};1)$ with $n = 5$ as well. The bright lines in Fig. 4.3.1 show the uncertainty product over the dimensionless time τ for different forces. Again, a minimum is obtained in the equilibrium limit

$$\begin{aligned} \mathcal{Q}_5^0(\mathcal{T};1) &= \frac{2}{\tau}\left(\frac{449}{225}\tau - \frac{4447}{3375} + e^{-\tau} + \frac{8}{27}e^{-3\tau} + \frac{8}{375}e^{-5\tau}\right) \\ &\approx \begin{cases} \frac{21}{5}\tau & \tau \ll 1 \\ \frac{898}{255} & \tau \to \infty. \end{cases} \end{aligned} \tag{4.3.10}$$

This result for $n = 5$ lies above the uncertainty product for the lower v-orders $\mathcal{Q}_3^0$ and $\mathcal{Q}_1^0$.

As already pointed out in Sec. 4.1.1, a TUR is not expected to hold for even observables. In accordance to the discussion presented earlier, the results for free diffusion look quite different for an even exponent, as plotted exemplary for $n = 2$ in Fig. 4.3.1. The curves settle below 2 in the long-time limit and become smaller for a decreasing driving force. The minimum of the uncertainty product is attained in the equilibrium limit $f \to 0$ where the product is 0 for all times.

4.4 Consequences on a putative underdamped TUR

The results obtained in this chapter show that a TUR is not expected to hold generally in the underdamped regime. Although exemplary in nature, the results for free diffusion allow to identify general constraints on the validity of a putative underdamped TUR.

Overall, the general class of observables introduced in Sec. 4.1 is more versatile than its overdamped analogous. When we allow the weight to depend on all degrees of freedom, including the velocity, there is no definite symmetry under time reversal. However, as for the overdamped case, the original TUR cannot hold for even observables.

Even for odd observables, the TUR does not hold generally as it is inherently broken for short times as a consequence of the inertia, see Sec. 4.2.1. An underdamped uncertainty relation that is valid for all times must capture this regime as well. In other words, the bound on the uncertainty product $\mathcal{Q}$ must depart from 0 and be time-dependent.

The results for free diffusion indicate that a long-time TUR can still exist in its original form. For times larger than the characteristic time $\gamma/m \gg 1$, the uncertainty product approaches 2 and saturates the orignal TUR for a current of first order in v. Such a first order current

$$Y_1(\mathcal{T}; w(x)) = \int_0^T dt w(x(t)) \circ dx(t) \tag{4.4.1}$$

can be interpreted as the rigorous underdamped analogous of the overdamped current, Eq. (3.47). In contrast to observables with higher v-order it is well defined in the overdamped limit. Such first-order observables are highly relevant in stochastic thermodynamics. Examples include the work done on the particle or the distance travelled. A putative TUR is expected to converge to the overdamped TUR for an order-1-current in the appropriate limit.

For currents that display an higher but still odd v-order, the uncertainty product for free diffusion lies above the TUR bound, but does not become tight.

In the following we first focus on the important class of currents with v-order 1 to further assess the validity of a TUR in the underdamped regime. Later, we consider other observables as well.

Chapter 5

The underdamped LDF in one dimension

The LDF takes on an important role in the proof of the overdamped TUR. To discuss the option of generalizing the proof to underdamped dynamics, a better understanding of the LDF is required in this regime. In this chapter we will introduce a method to calculate the LDF for an underdamped particle in a periodic potential and discuss its form. Due to the insights from the previous section, we focus on the long-time limit.

To further simplify the problem, we consider the simplest observable which is the distance traveled in time $\mathcal{T}$

$$Y_1(\mathcal{T};1) = \int_0^{\mathcal{T}} dt v(t) \tag{5.0.1}$$

or, related, the particle current

$$J_1(\mathcal{T};1) \equiv \frac{1}{\mathcal{T}} \int_0^{\mathcal{T}} dt v(t) \tag{5.0.2}$$

It is worth noting that any observable of v-order 1 with periodic weight can be traced back to this observable in the long-time limit since the integrated current is dominated by the number of completeted periods for large times.

5.1 LDF for free diffusion

To make the rather abstract concept of large deviations more applicable, we first calculate the LDF for free diffusion with drift as an example. To this end, we follow the path outlined in Sec. 3.4.2. In more detail we calculate the CFG by finding the largest eigenvalue of the tilted operator and then transform it into the LDF using the Gärtner-Ellis theorem. Finally, we discuss the empirical densities that are associated with the respective fluctuations.

By means of the Gärtner-Ellis theorem, Eq. (3.25), we can calculate the long-time LDF from the CFG that is in turn the largest eigenvalue of the tilted

operator, Eq. (3.4). For the traveled distance, Eq. (5.0.1), the tilted operator is given as

$$\mathcal{L}(\lambda) = -\partial_x v - \partial_v \frac{1}{m}(\gamma v - f) + \frac{D}{m^2}\partial_v^2 + \lambda v. \tag{5.1.1}$$

A right eigenfunction of this tilted operator is given by the shifted Gaussian

$$H_{\mathrm{r}}(\lambda, v) = \exp\left[-\frac{m}{2T}\left(v - \frac{f}{\gamma} - \lambda\frac{T}{\gamma}\right)^2\right]. \tag{5.1.2}$$

The corresponding eigenvalue is

$$\alpha(\lambda) = \frac{T}{\gamma}\left(\lambda + \frac{f}{2T}\right)^2 - \frac{f^2}{4T}. \tag{5.1.3}$$

For $\lambda = 0$ the largest eigenvalue is known to be 0 as is the eigenvalue of the shifted Gaussian. Since the eigenvalue must be continuous in λ, the parabula (5.1.3) indeed corresponds to the largest eigenvalue for all values of λ as required for the CGF. The corresponding left eigenfunction is the exponential function

$$H_{\mathrm{l}}(\lambda, v) = \exp\left[-\lambda\frac{m}{\gamma}v\right] \tag{5.1.4}$$

as can be checked by applying the adjoint tilted operator.

The Legendre-Fenchel transform of the CGF, Eq. (5.1.3), yields the LDF for free diffusion. It also has the form of a parabula

$$I^{\mathcal{T}}(J) = \frac{\gamma}{4T}\left(J - \frac{f}{\gamma}\right)^2 \tag{5.1.5}$$

where J is a certain realization for the mean velocity $J_1(\mathcal{T};1)$. As discussed in Section 3.4, the probability collapses on the unique steady-state value $J^{\mathrm{ss}} = \langle v\rangle = f/\gamma$ and thus the LDF vanishes at this particular point. Furthermore, the LDF reflects the symmetry introduced by the asymptotic DFT, Eq. (3.22). Since the observable $J_1(\mathcal{T};1)$ is proportional to the medium entropy production by means of Eq (2.36), we can apply the DFT to the distribution $P(J,\mathcal{T})$ for large times and derive the symmetry

$$\begin{aligned} I^{\mathcal{T}}(-J) &= \lim_{\mathcal{T}\to\infty}\frac{1}{\mathcal{T}}\ln P(-J\mathcal{T},\mathcal{T}) \\ &= \lim_{\mathcal{T}\to\infty}\frac{1}{\mathcal{T}}\ln e^{\mathcal{T}fJ/T}P(J\mathcal{T},\mathcal{T}) = I^{\mathcal{T}}(J) + \frac{fJ}{T}. \end{aligned} \tag{5.1.6}$$

We can further visualize the fluctuations by evaluating the typical distributions associated with a specific tilting λ or value J. This typical distribution is the product of the left and right eigenfunction, Eqs. (5.1.2) and (5.1.4)

respectivelly. After appropriate normalization, the typical distribution for given tilting λ becomes the Gaussian distribution

$$\rho_{\text{typ}}(v,\lambda) = \sqrt{\frac{m}{2\pi T}} \exp\left[-\frac{m}{2T}\left(v - \frac{f}{\gamma} - 2\lambda\frac{T}{\gamma}\right)^2\right] \tag{5.1.7}$$

which generates the mean velocity

$$J[\rho_{\text{typ}}(\lambda,v)] = \int dv \rho_{\text{typ}}(\lambda,v) v = \frac{f}{\gamma} + 2\lambda\frac{T}{\gamma}. \tag{5.1.8}$$

By inverting the expression for the mean velocity with respect to λ we find the tilting that is associated with a specific fluctuation $\tilde{J}$ which in turn allows to express the empirical distribution with respect to the desired current $\tilde{J}$ as

$$\rho(v,\tilde{J}) = \sqrt{\frac{m}{2\pi T}} \exp\left[-\frac{m}{2T}\left(v - \tilde{J}\right)^2\right]. \tag{5.1.9}$$

Hence, the empirical distribution for a specific fluctuation $\tilde{J}$ is the steady state distribution but with the mean shifted. Microscopically, a non-stationary current is realized by the noise consistently pushing the particle in a specific direction, just like an increased non-conservative force would.

5.2 LDF in a periodic potential

In presence of a periodic potential, we can follow the same path as outlined in Sec. 5.1. The tilted operator

$$\mathcal{L}(\lambda) = -\partial_x v - \partial_v \frac{1}{m}\left(\gamma v - F(x)\right) + \frac{D}{m^2}\partial_v^2 + \lambda v \tag{5.2.1}$$

then contains the periodic force $F(x) = F(2\pi x)$ with appropriate rescaling of the position x to normalize the periodicity.

5.2.1 Symmetry of the CGF

The tilted operator satisfies an identity [48] that on the level of the cumulant generating function manifests itself in the so-called *Gallavotti-Cohen symmetry* [49]

$$\alpha(\lambda) = \alpha(-\lambda - f/T) \tag{5.2.2}$$

which reflects the asymptotic DFT as proven before, Eq. (3.22). Moreover, it relates the corresponding left and right eigenfunctions as [48]

$$H_{\text{l}}(x,v,\lambda) = e^{E(x,v)/T} H_{\text{r}}(x,-v,-\lambda - f/T). \tag{5.2.3}$$

with the energy

$$E(x,v) \equiv \frac{1}{2}mv^2 + V(x). \tag{5.2.4}$$

For the tilting $\lambda = -f/T$, the symmetry of the eigenfunctions can be expressed as a symmetry of the typical density

$$\rho_{\text{typ}}(x,v,-f/T) = p^{\text{ss}}(x,-v). \tag{5.2.5}$$

In other words, the stationary density flipped in the velocity is associated with producing the negative of the stationary velocity.

5.2.2 A numerically convenient expansion

In order to numerically calculate the eigenvalue, we discretize the operator $\mathcal{L}(\lambda)$. Inspired by previous work considering steady state distributions [28, 50], we expand the right eigenfunction basis of the tilted operator (5.2.1) in a Fourier-Hermite basis

$$r_p^n(x,v) \equiv \frac{\sqrt{T}}{2\pi R\sqrt{m}} e^{inx/R}\phi_0(v)\phi_p(v), \tag{5.2.6}$$

consisting of Fourier modes in x and Hermite functions $\phi_p(v)$ in v. The Hermite functions are defined as

$$\begin{aligned}\phi_p(v) &\equiv \frac{(-1)^p}{\sqrt{2^p p!\sqrt{\pi}}}\left(\frac{m}{T}\right)^{\frac{p}{2}} e^{mv^2/(4T)}\frac{\mathrm{d}^p}{\mathrm{d}v^p}e^{-mv^2/(2T)} \\ &\equiv He_p(v)\frac{1}{\sqrt{2^p p!\sqrt{\pi}}}e^{-mv^2/(2T)}\end{aligned} \tag{5.2.7}$$

where the second line introduces the Hermite polynomials $He_p(v)$. For the left eigenfunction, we use the basis

$$l_p^n(x,v) \equiv \frac{1}{\sqrt{2^p p!\sqrt{\pi}}}e^{inx/R}He_p(v) \tag{5.2.8}$$

with Hermite polynomials $He_p(v)$ instead of Hermite functions. This has the advantage that the left eigenfunction 1 for $\lambda = 0$ can be trivially represented using only the zeroth order Hermite polynomial. The basis vectors $l_p(x,v)$ and $r_p(x,v)$ are orthogonal and normalised, such that the matrix elements of the tilted operator are given by the integral

$$\mathcal{L}(\lambda)_{pp'}^{nn'} = \int_0^{2\pi} dx \int_{-\infty}^{\infty} dv \;\; l_p^n(x,v)\mathcal{L}(\lambda)r_{p'}^n(x,v). \tag{5.2.9}$$

Since the v-derivatives and -factors in the tilted operator only cause an index shift of the right basis vectors, most of the matrix elements vanish. As a result, $\mathcal{L}(\lambda)$ becomes a tridiagonal block matrix with entries

$$\begin{aligned}\boldsymbol{\mathcal{L}}(\lambda)_{pp'} = &- \sqrt{p}\left(\hat{\mathbf{D}} - \lambda\sqrt{\frac{T}{m}}\boldsymbol{I}\right)\delta_{p-1,p'} - p\frac{\gamma}{m}\delta_{p,p'} \\ &- \sqrt{p+1}\left(\mathbf{D} - \lambda\sqrt{\frac{T}{m}}\boldsymbol{I}\right)\delta_{p+1,p'}\end{aligned} \tag{5.2.10}$$

with the identity matrix $\boldsymbol{I}$ and the matrices

$$\hat{\mathsf{D}}_{nn'} \equiv \left(\delta_{n,n'}\left(inT - F_{\text{ext}}\right) + \tilde{F}_{nn'}\right)/\sqrt{Tm} \tag{5.2.11}$$

$$\mathsf{D}_{nn'} \equiv in\delta_{n,n'}\sqrt{T/m} \tag{5.2.12}$$

where

$$\tilde{F}_{nn'} \equiv \int_0^{2\pi} dx\, e^{i(n'-n)x}V'(x) \tag{5.2.13}$$

is the Fourier transform matrix of the potential force acting on the particle.

For the simple case of a cosine potential

$$V(x) = V_0\cos(x), \tag{5.2.14}$$

the Fourier transformation yields

$$\tilde{F}_{nn'} = \frac{iV_0}{2}\left(\delta_{n,n'-1} - \delta_{n,n'+1}\right). \tag{5.2.15}$$

The same expression for the discretized tilted operator (5.2.10) has also been derived in the context of Josephson junctions using a slightly different approach in [51].

5.3 Numerical case study in a periodic potential

Using the discretized version of the tilted operator, Eq. (5.2.10), both the CGF and the LDF can be evaluated numerically. The eigenvalues and eigenfunctions of the truncated operator can be evaluated for an arbitrary value of λ using standard methods as long as the influence of higher modes decays sufficiently fast. For underdamped dynamics in a cosine potential, Eq. (5.2.14), using 64 Hermite modes and Fourier modes in the range of $-80 \leq n \leq 80$ proved to be suitable for moderate values of γ and m. Solving the eigenproblem for the resulting matrix with roughly $10\,000 \times 10\,000$ is still feasible on standard hardware. To probe into the extremely underdamped regime where $m/\gamma \gg 1$ the v-dependence becomes more complicated so that especially the number of Hermite modes must be increased.

To further shorten the computation time, we can employ the Gallavotti-Cohen symmetry (5.2.2) of the generating function and restrict ourselves to $\lambda \geq -f/2T$.

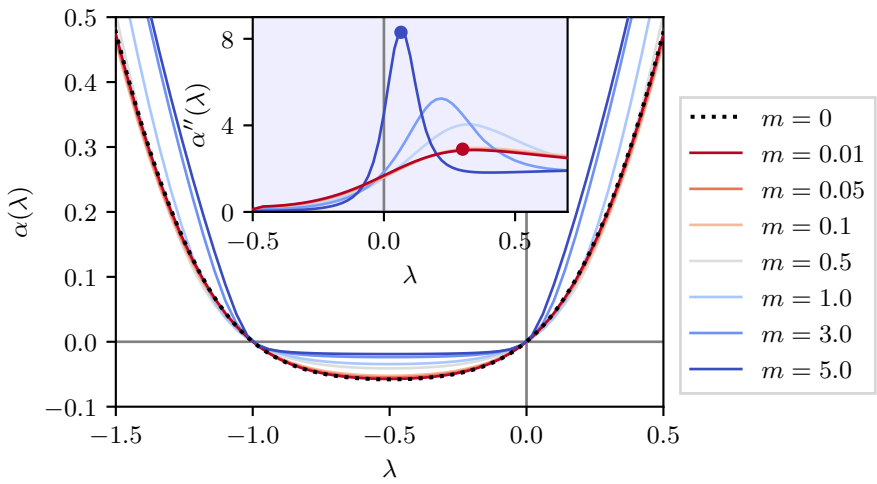

FIGURE 5.3.1: Generating function $\alpha(\lambda)$ for the particle current in a cosine potential for different masses with $T = 1$, $\gamma = 1$ and $V_0 = 2$, $f = 1$. The second derivative is shown in the inset, with the points of largest curvature marked by coloured dots.

5.3.1 Two different modes of transport

Figure 5.3.1 shows the generating function for three different masses with $T = 1$ and an intermediate driving force $f = 1$ with respect to the potential barrier of amplitude $V_0 = 2$.

In contrast to the CGF for free diffusion, see Eq. (5.1.3), the potential introduces a pronounced plateau around the center of symmetry with significantly reduced curvature. This has already been reported for overdamped motion [52]. Away from this plateau, the generating function converges towards a parabola with the characteristics of free diffusion, in particular the curvature matches free diffusion $\alpha''(\lambda) = 2D$ for $|\lambda| \gg 0$ with the bare diffusion coefficient $D \equiv T/\gamma$.

The two regimes of the generating function can be associated with different properties of the typical distributions $\rho_{\text{typ}}(x, v, \lambda)$ as shown in figure 5.3.2. For the center of symmetry $\lambda = -f/2$, shown in the first column, the typical distribution is symmetrical in v as evident from Eq. (5.2.3). The mean particle current associated with this distribution vanishes. In the vicinity of this value of λ, the distributions of the velocity are approximately Gaussian with mean close to zero for all x. Along the x direction the densities show a local maximum at approximately π. Around $x = 0$, on the other hand, the probability is close to zero. The trajectories producing this phase-space density can be imagined as "locked in" by the potential landscape. They rarely cross the potential barrier. When the distributions for small and high mass in the first column of Fig. 5.3.2 are compared, they show only minor differences.

As the tilting parameter λ increases to larger values, the particle flux increases as well, which gives rise to stripes of elevated probability spreading over the complete x range as shown in the third column. These stripes correspond to "running" trajectories that can overcome the potential barrier. Even though these stripes occur at large tilting for both large and small masses, they show a mass-dependent characteristic. For large mass, the stripes tightly follow the contour lines of the internal energy $E(x, v)$. This behaviour is due to the fact that the noise intensity in v scales like $1/m$, leading to only small deviations from deterministic trajectories for large mass.

For small mass, in contrast, the probability distribution resembles a Gaussian distribution in v with little dependence on x similar to free diffusion. In this regime, the relaxation time becomes small thus inhibiting the memory effects of energy conservation. In the overdamped limit $m/\gamma \to 0$, the relaxation time vanishes. Through the arising time-scale separation the distribution in v becomes independent from its energy at a previous time thus becoming a Gaussian that only reflects the local mean speed. Furthermore, the small mass increases the noise intensity on v and broadens the distributions. With respect to the width of the local distribution in v, the variation in local mean speed becomes small. Consequently, the distributions shown in Fig. 5.3.2 seem flat in x.

In an intermediate regime the typical densities display both characteristics, a "running" stripe and the "locked" local maximum around $v = 0$, corresponding to "running" and "locked" parts of trajectories, respectively. The value of λ in this intermediate regime coincides with the position λ_c of the maximum in the second derivative of the generating function, marked with dots in the inset of figure 5.3.1. This point marks the transition from the flat plateau to the quadratic regime. The plateau of the generating function is consequently bound between $-\lambda_c - f/T$ and λ_c.

With increasing mass, the inertia increases and the motion becomes less prone to the noise thus stabilizing the respective solutions. Consistently, the plateau associated with the "locked" solutions becomes flatter. In addition, the intermediate regime becomes narrower, leading to a larger second derivative of the generating function around $-\lambda_c - f/T$ and λ_c.

5.3.2 Manifestation of the different regimes in the LDF

The LDF for the presented generating functions can be calculated via Legendre-Fenchel transformation, see Eq. (3.25). The results are plotted in Fig. 5.3.3.

For different masses, the typical current J^{ss} shifts as the inertia allows to surpass energy barriers more easily. The change of the mean speed with respect to the mass has been discussed and characterized intensively, for instance in Ref. [28].

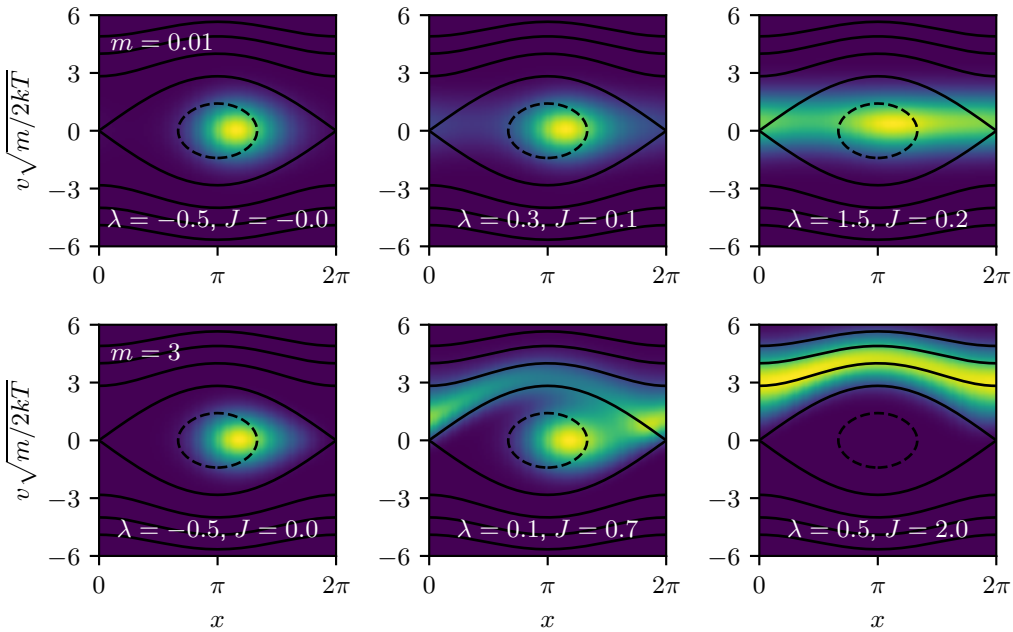

FIGURE 5.3.2: Typical densities for small mass $m = 0.01$ (top row) and large mass $m = 3$ (bottom row) with $T = 1$, $\gamma = 1$ and $V_0 = 2$. Darker colors depict small probability densities. The tilting λ of the operator (5.2.1) and with it the empirical current J is varied along the columns as specified at the bottom of each plot. The first column corresponds to the state with vanishing current $J = 0$. The contour lines of the energy landscape are plotted as black lines.

In the limit of both small and large mass the LDF seems to converge to limiting functions. In the limit of small masses, the exact overdamped LDF is reproduced. For large masses, the LDF becomes quadratic for large empirical currents with a pronounced plateau between 0 and the stationary current J^{s}. This degeneration of the minimum of the LDF and divergence of the variance is a consequence of the bistability in the deterministic limit. Dependent on the initial condition, the particle can either escape the potential or is tied to its minimum.

The plateau of the generating function translates to a kink in the LDF at $J = 0$, which becomes sharper when the second derivative at λ_{c} becomes larger. Such a kink in the LDF is a common feature and has been observed and discussed in a wide variety of systems such as models describing driven overdamped systems [53] and molecular motors [54]. In some cases, the kink in the LDF has been attributed to intermittent or flashing states [55, 56]. In the underdamped system, the bistability between "running" and "locked" dynamics causes such an intermittence [50].

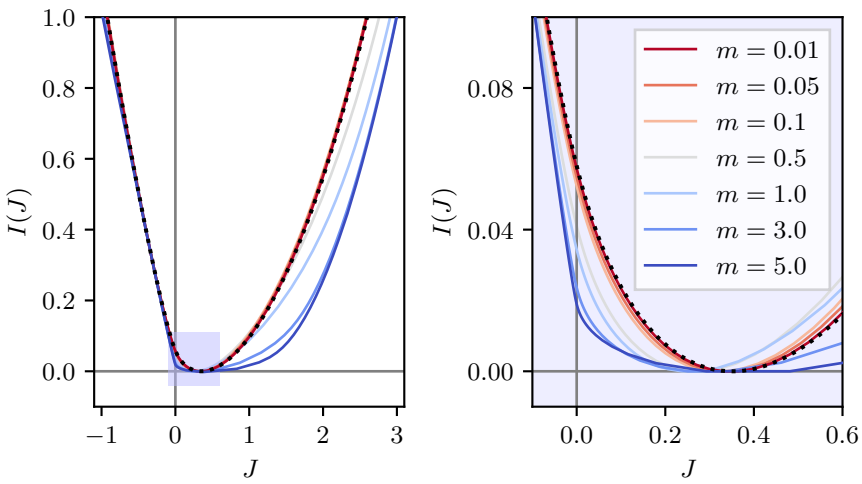

FIGURE 5.3.3: Large deviation function $I(J)$ for the CGFs shown in Fig. 5.3.3. The right panel shows the LDF in the vicinity of the vanishing and most probable current as highlighted on the left hand side.

The sharpening of the kink for increasing mass at $J = 0$, displayed in the right panel of Fig. 5.3.3, can be interpreted as a tightening regime of intermittent states. This is due to the fact that a particle with larger inertia survives longer in a running state compared to a lighter particle. Hence, the intermittent switching between running and trapped trajectories becomes more sensitive for the tilting λ for large masses.

As mentioned before, the inverse of the second derivative at the minimum of the LDF corresponds to the variance for the current J. The sharpening kink at $J = 0$ thus has an indirect impact on the decreasing curvature as shown in the right panel of Fig. 5.3.3. The, in turn, increased effective diffusion for intermittent trajectories suggests that the phenomenon of *enhanced* or *giant diffusion* originally reported for overdamped dynamics [57] is interlinked with a sharpening of the kink. The maximal diffusion is observed, when locked and running trajectories with a different typical current have a comparable influence on the motion. In terms of the CGF, the maximum of the second derivative then is located near $\lambda = 0$ and enhances the diffusion. Since changes between the different regimes of motion are mediated by diffusive effects, the effect of such effects can be enhanced significantly if the different modes of motion are stable and display a small relaxation time.

As a side note, extreme fluctuations have also observed in bistable models for active matter [58] or biochemical oscillators [59]. As for the periodic system discussed here, the diffusion coefficient increases when the individual modes become more stable. This is, however, only observed when there

is a different mean contribution to the observable for the modes, i.e. a different mean rate. In this sense enhanced diffusion is a sign for distinct modes contributing to the observable. The empirical distribution could be used to identify and characterize the involved modes of motion in such systems.

5.4 Qualitative reconstruction of the LDF via Bounds

In the previous section the LDF has been evaluated for an exemplary driven system. The qualitative discussion outlined features of the LDF and how they reflect in the typical densities. In this chapter, these observations are put on a broader foundation by bounds that approximate the behavior of the LDF. To this end, we mime the observed form of the empirical densitites in the respective regimes and make suitable ansatzes to derive bounds by means of the contraction principle (3.43).

An overview with all bounds and the appropriate regimes where the bounds become suitable is presented in Fig. 5.4.1.

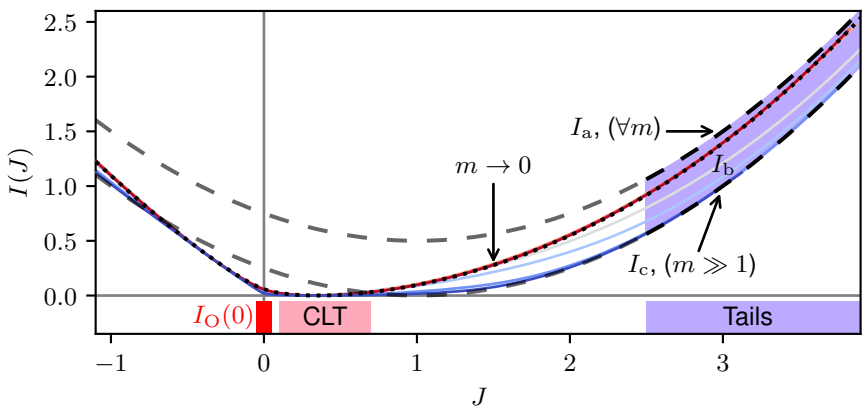

FIGURE 5.4.1: Overview of all bounds on the underdamped LDF derived in this section. The solid lines are the same LDFs as plotted in Fig. 5.3.3. The dashed lines depict the bounds I_a, Eq. (5.4.4) and I_c, Eq. (5.4.12). For typical events, in the vicinity of the stationary current J^{ss}, the LDFs are governed by the central limit theorem (CLT). In the tail of the LDF for rare events, the asymptotic bound I_a imposes a bound for arbitrary mass. It can be refined for specific mass using I_b, Eq. (5.4.11). In the limit $m \to \infty$, I_c forms an upper bound. Finally, for $J = 0$ the LDF is bounded from above by the corresponding overdamped LDF as described in Sec. 5.4.3. The ansatz also describes the transition to the overdamped regime as indicated by the dotted line.

5.4.1 A master ansatz

The constraints of the empirical current, Eq. (3.39) in the underdamped functional LDF, poses two challenges for finding analytical bounds on the LDF. First, the mean current associated with the ansatz must be known as otherwise it is not possible to reconstruct the LDF with respect to this observable. Second, to get an analytical bound the empirical current associated with a given density must also be expressable analytically.

A versatile ansatz that meets this requirement is the function

$$\begin{aligned}\rho(x,v;\tilde{J}) &= \rho(x)\sqrt{\frac{m}{2\pi T}}\exp\left[-\frac{m}{2T}\left(v-\frac{\tilde{J}}{2\pi R\rho(x)}\right)^2\right] \\ &\equiv \rho(x)\hat{\rho}(x,v;\tilde{J})\end{aligned} \tag{5.4.1}$$

with an arbitrary normalized distribution $\rho(x)$. This function corresponds to a Gaussian distribution for fixed x. The variance of the distribution matches the equilibrium distribution of the velocity, but the center is shifted to $\tilde{J}/(2\pi\rho(x))$. By construction, the mean current $J[\rho]$ is equal to $\tilde{J}$. The advantage of the ansatz is that the associated empirical current $\mu_v^\rho(x,v;\tilde{J})$ can be cast in the closed form

$$\mu_v^\rho(x,v;\tilde{J}) = \rho'(x)\hat{\rho}(x,v)\left[\frac{T}{m}-\frac{\tilde{J}v}{2\pi R\rho(x)}\right]. \tag{5.4.2}$$

Plugging these terms in the functional LDF (3.37) in the long-time limit with still undetermined distribution $\rho(x)$ yields, after some simplifications, the somewhat lengthy master bound

$$\begin{aligned}I(\tilde{J}) \leq I_{\mathrm{M}}(\tilde{J}) \equiv \min_{\rho(x)} \frac{1}{4\gamma T}\int dx \Bigg\{ &\frac{1}{\rho(x)}\left[T\rho'(x)-F(x)\rho(x)+\gamma\frac{\tilde{J}}{2\pi}\right]^2 \\ &+ m\left(\frac{\tilde{J}}{2\pi}\right)^2\frac{\rho'(x)}{\rho(x)^3}\left[2\rho(x)F(x)-T\rho'(x)\right] \\ &+m^2\left(\frac{\tilde{J}}{2\pi R}\right)^4\frac{\rho'(x)^2}{\rho(x)^5}\Bigg\}.\end{aligned} \tag{5.4.3}$$

In the following, we discuss some special realizations and implications of this bound.

5.4.2 Overdamped asymptotic bound

The simplest realization of the ansatz (5.4.1) is obtained with an uniform distribution $\rho(x) = 1/2\pi$. The resulting distribution is just a shifted Gaussian as encountered for free diffusion, see Eq. (5.1.9). Furthermore, such a distribution can be recognized in the periodic potential for small mass and large

currents (see the upper row in Fig. (5.3.2)). Consequently, the ansatz is expected to be a suitable approximation in the tails of the LDF for small mass, albeit forming an upper bound for all masses.

Since $\rho(x)$ is flat, the first derivative vanishes as well as the associated current (5.4.2). This renders most of the terms in $I_{\mathrm{M}}(J)$ zero. For an arbitrary potential, the corresponding bound I_{a} reads

$$I(\tilde{J}) \leq I_{\mathrm{M}}(\tilde{J}) \leq I_{\mathrm{a}}(\tilde{J}) \equiv \frac{\gamma}{4T}\left(J - \frac{f}{\gamma}\right)^2 + \frac{1}{4T\gamma}\left\langle V'(x)^2\right\rangle_\rho \tag{5.4.4}$$

where the last average is an integral over the flat distribution $\rho(x)$. Interestingly, the bound is independent of the mass m.

The bound is plotted in Fig. 5.4.1. As expected, it becomes tight for $m \to 0$ in the tails of the LDF. For larger masses, however, there is an offset between the bound and the LDFs. This discrepancy implies that strongly directed realizations for large masses behave differently. Since it has the same form as the asymptotic bound reported in [52] for the overdamped limit, the bound can be considered a generalization of said bound that is valid for arbitrary underdamped (and overdamped) processes.

5.4.3 LDF in the overdamped limit

The underdamped LDF converges to the overdamped LDF in the limit of small masses, as can be observed in Fig. 5.3.2. In this section, we examine how the typical distribution behaves in this limit. In particular, we are driven by the question of how the two-dimensional empirical density reduces to effectively one-dimensional ones.

Interestingly the master bound, Eq. (5.4.3), converges to the apparent overdamped contraction

$$I_{\mathrm{O}}(\tilde{J}) = \min_{\rho(x)} \frac{1}{4T\gamma}\int dx\, \left[\gamma\frac{\tilde{J}}{2\pi} - (F(x) - T\partial_x)\rho(x)\right]^2 / \rho(x). \tag{5.4.5}$$

for $m \to 0$. In fact this is the contraction for the overdamped analogous of this system, where the empirical current μ is a scalar and fixed to $\tilde{J}$ by the condition of the contraction. The density ansatz (5.4.1) with the optimal empirical distribution $\rho(x)$ then represents the exact phase space density in the limit $m \to 0$.

In this sense the master ansatz governs the transition from a level 2 LDF in the underdamped case to the overdamped level 2.5 LDF. As outlined in Sec. 2.1.4, the velocity becomes a fast variable in the overdamped limit and thus relaxes instantly on the timescale of the spatial motion. As a consequence, there is no memory effect for the velocity and it relaxes in the local "equilibrium" that is a Gaussian with the appropriate mean velocity at that

particular point. For arbitrary mass a more involved coupling between the velocity and position is expected due to the finite relaxation time of the velocity. As this, in general, exceeds the possibilities of the master ansatz, a true two-dimensional ansatz is required for the exact underdamped LDF.

Beyond the master ansatz governing the transition to overdamped dynamics, it imposes an upper bound to the LDF at $\tilde{J} = 0$. Here, all terms involving the mass in the bound $I_{\mathrm{M}}(\tilde{J})$, Eq. (5.4.3), vanish and the overdamped contraction is retrieved directly. As a result, the stalled large deviation function can be bound as

$$I(0) \leq I_{\mathrm{O}}(0) = \lim_{m \to 0} I(0). \tag{5.4.6}$$

In other words, its more likely for an underdamped particle to observe a vanishing current compared to a overdamped particle with the same friction coefficient and temperature. This behavior is plotted in the inset of figure (5.3.2).

From this bound at $\tilde{J} = 0$ one can motivate the validity of the TUR for the particle current in the linear response regime. In this regime, a small force ϵf drives the system out of equilibrium which leads to small stationary current J^{ss} in the order of ϵ. As a consequence the stalled state is in the vicinity of the regime of the central limit theorem. The curvature of the parabula is limited through Eq. (5.4.6) by the overdamped curvature and in turn by means of the TUR. A rigorous proof for higher dimensions and arbitrary forces is provided in Refs. [60, 61] as long as the time-reversal symmetry is not broken.

5.4.4 Underdamped asymptotic bound

Although designed as an asymptotic bound, $I_{\mathrm{a}}(\tilde{J})$ in Eq. (5.4.4) is not saturated by the LDF in the tails for large mass, as shown in Fig. 5.3.2. In this limit, the impact of thermal noise on the velocity is marginal. As a result, we observe approximate energy conservation, leading to trajectories that mainly follow the contour lines of the internal energy $E(x, v)$. The marginalized probability in x, i.e. the mean time spent at a certain position x, is proportional to the inverse mean velocity at this position. Following this rationale we make the ansatz

$$\rho(x, v; E) = \frac{\sqrt{m/(2\pi T)}}{N(E)\bar{v}(x; E)} \exp\left[-\frac{m}{2T}\left(v - \bar{v}(x; E)\right)^2\right], \tag{5.4.7}$$

where $\bar{v}(x; E)$ is the local mean velocity and follows the contour line of the internal energy with suitably large level E

$$\bar{v}(x; E) = \sqrt{\frac{2}{m}\left(E - V(x) + V(0)\right)}, \tag{5.4.8}$$

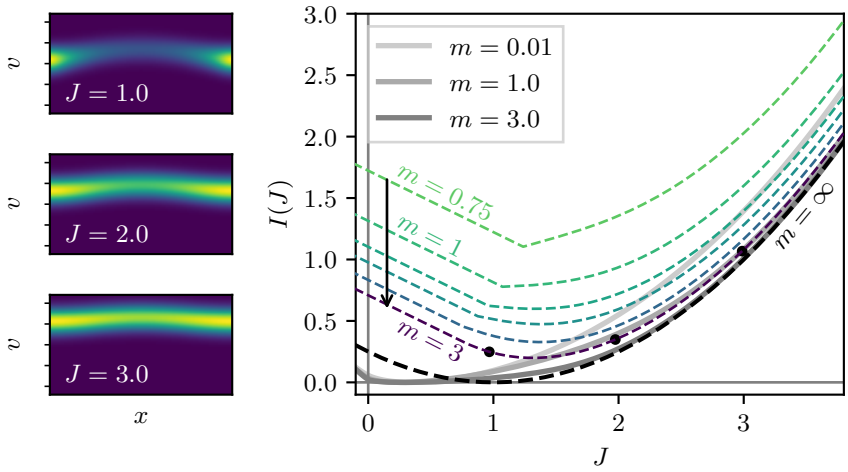

FIGURE 5.4.2: Illustration of the bound I_b, Eq. (5.4.11), in a cosine potential for different masses $m = [0.75, 1, 1.25, 1.5, 2, 3]$ from top to bottom. Plotted as thick grey line are exemplarily LDFs for three masses (see legend). The black dashed line corresponds to the limit $m \to \infty$ or bound I_c, Eq. (5.4.12). The further parameters are $\gamma = 1$, $V_0 = 2$, $f = 1$, $T = 1$.

and N is the normalisation

$$N(E) = \int dx\, \bar{v}(x;E)^{-1}. \tag{5.4.9}$$

The idea of the ansatz, Eq. (5.4.7), can be cast in the form of the master ansatz, Eq. (5.4.1), with

$$\rho(x;E) = \frac{1}{N(E)\bar{v}(x;E)} \quad , \quad J(E) = \frac{2\pi}{N(E)} \tag{5.4.10}$$

for E sufficiently large overcome the potential barriers. Using these terms as trial function for the minimization in Eq. (5.4.3) gives the bound

$$\begin{aligned} &I(J(E)) \leq I_M(J(E)) \leq I_b(J(E)) \\ &\equiv \frac{1}{4T\gamma N(E)} \int dx \left\{ \frac{1}{\bar{v}(x;E)} \left(F - \gamma \bar{v}(x;E)\right)^2 + \frac{T}{m} \frac{V'(x)^2}{\bar{v}(x;E)^3} \left(\frac{T}{m\bar{v}(x;E)^2} + 1 \right) \right\} \end{aligned} \tag{5.4.11}$$

for $E \geq \max_x(V(x) - V(0))$. The mirrored side follows from the symetry of the LDF, Eq. (5.1.6).

In principle this expression can be evaluated for arbitrary masses using numerical integration schemes. Fig. 5.4.2 shows the bound for some selected masses. Although the bound cannot be evaluated when $\bar{v}(x;E)$ becomes imaginary, the convex hull of the bound is still a bound. The intervals where

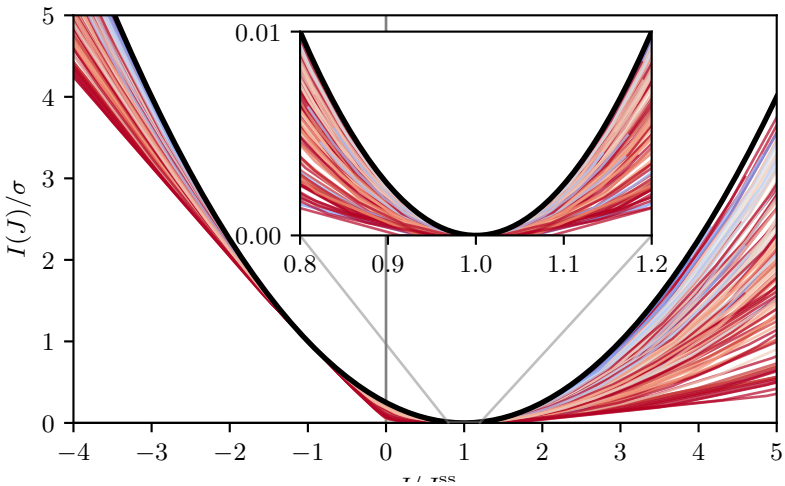

FIGURE 5.5.1: Rescaled LDF for 100 randomly selected parameters and potentials consisting of 5 cosine modes also chosen at random. The black curve corresponds to the parabolic bound that implies the TUR, Eq. (5.5.2).

the energy is to low stand out through linear parts in the bounds shown in Fig. 5.4.2.

In the limit $m \to \infty$ with $J(E)$ kept fix the bound reduces to the simpler expression

$$\lim_{m\to\infty} I\left(\tilde{J}\right) \leq \lim_{m\to\infty} I_{\mathrm{b}}\left(\tilde{J}\right) = \frac{\gamma}{4T}\left(\tilde{J} - \frac{f}{\gamma}\right)^2 \equiv I_{\mathrm{c}}(\tilde{J}), \tag{5.4.12}$$

due to the energy E scaling linearly in m and $\bar{v}(x;E)$ becoming independent of x. This parabolic function coincides with the exact LDF for free diffusion, Eq. (5.1.5). Moreover, the typical densities obtained for free diffusion, Eq. (5.1.9), can be retrieved from Eq. (5.4.7) by setting the potential to 0.

The quality of the underdamped asymptotic bound as an approximation of the actual LDF in the limit of large mass can be appreciated in figure 5.3.2. For an intermediate mass of $m = 3$, the bound $I_{\mathrm{c}}(\tilde{J})$ already matches the tails of the LDF. In this regime, the ansatz (5.4.7) describes well the typical distributions resulting from running trajectories with high energy that have only small modulations in the velocity.

5.5 A parabolic bound on the LDF?

One of the more practical aspects of the LDF is its role in the proof of the overdamped TUR. It follows from a parabolic upper bound on the LDF that coincides with the free diffusion LDF derived earlier. In this section we will

asses the validity of this bound for underdamped dynamics using numerical simulations.

Using the numerical procedure described in Sec. 5.2, we can go beyond the single cosine potential that has been considered in the previous section and expand arbitrary potentials in Fourier-modes. To randomly sample different potentials, we select 5 amplitudes c_n in the interval $[-1/2, 1/2]$ and construct the potential as

$$V(x) = \sum_{n=1}^{5} c_n \cos(2\pi n x). \tag{5.5.1}$$

The system parameters for mass, temperature and friction are also randomly generated for each run. Depending on the overall height of the potential and the other parameters the constant force of $f = 1$ covers the range from systems that are almost locked (10 % of the free diffusion current) and "running" parameters with J^{ss} at over 90 % of the average current without potential.

Fig. 5.5.1 shows the rescaled LDF for 100 sampled parameter sets. The solid black line corresponds to the parabolic bound on the overdamped LDF, (3.55),

$$I^{\mathrm{TUR}}(\tilde{J}) = \frac{\sigma}{4}\left(1 - \frac{\tilde{J}}{J^{\mathrm{ss}}}\right). \tag{5.5.2}$$

For the considered parameters no violation of the parabolic bound can be observed both in the typical regime and for rare events in the tails of the LDF. This result gives further credence to the validity of the TUR in underdamped dynamics but also to the existence of a parabolic bound that implies said relation.

5.6 Conclusion

In principle, the form of the LDF for underdamped dynamics is similar to that of an overdamped particle in a periodic potential. In both cases a crossover from "locked" to "running" trajectories can be observed that is accompanied by a kink in the LDF, a pronounced plateau in the CGF, respectively. Differences do, however, stand out when the empirical densities are compared. While the distributions are relatively flat in x and show a Gaussian behavior in v in the overdamped dynamics, they follow the isolines of the energy when the inertia comes into play.

The derived bounds provide further insight in the LDF. The asymptotic bounds I_{a} for arbitrary mass and its refinement I_{b} capture the discussed differences of empirical distributions from the overdamped to the underdamped regime. Furthermore, the overdamped bound I_{O} illustrates how the transition to the overdamped regime is accompanied in the underdamped phase space. This bound also illuminates how the empirical distribution in x

and v transforms to the overdamped pair of empirical distribution in x and an empirical current.

Deriving bounds on the LDF also revealed challenges that have to be met when using the contraction principle. The ansatz has to be chosen carefully to produce an associated current, Eq. (3.39), that can be expressed in a closed form. That ansatz further has to cover the wide range from a regime that is dominated by noise, i.e. the nearly overdamped regime, to the underdamped regime with inherent long-ranged correlations due to the inertia. This challenge becomes apparent in the derived bounds for the tails of the LDF. The characteristics of the empirical distributions are known and it is possible to find bounds that adequately describe the tails in either the overdamped or the underdamped regime. However, the ansatzes that are necessary to derive the bounds are very different and cannot be connected easily to obtain a tight bound for arbitrary mass.

The numerical results presented in Sec. 5.5 indicate that a parabolic bound in the spirit of the TUR exists for observables of v-order 1. In the next chapter we will apply the insights obtained here to bounds that could be used to derive bounds on thermodynamic quantities.

Chapter 6

Thermodynamic bounds for underdamped motion

As demonstrated in the previous chapter, bounds on the LDF can be derived from the contraction (3.43) by inserting trial densities tailored to produce a specific particle current. However, the bounds derived to characterize the LDF in Sec. 5.4 cannot be employed to derive bounds on thermodynamic quantities since they structure the LDF for rare events which typically have little influence on thermodynamics. In order to characterize the typical events, it is essential to find differentiable bounds on the LDF that are saturated in the vicinity of its minimum. In other words, the ansatz for the density has to become the solution of the Fokker-Planck equation p^{ss} at one point.

In Sec. 5.5 a parabolic bound on the LDF that would imply the TUR was numerically observed, awakening the hope that the TUR can be proven in the same fashion as for overdamped motion. However, the constraint of the empirical current (3.39) in the underdamped functional LDF poses a new problem for finding bounds on the LDF. The level 2 LDF does not allow for a variation of the current independently from the density, as was possible in the overdamped case [38, 39]. Instead, a suitable ansatz has to be developed for the complete phase space density.

In this chapter we introduce suitable ansatzes and bounds, assess their tightness and discuss their relation to the most prominent thermodynamic bound: The TUR.

6.1 Activity bound

The ansatz that leads to the TUR for overdamped dynamics can be interpreted as a "time-lapse" transformation of steady state trajectories, where all trajectories are scaled linearly in time. Such an ensemble of "time-lapsed" trajectories reproduces the stationary density but leads to a scaled current. In this section we apply this idea for underdamped dynamics and derive the so-called activity bound.

6.1.1 Proof of the bound

The notion of a time-scaling can be implemented for underdamped Brownian dynamics by introducing a scaling factor $(1+c)$ in the density

$$\rho^{\mathrm{TL}}(\boldsymbol{x},\boldsymbol{v};c) \equiv \frac{1}{(1+c)^d} p^{\mathrm{ss}}\left(\boldsymbol{x}, \frac{\boldsymbol{v}}{1+c}\right) \tag{6.1.1}$$

where d is the number of dimensions of $\boldsymbol{x}$ and $\boldsymbol{v}$. By construction, the marginalized $\boldsymbol{x}$-distribution of this density is the same as for the stationary distribution, but the particle moves faster or slower. This ansatz was first introduced in Ref. [48] and later generalized in Ref. [62].

Despite the known discrepancy for observables that are even under time-reversal we consider the general class of observable

$$Y_n(\mathcal{T};\boldsymbol{w}(\boldsymbol{x}) \equiv \int_0^{\mathcal{T}} dt \sum_i^d w_i(\boldsymbol{x}(t)) v_i(t)^n \tag{6.1.2}$$

with variable v-order n. The mean of such an observable for the density of the ansatz, Eq. (6.1.1), is

$$\begin{aligned}\langle Y_n(\mathcal{T};\boldsymbol{w}(\boldsymbol{x}))\rangle_{\rho,c} &= \mathcal{T}\int d\boldsymbol{x}\int d\boldsymbol{v}\, \rho^{\mathrm{TL}}(\boldsymbol{x},\boldsymbol{v};c)\sum_{i=1}^d w_i(\boldsymbol{x}) v_i^n \\ &= (1+c)^n \langle Y_n(\mathcal{T};\boldsymbol{w}(\boldsymbol{x})\rangle \end{aligned} \tag{6.1.3}$$

where the last ensemble average is taken with respect to the steady-state distribution. As desired, the mean is just rescaled in the time-scaled image.

Plugging the trial function into the contraction (3.43) with the diagonal diffusion matrix $D_{ii} = T_i\gamma_t/m_i^2$ and expanding around the stationary state at $c=0$ gives, after some algebraic simplifications, the bound

$$I\left(\tilde{Y},\mathcal{T}\right) \leq I^{\mathrm{TL}}\left(c,\mathcal{T}\right) \equiv I[\rho^{\mathrm{TL}}(\cdot,c),\mathcal{T}] = \left(\frac{\mathcal{T}}{4}\mathbb{A} + \frac{1}{2}\mathbb{B}\right)c^2 + \mathcal{O}(c^4) \tag{6.1.4}$$

with the time extensive measure

$$\mathbb{A} \equiv 9\sigma + 4\sum_{i=1}^d \left[\frac{4\gamma_i}{m_i} - \frac{3\gamma_i}{T_i}\langle v_i^2\rangle + \frac{1}{T_i\gamma_i}\langle F_i(x)^2\rangle\right] \tag{6.1.5}$$

and a constant term that stems from the expansion of the Kullback-Leibler divergence $K(\rho^{\mathrm{TL}} \mid p^{\mathrm{ss}})$

$$\mathbb{B} \equiv \left\langle \left(\frac{\boldsymbol{v}\cdot\nabla_{\boldsymbol{v}} p^{\mathrm{ss}}(\boldsymbol{x},\boldsymbol{v})}{p^{\mathrm{ss}}(\boldsymbol{x},\boldsymbol{v})}\right)^2\right\rangle - d^2. \tag{6.1.6}$$

By taking the second derivative, this timelapse bound on the LDF implies a bound on the variance of the observable $Y_n(\mathcal{T} \mid w(\boldsymbol{x}))$ as

$$\begin{aligned}\mathrm{Var}[Y_n(\mathcal{T};\boldsymbol{w}(\boldsymbol{x})] &\geq \left(\partial_c^2 I^{\mathrm{TL}}(0,\mathcal{T})\right)^{-1} \left(\partial_c \left\langle Y_n(\mathcal{T};\boldsymbol{w}(\boldsymbol{x})\right\rangle_{\rho,c}\right)^2\Big|_{c=0} \\ &= 2\left(\mathcal{T}\mathbb{A}+2\mathbb{B}\right)^{-1} n^2 \left\langle Y_n(\mathcal{T};\boldsymbol{w}(\boldsymbol{x})\right\rangle^2 \end{aligned} \tag{6.1.7}$$

or in the form of an uncertainty product adapted to this bound

$$\mathbb{Q}_n^{\mathrm{TL}}(\mathcal{T};w(\boldsymbol{x}) \equiv \frac{\mathrm{Var}[Y_n(\mathcal{T};\boldsymbol{w}(\boldsymbol{x})]}{\left\langle Y_n(\mathcal{T};\boldsymbol{w}(\boldsymbol{x})\right\rangle^2}\left(\mathcal{T}\mathbb{A}+2\mathbb{B}\right)/n^2 \geq 2 \tag{6.1.8}$$

that defines the uncertainty product that is associated with the timelapse bound $\mathbb{Q}_n^{\mathrm{TL}}$. It is worth noting that the bound can readily be generalized to currents with general v-dependent weight $Y(\mathcal{T};w(\boldsymbol{x},\boldsymbol{v}))$. In this case the derivative $\partial_c \left\langle Y\right\rangle_{\rho,c}$ in Eq. (6.1.7) must be evaluated as shown in Ref. [45].

Since the ansatz ρ^{TL} does not coincide with the stationary distribution for $\mathcal{T}=0$, the Kullback-Leibler divergence in the level 2 LDF leads to an offset $\mathbb{B}$ that is independent of $\mathcal{T}$. This constant ensures that the bound is valid even in the limit $\mathcal{T}\to 0$, where the uncertainty ϵ becomes constant (see Sec. 4.2.1). If the term $\mathbb{B}$ vanished, the bound could be broken for small times.

For large times, the time extensive term $\mathbb{A}$ dominates. In contrast to the TUR for overdamped motion, the bound (6.1.7) does, however, not only depend on the irreversibly σ but also on terms that can be identified as a measure of the dynamical activity [63, 64, 65, 66]. This is the time-symmetric part of the path integral without the term that is proportional to $\dot{\boldsymbol{v}}\boldsymbol{D}^{-1}\dot{\boldsymbol{v}}$ [66]. It can be argued that this term has to be attributed to the path weight itself.

The discrepancy between the timelapse ansatz for overdamped and underdamped dynamics is due to the presence of reversible currents in the latter regime. For overdamped dynamics, no reversible currents are present and the ansatz scales the irreversible current in the level 2.5 LDF. For underdamped dynamics, on the other hand, reversible currents are amplified by the time-scaling as well. This leads to additional terms in the bound, in particular the activity terms.

An advantage of the bound is that it does not vanish in equilibrium which is particularly relevant for observables that are even under time-reversal. For such observables, the bound can be applied for arbitrary driving, particularly in the equilibrium limit where the original uncertainty product $\mathcal{Q}$ approaches zero. A bound that is similar in spirit can be derived for time-symmetric traffic in Markovian jump dynamics [46] as well. Furthermore, the precision of current-like observables can also be be bound by the activity in such systems [47]. This bound on the precision can be derived by increasing the general activity in the system instead of the currents as done for the TUR prove.

This approach has some similarities to the ansatz considered here. The definition of the activity in such discrete systems does, however, not translate to the continuous case. Consequently, the similarities between the bounds for discrete dynamics and the timelapse bound is of a more qualitative nature.

It is worth noting that the decomposition in a term that involves the entropy production σ and other terms is ambiguous. Expanding the expression for the entropy production, Eq. (2.34), yields after some simplifications

$$\sigma = \sum_i \frac{1}{T_i} \langle f_i v_i \rangle = \sum_i \left(\frac{\gamma_i}{T_i} \left\langle v_i^2 \right\rangle - \frac{\gamma_i}{m_i} \right). \tag{6.1.9}$$

Notably, all terms on the right hand side are averages over time-reversible terms. Using this identity, the bound as presented in Eq. (6.1.7) can be cast in the form of Ref. [48].

6.1.2 Benchmark using free diffusion

Evaluating the bound in practice is challenging, especially for small times where $\mathbb{B}$ has a significant impact. The problem with $\mathbb{B}$ is that the distribution appears in the denominator which can lead to an amplification of numerical errors in the tails of the distribution if it is not accessible analytically. To further assess the validity and tightness of the bound, we thus benchmark it using an analytically accessible model and revisit free diffusion with drift in one dimension. Furthermore we chose constant weights along x, i.e. $w(x) = 1$.

The uncertainty can be calculated as described in Sec. 4.2. All averages occurring in the two measures $\mathbb{A}$ and $\mathbb{B}$ can be calculated analytically using the stationary distribution, Eq. (4.3.2), leading to

$$(\mathcal{T}\mathbb{A} + 2\mathbb{B}) = \left(\sigma + 4\frac{\gamma}{m}\right)\mathcal{T} + 2\frac{f^2}{T\gamma^2} + 4. \tag{6.1.10}$$

The resulting products $\mathbb{Q}^{\mathrm{TL}}$ are plotted against the dimensionless time τ in Fig. 6.1.1.

As mentioned before, the Kullback-Leibler divergence induces a time-independent constant offset. As the offset depends on the driving force, one can observe a transition in time for large forces. While for large and small times the terms $\mathbb{A}$ and $\mathbb{B}$ dominate, respectivelly, for intermediate times both terms are significant and add up the maximum in the third and fourth panel of Fig. 6.1.1.

Due to the crossover, it is hard to make general statements as non-systematic crossings of the curves occur. Given that the bound is dominated by the undesired and somewhat unphysical influence of the Kullback-Leibler divergence for small times, we restrict our discussion on the long-time limit in the following.

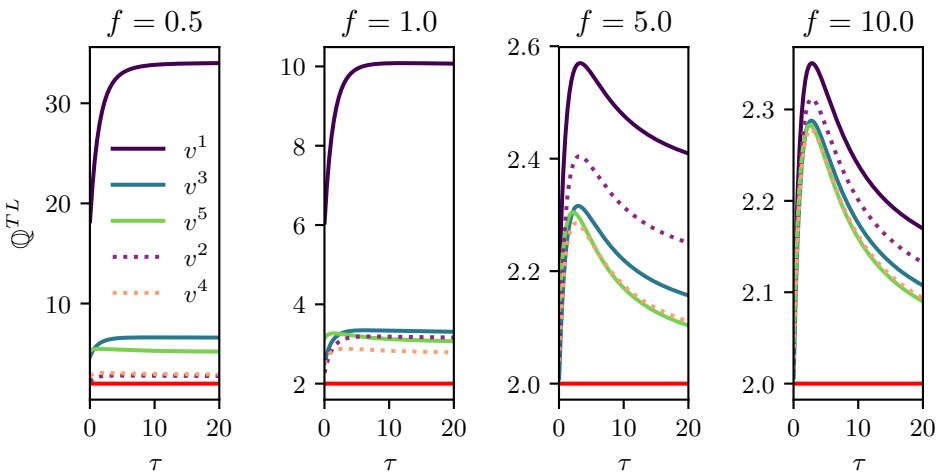

FIGURE 6.1.1: The timelapse bound, Eq. (6.1.7), evaluated for free diffusion with drift. The driving force f is increased from left to right from 0.5 to 10. The plotted lines correspond to the adjusted uncertainty product for the current $Y_n(\mathcal{T};1)$ with v-order n. Dotted lines highlight even observables. The red line depicts the lower bound 2 of the product $\mathcal{Q}^{\mathrm{TL}}$.

Overall, we can observe a dependency on the v-order that is contrary to the observations made for the uncertainty product $\mathbb{Q}$ in Sec. 4.2. While $\mathbb{Q}^{\mathrm{TL}}$ diverges for odd observables in the linear response limit, even observables converge in the same limit.

This observation can also be put on a more formal basis. For a current of v-order 1, the uncertainty product is given by

$$\lim_{\mathcal{T}\to\infty} \mathbb{Q}_1^{\mathrm{TL}}(\mathcal{T};1) = 2 + \frac{8T\gamma^2}{f^2 m} \tag{6.1.11}$$

in the long-time limit. The latter term shows that the distance between $\mathbb{Q}^{\mathrm{TL}}$ and its bounding value 2 grows with f^{-2}. The products for $n = 3$ and $n = 5$ qualitatively show the same behavior and diverge in the limit $f \to 0$ as can be observed in Fig. 6.1.1. An offset of potentially several orders of magnitude for an order 1 current has been reported in more advanced models as well [62].

For even observables, as plotted with broken lines in Fig. 6.1.1, the performance of the bound generally looks better, especially in the linear response limit. In this limit, the bound can be saturized for free diffusion and an observables that grows with weight v^2. For an observable of order $n = 4$ the limit is given by the slightly larger value $7/3$.

In the large driving limit $f \to \infty$ or for large mass, the bounding function, Eq. (6.1.10), is dominated by the entropy production σ for free diffusion. In

this limit, the bound also becomes tight independent from the v-order. Simultaneously, its statement reduces to the statement of a putative TUR as the timelapse product $\mathbb{Q}_n^{\mathrm{TL}}$ reduces to the entropy uncertainty product $\mathcal{Q}_n$. Although this is only true for free diffusion, the statement might be valid for other systems as well when they approach free diffusion in the large driving limit. Most prominently, this is true for diffusion over periodic potential landscapes. In this case, the details of the potential vanish when dominated by a large driving force.

Besides the more complex and less transparent form of the timelapse bound impeding its applicability in practice, it does not seem particularly tight in general. Although the bound can be saturated in some limiting cases, in general it only gives a loose bound on the precision. The different behavior for odd and even observables in the linear response limit, however, also indicates that the timelapse ansatz might incorporate two conceptually different bounds that could also hold individually: One that is based on the irreversibility and dominates for large forces and one that is based on the activity and dominates in the linear response regime.

6.2 Virtual pertubative forces

A different proof for the overdamped TUR has been presented more recently in Ref. [24]. Here, a bound on the CGF is derived by making an ansatz for a virtual, not-necessary physically motivated force that models the vicinity of $\alpha(0)$ to second order in the tilting λ.

Although initially formulated as an expansion for the CGF, such virtual dynamics are used in the proof of the level functional LDF as well (compare Eq. (3.A.1)). While the large deviation approach allows one to choose an empiric density and possibly current to an unknown virtual force, the described method makes an ansatz for the virtual forces directly without knowing the associated distributions from the start. Keeping the tight connection between the CGF and the LDF in mind (Sec. 3.4.2), the both methods can be regarded as equivalent with a difference only in the interpretation of the ansatzes.

In this section we use this equivalence to derive the class of bounds presented in [24] from the level 2 LDF. As a next step, we follow the derivation of the overdamped TUR to discuss its implications on underdamped dynamics.

6.2.1 Bounds based on virtual pertubation

The central result of the method can be retrieved from the contraction principle by inserting the stationary current and density that follows from a Fokker-Planck equation with a specific virtual force. Let ρ be a stationary solution to

the pertubed Fokker-Planck equation

$$0 = -\nabla_x \cdot v\rho(x,v;c) - \frac{1}{m}\nabla_v \cdot \left(F(x) - \gamma v + cF^{(1)}(x,v)\right)\rho(x,v;c) + \nabla_v^{\intercal}\left(D + cD^{(1)}\right)\nabla_v \rho(x,v;c) \tag{6.2.1}$$

with an additional, not necessarily physically motivated force $F^{(1)}$ and an altered diffusion matrix $D + D^{(1)}$. In the following we will refer to these pertubed dynamics as virtual dynamics.

It is straightforward to identify the empirical current that is associated with this distribution from the altered Fokker-Planck equation

$$\mu_v(x,v;c) = \frac{1}{m}\left(F(x) - \gamma v + cF^{(1)}(x,v)\right)\rho(x,v) + \left(D + cD^{(1)}\right)\nabla_v \rho(x,v). \tag{6.2.2}$$

Plugging the ansatz for the distribution ρ and associated current in the level 2 LDF yields for large times

$$I[\rho] = \frac{c^2\mathcal{T}}{4}\sum_i \frac{1}{D_{ii}}\left\langle\left(\frac{F_i^{(1)}/m_i p^{ss} - D_{ii}^{(1)}\partial_{vi}p^{ss}}{p^{ss}}\right)^2\right\rangle + \mathcal{O}(c^3) \quad (\mathcal{T} \gg 1) \tag{6.2.3}$$

with p^{ss} being the stationary distribution of the unperturbed Fokker-Planck equation, i.e. the stationary distribution of Eq. (6.2.1) with $c = 0$. Trivially, $I[\rho(x,v,t,0)] = 0$ in the long-time limit.

As shown in the previous section, we can derive a bound on the variance of an observable $Y(\mathcal{T}; w(x,v))$ from the LDF as

$$\mathrm{Var}[Y] \geq \left[\mathcal{T}\sum_i \frac{1}{2D_{ii}}\left\langle\left(\frac{F_i^{(1)}/m_i p^{ss} - D_{ii}^{(1)}\partial_{vi}p^{ss}}{p^{ss}}\right)^2\right\rangle\right]^{-1}\left(\partial_c \langle Y\rangle_{\rho,c}\right)^2\Big|_{c=0} \tag{6.2.4}$$

which is valid for large times ($\mathcal{T} \gg 1$).

In principle the proof can be extended to finite times. Calculating the virtual bound, however, involves the expansion of the Kullback-Leibler divergence as seen for the activity bound in Sec. 6.1.1. This contribution ensures the validity of the bound for small times where the regular uncertainty product becomes 0. The expansion of the Kullback-Leibler divergence yields

$$K(\rho(x,v;c) \mid p^{ss}(x,v)) = \frac{c^2}{2}\int dx \int dv\, \frac{\rho^{(1)}(x,v)^2}{p^{ss}(x,v)}, \tag{6.2.5}$$

with the pertubative expansion of the probability distribution $\rho(x,v;c) = p^{ss}(x,v) + c\rho^{(1)}(x,v)$.

In addition, we can consider an arbitrary initial states, as demonstrated in Ref. [67] for the CGF expansion. In this case, the altered Fokker-Planck equation contains a partial time-derivative and and the empirical functions become time-dependent. The advantage is that we can now chose the stationary distribution as initial state, i.e. $\rho(\boldsymbol{x}, \boldsymbol{v}, 0; c) = p^{\mathrm{ss}}(\boldsymbol{x}, \boldsymbol{v})$. This choice leads to a vanishing Kullback-Leibler divergence in limit $\mathcal{T} \to 0$, but comes at the cost of a vanishing derivative of the mean observable with respect to c. This ultimately ensures the validity of the bound for small times.

A more subtle point of the bound is its convergence when the diffusion matrix is changed. Following the original paper that builds upon the expansion of the generating function, one has to calculate the probability ratio of the original process with respect to a process governed by the virtual dynamics. The probability measure is, however, not absolutely continuous when the diffusion matrix is changed [44] leading to a diverging ratio (see [68] for a comprehensive explanation). Since we are only interested in a small pertubation in c, a change in the diffusion matrix can be translated to an additional force by expanding in c [69] thus circumventing this limitation.

Using the large deviation framework this issue does not arise, since we do not dictate the microscopic dynamics but rather an observed distribution. In fact, the same ratio of two path measures has to be evaluated in the proof of the level 2 LDF as well, see Sec. 3.4.3. In contrast to the aforementioned method, the compared process is, however, not the process that includes the virtual dynamics (and diffusion) but rather a process that has a force taylored to reproduce the empirical density of the virtual dynamics. This leaves an ambiguity in the microscopic details of the underlying trajectories which ensures the convergence of the ratio.

6.2.2 Rescaling the friction

In the previous section we have derived a general bound, Eq. (6.2.4), that can be evaluated for an arbitrary virtual force. If we want to proof the TUR, a straightforward choice is

$$F_i^{(1)} = -\gamma_i v_i \qquad D_{ii}^{(1)} = D_{ii} \tag{6.2.6}$$

which is chosen in a way that yields the entropy production, Eq. (2.34) on the right hand side of Eq. (6.2.4). The ansatz can also be expressed as a rescaled friction $\gamma' = (1+c)\gamma$ with the vector γ containing the friction coefficients γ_i for each spatial dimension. In first order of c, this virtual dynamics can be interpreted a simple rescaling of the irreversible current.

For this choice, the ensemble average takes on the form of the mean entropy production and thus the corresponding bound takes on the long-time form

$$\mathrm{Var}[Y] \geq \frac{2}{\mathcal{T}\sigma}\left(\gamma \cdot \nabla_\gamma \langle Y \rangle_\gamma\right)^2 \qquad (\mathcal{T} \gg 1) \tag{6.2.7}$$

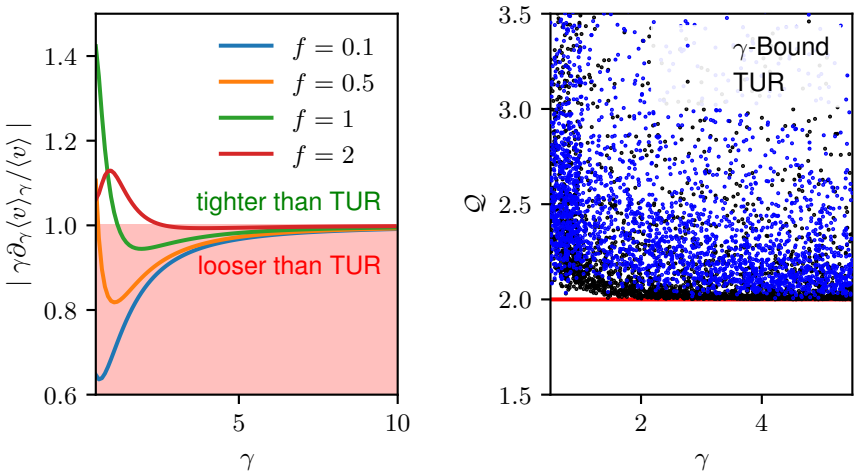

FIGURE 6.2.1: In the left panel: The condition (6.2.9) in form of the ratio of left and right side plotted against the friction γ for a particle of unit mass in a cosine potential with amplitude $V_0 = 1$ and three different driving forces f. The considered current is the particle current $Y_1(\mathcal{T};1)/\mathcal{T} = \langle v\rangle$. In the regime highlighted in bright red the condition is violated.
In the right panel: The uncertainty product of the γ-bound, Eq. (6.2.10) (blue), is plotted in comparison to the putative TUR (black) for 2700 parameters. Both uncertainty product are expected to be above 2.

where $\nabla_\gamma \langle Y\rangle_\gamma$ describes the change of the average value of the observable Y under a change of the friction γ.

In the overdamped regime this choice indeed proofs the TUR as no reversible currents are present in this limit. As a consequence, rescaling the irreversible current via virtual forces is equivalent to rescaling the overall current as done in the LDF based proof of the TUR (see Sec. 3.5.2). As a consequence, the last term in Eq. (6.2.7) becomes

$$\left(\gamma \cdot \nabla_\gamma \langle Y\rangle_\gamma\right)^2 = \langle Y\rangle^2 . \tag{6.2.8}$$

For underdamped dynamics, in contrast, evaluating the change of the average is not so straightforward. Since only the irreversible part is rescaled, one has to solve the Fokker-Planck equation to obtain the PDF and in turn the change on the overall current for changed friction. In this sense, we meet the same challenge as for the timelapse bound: The separation of the overall microscopic current into an irreversible and a reversible contribution obstructs the proof of the uncertainty relation. We can either choose how the ansatz effects the overall current or how it renders the term that bounds the precision.

Nevertheless, Eq. (6.2.7) would be a proof for the TUR if

$$|\gamma \cdot \nabla_\gamma \langle Y \rangle_\gamma| \overset{?}{\geq} |\langle Y \rangle|. \tag{6.2.9}$$

For driven free diffusion in one dimension with probability density as shown in Eq. (4.3.2), the terms can be compared analytically. In this case this condition is true only for odd observables with equality prevailing. This is in accordance with the observations made for free diffusion in Sec. 4.2.

When an external potential, such as a cosine potential $V(x) = V_0 \cos(2\pi x)$, is added the condition is generally violated. The left panel of Fig. 6.2.1 shows the ratio of the left and right side of condition (6.2.9) with respect to the friction γ and constant mass $m = 1$. The results are obtained numerically as described in Sec. 5.3.

In the red highlighted regime the bound obtained by rescaling γ is looser than the TUR and can thus not be reduced to the latter. Especially for small driving forces that result in a small particle current, the bound can not beat the TUR. For large driving, the potential landscape becomes negligible and the motion becomes more similar to free diffusion. This manifests in the ratio approaching 1, as free diffusion. In the overdamped limit, this is for $\gamma/m \gg 1$, the bound obtained by rescaling γ is known to converge to the TUR. Hence, the ratio approaches 1 in this limit as well.

To assess the tightness of the bound, we revisit the particle on a ring and evaluate the bound for the particle current numerically for 2700 parameter sets as described in Sec. 5.5. The derivative with respect to γ is evaluated numerically by calculating the average current in the vicinity of a certain γ. The associated uncertainty product in the long-time limit

$$\mathcal{Q}^\gamma \equiv \lim_{\mathcal{T}\to\infty} \frac{\mathrm{Var}[Y]}{\left(\gamma \cdot \nabla_\gamma \langle Y \rangle_\gamma\right)^2} \mathcal{T}\sigma \geq 2 \tag{6.2.10}$$

is plotted in the right panel of Fig. 6.2.1. As a comparison, the putative TUR is indicated by black dots.

Although the bound is not as easy to evaluate in practice due to the derivative in γ, it is much tighter than the timelapse bound, Eq. (6.1.7). Unfortunately, it is not possible to build a hierarchy of bounds with either bound being a tighter version of the other. For some regimes the friction bound gives a tighter estimate of the variance, while in others the bound is looser. In general, however, the original TUR seems to be tighter with the uncertainty product typically agglomerating in the vicinity of 2.

For the sake of completeness we shortly discuss how a rescaling of the reversible current affects the bound. Such a rescaling corresponds to the virtual

forces $F_i^{(1)} = F_i(x)$ and gives the bound

$$\mathrm{Var}[Y] \geq \left[\mathcal{T}\sum_i \frac{1}{2T_i\gamma_i}\left\langle F_i(x)^2\right\rangle\right]^{-1}\left(\partial_c \left\langle Y\right\rangle_{\rho,c}\right)^2\Big|_{c=0}. \tag{6.2.11}$$

Which also appears as term in the activity bound, Eq. (6.1.7). Combining the two ansatzes allows to identify the contributions in the activity bound as parts that arise through irreversible and reversible contributions and their combination.

6.3 A conjecture based on free diffusion

As shown in Sec. 4.2, the uncertainty product of free diffusion at finite times becomes smaller than the original, overdamped formulation of the TUR, Eq. (3.45), for all driving forces. In contrast to the overdamped TUR, the results obtained for free diffusion suggest that a putative bound should be time-dependent to cover the linear regime of the uncertainty product for small times. Consequently, the overdamped TUR cannot be straightforwardly generalized to underdamped motion.

In the long-time regime, evidence of the validity of a generalized TUR has been collected. For instance, the parabolic bound on the LDF that is established for overdamped motion seems to hold for underdamped dynamics, see Sec. 5.5. In the linear response regime, the validity is proven in the long-time limit for observables with v-order 1.

In this section we conjecture a bound on the uncertainty product that is valid for all times and substantiate it by extensive numerical results.

6.3.1 The conjecture

Conceptually, the original, overdamped TUR can also be interpreted as a bound generated by free diffusion. One of the features of the original TUR for overdamped dynamics is that it becomes saturated for free diffusion. In the proof, the TUR follows from a bound on the large deviation function (LDF) [70] or on the scaled cumulant generating function [24]. In both versions, the bounding function on the LDF (the generating function) is the one from free diffusion. In this sense, one could also say that the TUR states that the uncertainty product $\mathcal{Q}$ is bounded from below by the uncertainty product of free diffusion. The same interpretation holds for an approach to the TUR for the entropy production that is based on a Martingale decomposition [23]. For free diffusion, the stochastic entropy is subdivided in a linear part and a Martingale that embeds free diffusion without drift.

In extensive numerical simulations for diffusion in a periodic potential we recognize the same relationship for underdamped motion. In detail, we find that the uncertainty product $\mathcal{Q}_n(\mathcal{T}; w(x))$ of an odd n-order current

$$Y_n(\mathcal{T}; w(x)) = Y(\mathcal{T}; w(x)v^n), \quad n \in \{1, 3, 5...\} \tag{6.3.1}$$

for a one-dimensional system described by the underdamped dynamics (2.7) without forces that depend on the velocity (e.g. the Lorentz force) is bounded from below by the respective result for one-dimensional free diffusion in the equilibrium limit with homogeneous weight $w(x) = 1$

$$\mathcal{Q}_n^{F(x)}(\mathcal{T}; w(x)) \geq \mathcal{Q}_n^0(\mathcal{T}; 1). \tag{6.3.2}$$

We will refer to this conjecture as the *free diffusion bound* (FDB). The right hand side of (6.3.2) has been calculated in Sec. 4.2.

Most prominently, for the important class of currents Y_1 with v-order 1 the conjecture takes on the form

$$\mathcal{Q}_n^{F(x)}(\mathcal{T}; w(x)) \geq 2 - \frac{2m}{\gamma\mathcal{T}}\left(1 - \exp[-\frac{\gamma}{m}\mathcal{T}]\right). \tag{6.3.3}$$

For $\mathcal{T} \to \infty$ the second term on the right hand side vanishes and the statement of the overdamped TUR is recovered.

In the following we substantiate our conjecture by numerical data.

6.3.2 Driven diffusion in a periodic potential

We consider one-dimensional driven diffusion in a 2π-periodic potential $V(x)$. The process is described by the Langevin equation (2.7) with scalar variables x and v. The spatial coordinate x is projected on a ring of perimeter 2π to get a unique steady state. The potential consists of sine and cosine modes up to second order and random amplitudes $c_i^{\pm}$ where the superscript $+$ $(-)$ denotes the amplitude of the cosine (sinus) mode. In addition, a constant force f is applied. We randomly choose 500 parameter sets ($f \in [0, 3.5]$, $T \in [0.5, 1.5]$, $\gamma \in [0.5, 5]$, $c_i^{\pm} \in [-2, 2]$) and sample at least 50 000 trajectories of fixed length from the steady state for each set using a Verlet type integrator [71] with timestep $\Delta t = 10^{-3}$.

The variance and mean value of the currents $Y_1(\mathcal{T}; 1)$ and $Y_3(\mathcal{T}; 1)$ are computed for constant time along the different trajectories. Analogously, we extract the mean entropy production rate σ by tracking the dissipation.

The simulation results for the observable $Y_1(\mathcal{T}; 1)$ are summarized in the left panel of Fig. 6.3.1, where each thin line corresponds to one parameter set. The conjectured FDB, which is the uncertainty product for free diffusion $\mathcal{Q}_1^0$, Eq. (4.3.7) is plotted as thick, black line. Within the considered parameter range we see no violation of our conjecture, Eq. (6.3.2).

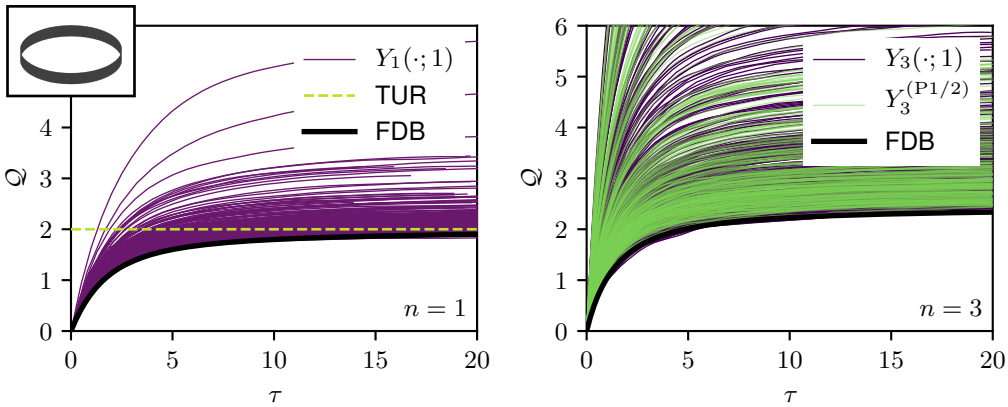

FIGURE 6.3.1: Finite-time uncertainty product for different currents numerically evaluated for an underdamped particle on a ring. The left panel shows the data for the current $Y_1(\mathcal{T};1) = \int v dt$ where each line corresponds to a diffusion process in a random potential characterized by its amplitudes $c_i^{\pm} \in [-2,2]$ and randomly sampled parameters with $f \in [0,3.5]$, $T \in [0.5,1.5]$, $\gamma \in [0.5,5]$. The conjectured bound for v-currents of order 1, Eq. (6.3.3), is plotted as solid black line, the (overdamped) TUR and coincident the asymptotic behavior is indicated by the dashed line. The right panel shows the uncertainty product for the current $Y_3(\mathcal{T};1) = \int v^3 dt$ and two exemplary x-dependent currents (P1) and (P2) (see Eqs. (6.3.4) and (6.3.5)). The solid black line depicts the more general bound for $n = 3$, Eq. (6.3.2).

For $n = 3$ we can establish the same role of free diffusion. In detail, the equilibrium limit of the uncertainty product obtained for free diffusion $\mathcal{Q}_3^0$, see Eq. (4.3.8), bounds the uncertainty product from below for all times. We, again, validate this by randomly selecting 270 different parameter sets and plotting them as dark lines in the right panel of Fig. 6.3.1. To check that the conjecture holds with x-dependent weights as well, we furthermore evaluate the uncertainty product of the two currents

$$Y_3^{(P1)}(\mathcal{T}) \equiv Y_3\left(\mathcal{T};1+\frac{1}{2}\cos\left(2\pi x(t)\right)\right) \tag{6.3.4}$$

and

$$Y_3^{(P2)}(\mathcal{T}) \equiv Y_3\left(\mathcal{T};\cos\left(2\pi x(t)\right)^2\right) \tag{6.3.5}$$

which are plotted as bright lines in the right panel of Fig. 6.3.1.

The procedure is repeated for 200 parameter sets with a randomly constructed weighting factor

$$w(x) = \tilde{c}_0 + \sum_{n=1}^{2} \tilde{c}_n^+ \cos(2\pi n) + \tilde{c}_n^- \sin(2\pi n) \tag{6.3.6}$$

and v-orders $n = 1$ and $n = 3$ without any violations.

6.3.3 Case studies in higher dimensions

So far, we have focused on one spatial dimension. In higher dimensions, it is not obvious how to generalize our conjecture, Eq. (6.3.2), as different velocities of different directions can arise. The v-order of an observable involving different spatial dimensions is ambiguous as it can refer to either the overall order of all velocities or that of just one specific direction. In the following, we will exemplarily study two different systems to examine the applicability of the FDB to higher dimensions. It is important to emphasize that the results presented in the following are not conclusive, yet, but are rather intended as a starting point for further studies.

Underdamped diffusion on an torus

First, we consider driven diffusion in a two-dimensional periodic potential, i.e. diffusion on a two-dimensional torus. The process is described by coupled Langevin equations for the variables $x_{1,2}$ and $v_{1,2}$ with periodic boundaries along both spatial dimensions. We apply the non-conservative force

$$\boldsymbol{F}(\boldsymbol{x}) = (c_1 \sin(x_1 + x_2), c_2 \cos(x_1 - x_2))^T + \boldsymbol{f} \tag{6.3.7}$$

with parameters $c_{1,2}$ and external driving $\boldsymbol{f}$.

The time-integrated current can, in principle, depend on all velocity components. First, we restrict the current to the projected velocity in either the first or the second direction

$$Y_n^{(\mathrm{T1})}(\mathcal{T}) \equiv Y(\mathcal{T}; v_1^n) \;\text{ and }\; Y_n^{(\mathrm{T2})}(\mathcal{T}) \equiv Y(\mathcal{T}; v_2^n) \tag{6.3.8}$$

which correspond to a v-order $n = 1$ and $n = 3$, respectively. Furthermore, we consider the diagonal current

$$Y_n^{(\mathrm{T3})} \equiv Y_n^{(\mathrm{T1})} + Y_n^{(\mathrm{T2})}. \tag{6.3.9}$$

As either term can dominate the sum, a lower bound that is based on the v-order, if existent, must be given by the smallest bound of the respective terms. This smallest bound corresponds to the term with the lowest occurring v-order. In this case, both terms in the current $Y_n^{(\mathrm{T3})}$ have the same v-order so that we attribute the v-order of n to the observable (T3).

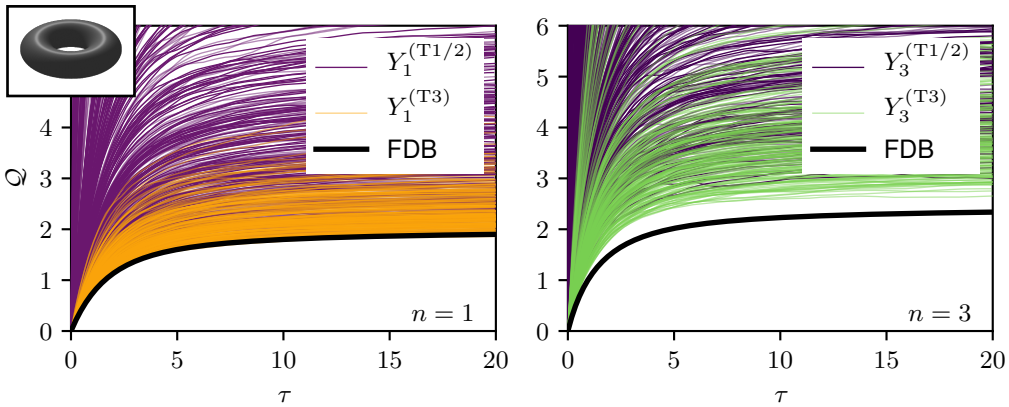

FIGURE 6.3.2: The uncertainty product $\mathcal{Q}$ plotted against dimensionless time τ for diffusion on a torus. Each line corresponds to one of 250 parameter sets for γ, T and the free parameters in the force (6.3.7). The dark lines correspond to the projected currents in one direction $Y_n^{(T1)}(\mathcal{T})$, $Y_n^{(T2)}(\mathcal{T})$ (see Eq. (6.3.8)) while the bright lines give the diagonal current $Y_n^{(T3)}(\mathcal{T})$, Eq. (6.3.9), with $n = 1$ in the left panel and $n = 3$ in the right panel. The thick black line depicts the expected free diffusion bound $\mathcal{Q}_n^0$.

We extract the uncertainty product numerically as described in Sec. 6.3.2. The results for the three currents (T1) – (T3) for $n = 1$ and 3 are shown in the both panels of Fig. 6.3.2. The numerical data give a first indication that the respective free diffusion bound for one dimension, plotted as thick black lines, could be generalized to higher dimensions as well.

The apparent validity of the conjecture is surprising as there is no straightforward mapping of the two-dimensional diffusion to a one-dimensional problem. Although the Langevin equation decouples for $c_1 = c_2 = 0$ and one arrives at effectively two one-dimensional processes, the diffusion process is a genuine two-dimensional process in general. One could, however, argue that the additional degrees of freedom increase the uncertainty product. First, there might be dissipation due to directed motion in a direction that does not contribute to the considered current, which increases $\mathcal{Q}$. For instance for the current (T1) the force in the 2-direction contributes only indirectly to the motion in 1-direction while it directly increases the entropy production rate σ. Second, the potential mediates energy transfer between the two directions, thus increasing the fluctuations and also the uncertainty for the current in one specific direction.

In principle, one can also consider mixed currents where both velocities are connected multiplicatively as in

$$Y\left(\mathcal{T}; w(x) v_1^n v_2^m\right) = \int_0^{\mathcal{T}} w(x) v_1^n v_2^m dt \qquad n, m \in \mathbb{N} \tag{6.3.10}$$

where one number n or m must be even and the other one odd in order to maintain the odd character under time-reversal. One example is the empirical correlation of the kinetic energy in 1-direction and the velocity in 2-direction measured along a trajectory. This quantity can be written in the form $Y(\mathcal{T}; m v_1^2 v_2/2)/\mathcal{T}$. In contrast to the previously analyzed currents, it is not obvious how to define the "v-order" of such a current. On the one hand, one could argue that the odd part v_1 does only appear in first order. On the other hand, the overall exponent of velocities is 3 thus suggesting that the uncertainty product can be estimated better by comparing with a one-dimensional $n = 3$ current. We briefly address this issue exemplarily for the above current.

For a flat potential $c_i = 0$ the uncertainty product can be solved analytically using the previously derived differential equations (4.2.1) and (4.2.2). The corresponding uncertainty product for arbitrary driving $\boldsymbol{f}$, as before, depends on the force. In the equilibrium limit $\boldsymbol{f} \to \mathbf{0}$ the uncertainty product takes on the form

$$\mathcal{Q}^{\mathbf{0}}\left(\mathcal{T}; \frac{m}{2} v_1^2 v_2\right) = \frac{2}{\tau}\left(\frac{5}{3}\tau - \frac{11}{9} + e^{-\tau} + \frac{2}{9} e^{-3\tau}\right) \tag{6.3.11}$$

which is larger than both, the uncertainty product obtained for free diffusion of observables of order 1 and 3 in the equilibrium limit

$$\mathcal{Q}^{\mathbf{0}}\left(\mathcal{T}; \frac{m}{2} v_1^2 v_2\right) \geq \mathcal{Q}_3^0(\mathcal{T}; 1) \geq \mathcal{Q}_1^0(\mathcal{T}; 1). \tag{6.3.12}$$

The tighter bound for the $n = 3$ current can be interpreted by considering the correlations between the velocities. Even when a potential mediates a correlation of the velocities in different spatial directions, the uncertainty of the current is still higher than that of a one-dimensional process where only one velocity exists.

To see whether a bound for such multiplicative currents holds in presence of a potential as well, we repeat the numerical analysis for the time-integrated current $Y(\mathcal{T}; m v_1^2 v_2/2)$ and evaluate 200 random parameter sets numerically. All results lie above the value obtained without an external potential in the equilibrium limit, $\mathcal{Q}^{\mathbf{0}}\left(\mathcal{T}; m v_1^2 v_2/2\right)$. To increase the transfer of energy between the two spatial directions via the potential we further consider the conservative potential

$$V(\boldsymbol{x}) = c_1 \sin(x_1 - x_2) \tag{6.3.13}$$

which essentially forms a well of lower energy diagonally along the torus. Here, driving in the direction x_1 results in a consistent motion in the direction 2 and vice versa. We simulate 100 different parameter sets with random values c_1, f, γ, T, never observing an uncertainty product that goes below Eq. (6.3.11). This finding does not only suggests that a lower bound based on free diffusion holds for such mixed currents as well, but also that it is possible to improve the bound by including more information on the considered observable, see Eq. (6.3.12).

The underdamped Brownian gyrator

A model that is conceptually different from diffusion on a torus is that of a Brownian gyrator [72]. This minimal model of a heat-engine at the nanoscale at heart consists of a particle in two dimensions that is coupled to two heat baths of different temperature. By adjusting the potential, work can be extracted by driving the particle up the potential dominated by the hot bath and using the gained potential energy. Due to its simplistic nature and analytical tractability that stems from the linear dynamics, the overdamped version of this system has been thoroughly studied [73, 74] and even experimentally realized [75, 76].

The dynamics of the underdamped analogous of the gyrator remains linear and can thus be solved analytically, as well. Being interested in the uncertainty, we consider a simplified version that consists of a particle in a two-dimensional harmonic potential with spring constant k that is driven with a constant torque κ. The particle is embedded in a medium with friction coefficient γ and single temperature T. The overall motion is described by the two-dimensional Langevin equation

$$\dot{\boldsymbol{x}} = \boldsymbol{v} \quad ; \quad m\dot{\boldsymbol{v}} = \begin{pmatrix} -k & \kappa \\ -\kappa & -k \end{pmatrix} \boldsymbol{x} + \begin{pmatrix} -\gamma & 0 \\ 0 & -\gamma \end{pmatrix} \boldsymbol{v} + \boldsymbol{\xi} \tag{6.3.14}$$

with the usual statistics for the noise $\boldsymbol{\xi}$ (see Eq. (2.7)).

As mentioned, the stationary state of the linear Langevin dynamics (6.3.14) can be solved exactly. The covariance matrix $\mathsf{C} = \langle (\boldsymbol{x}, \boldsymbol{v})^{\mathrm{T}} (\boldsymbol{x}, \boldsymbol{v}) \rangle - \langle (\boldsymbol{x}, \boldsymbol{v}) \rangle^2$ is given by

$$\mathsf{C} = \frac{T}{m\phi - \kappa^2 m/\gamma} \begin{pmatrix} \gamma & 0 & 0 & -\kappa \\ 0 & \gamma & \kappa & 0 \\ 0 & \kappa & \phi & 0 \\ -\kappa & 0 & 0 & \phi \end{pmatrix} \tag{6.3.15}$$

with $\phi \equiv \gamma k/m$ as long as the parameters satisfy the stability condition

$$\gamma k - \kappa^2 m/\gamma > 0. \tag{6.3.16}$$

Consequently, the particle is confined by the potential if the strength of torque $|\kappa|$ is moderate enough to satisfy the stability condition, otherwise the particle escapes from the potential.

A natural current arising in this system is the observable

$$Y_1^{(\mathrm{G1})}(\mathcal{T}) \equiv \int_0^{\mathcal{T}} dt\,[x_2(t)v_1(t) - x_1(t)v_2(t)]\,. \tag{6.3.17}$$

which corresponds to the distance travelled in the gyrator. This circular current is also proportional to the work performed by the torque κ. Since the velocity appears in first order, the circular current can be regarded as an $n = 1$ observable. Using the covariance matrix (6.3.15) the mean value is given by

$$\left\langle Y_1^{(\mathrm{G1})}(\mathcal{T})\right\rangle = \mathcal{T}\frac{2\kappa T\gamma}{m(\gamma\phi - \kappa^2)} \tag{6.3.18}$$

and using Eq. (2.36) the entropy production rate can be expressed as

$$\sigma = \frac{\kappa}{T}\partial_{\mathcal{T}}\left\langle Y_1^{\mathrm{Gyr}}(\mathcal{T})\right\rangle. \tag{6.3.19}$$

For small times the variance can be calculated with Eq. (4.2.3)

$$\begin{aligned}\mathrm{Var}\left[Y_1^{(\mathrm{G1})}(\mathcal{T})\right] &\approx \mathcal{T}^2\mathrm{Var}[x_2v_1 - x_1v_2] \\ &= \mathcal{T}^2\left(\left\langle x_2^2\right\rangle\left\langle v_1^2\right\rangle + \langle x_2v_1\rangle^2 + \left\langle x_1^2\right\rangle\left\langle v_2^2\right\rangle + \langle x_1v_2\rangle^2\right).\end{aligned} \tag{6.3.20}$$

Here, the second line follows from Wick's theorem and from $\langle x_1x_2\rangle = \langle x_iv_i\rangle = 0$. Plugging the covariances in and identifying the mean current, Eq. (6.3.18), finally yields

$$\mathrm{Var}[Y_1^{(\mathrm{G1})}(\mathcal{T})] = \mathcal{T}^2\left\langle Y_1^{(\mathrm{G1})}\right\rangle^2\frac{\gamma\phi + \kappa^2}{2\kappa^2} + \mathcal{O}(\mathcal{T}^2). \tag{6.3.21}$$

Combining the cumulants, we can express the uncertainty product in first order in time as

$$\mathcal{Q}_1^{(\mathrm{G1})}(\mathcal{T}) = \mathcal{T}\frac{\gamma}{m}\frac{\gamma\phi + \kappa^2}{\gamma\phi - \kappa^2} + \mathcal{O}(\mathcal{T}^2) \geq \mathcal{T}\frac{\gamma}{m} + \mathcal{O}(\mathcal{T}^2) \tag{6.3.22}$$

where the bound follows from minimizing in κ which is attained in the equilibrium limit $\kappa \to 0$.

This short-time expansion coincides with the corresponding free diffusion bound (4.3.7) to first order in time. As a result, the conjectured bound (6.3.2) holds in the Brownian gyrator in this order. It is due to the ballistic dynamics for small times.

To investigate the uncertainty product and its relation to our conjecture in this system, we numerically compute the finite-time uncertainty product of $Y_1^{(\mathrm{G1})}$ for 160 randomly sampled parameters ($\gamma \in [0.5, 1.5]$, $T \in [0.5, 1.5]$, $k \in [0.05, 4]$ and $\kappa \in [0, 2.5]$) and plot them with respect to the dimensionless

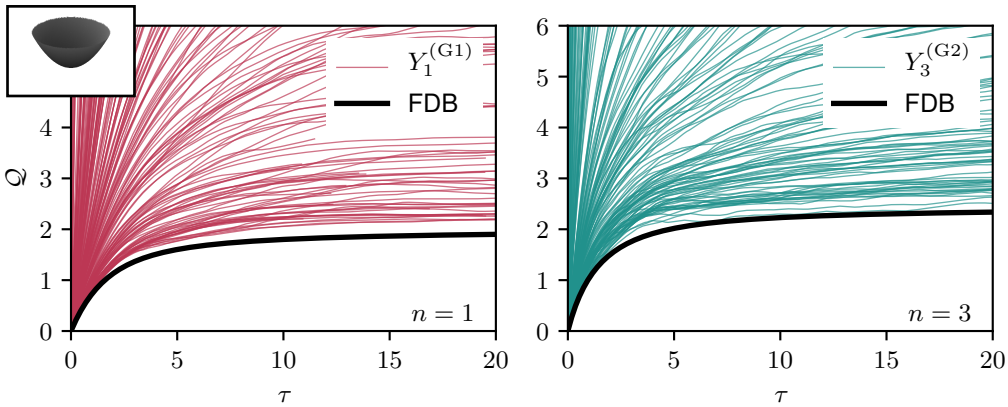

FIGURE 6.3.3: The uncertainty product for the two considered currents in the gyrator model, $Y_1^{(G1)}$ in the left panel and $Y_3^{(G2)}$ in the right panel, plotted against dimensionless time τ. Each line corresponds to a different parameter set that was chosen on random. The thick black line depicts the respective free diffusion bound $\mathcal{Q}_n^0$ that has been conjectured to be a lower bound for diffusion in one spatial dimension.

time τ in the left panel of Fig. 6.3.3. In agreement with our conjecture, all curves lie above the value obtained for one-dimensional free diffusion.

Motivated by the results for diffusion on a torus, we repeat the analysis for the more abstract order $n = 3$ current of the form

$$Y_3^{(G2)}(\mathcal{T}) \equiv \int_0^{\mathcal{T}} dt \left[x_2(t) v_1(t)^3 - x_1(t) v_2(t)^3 \right]. \tag{6.3.23}$$

Using the same rationale as for the diagonal current on a torus, we consider this observable a current of v-order 3. The numerical results for 160 parameter sets with $\gamma \in [0.5, 5]$, $T \in [0.5, 1.5]$, $k \in [0.05, 3]$ and $\kappa \in [0, 2.5]$ are plotted in the right panel of Fig. 6.3.3. Again, in accordance with the conjecture the uncertainty product does not become smaller than the value obtained for free diffusion in one dimension in the equilibrium limit.

6.4 Conclusion

Based on numerical evidence we conjecture that the uncertainty product for an odd current with arbitrary weight function in a one-dimensional periodic potential is bounded from below by the result obtained for free diffusion for an observable of same order in the velocity but constant spatial weight in the limit of vanishing driving force. The conjectured bound converges to the overdamped TUR in the corresponding limit, thus suggesting that our

conjecture is in fact the underdamped generalization of the TUR. By design, the bound is saturated for all times for free diffusion and thus is tight.

To our knowledge the conjectured free diffusion bound is the first bound that can be saturated for the important class of currents scaling with the first order in the velocity. Among this class of currents are, for instance, the integrated work current or the distance traveled in some time. Since such quantities can be measured experimentally, our bound can be used to infer bounds on the entropy production rate in systems where the latter is not directly accessible.

The presented simulation results, further, indicate that the conjecture could be generalized to higher dimensions. Surprisingly, the conjectured bound that is founded on free diffusion in one dimension also shows to bound diffusion in higher dimensions. Further analysis is, however, necessary especially regarding currents that contain velocities of different spatial directions multiplicatively. In this case, our data suggest that it is possible to get tighter bounds by adjusting the weight of the free diffusion process that is used for comparison.

The short-time behavior of the conjecture, however, also sparks the question how to proof such a dependence. One possibility, to achieve this short-time behavior using the established large deviations framework is to consider the steady state of the original dynamics as a transient initial condition [69, 67] that evolves according to a suited virtual dynamic, see Sec. 6.2. In the velocity, such a transition to a new steady state takes place on the same timescale γ/m as the observed change in the bounding function. Such an ansatz was outlined in Sec. 6.2.1, but requires to solve the complete relaxation in the perturbed steady state.

Underdamped thermodynamic bounds that have been derived so far can be associated with the activity bound or the bound obtained by γ-rescaling. A third class of bounds that is derived from the fluctuation theorem has been discussed [77, 78] more recently. The bound reduces to the statement of the TUR in the linear-response limit for overdamped and underdamped motion, thus providing another proof for the validity of the TUR in this limit [60, 61]. For larger driving, the tightness of the bound, however, rapidly decreases.

Additional bounds can be straightforwardly derived by making new ansatzes. A promising idea is to use the known collapse of the empirical density in the overdamped limit, see Sec. 5.4.3, and adapt it to reflect the ansatz used in the proof of the overdamped TUR. By doing so, the ansatz can be directly used in the underdamped regime. Plugging in the stationary overdamped density $p^{\mathrm{ov,\,ss}}(x)$ and the rescaled stationary current J^{ss} in the master ansatz Eq. (5.4.1) yields

$$\rho^*(x,v;\tilde{J}) = p^{\mathrm{ov,\,ss}}(x)\sqrt{\frac{m}{2\pi T}}\exp\left[-\frac{m}{2T}\left(v-\frac{\tilde{J}}{Lp^{\mathrm{ov,\,ss}}(x)}\right)^2\right] \tag{6.4.1}$$

in one dimension and for $x \in [0, L]$. Since the stationary distribution follows the same asymptotic transition, the overdamped ansatz can more generally be expressed as

$$\rho^*(x, v; \tilde{J}) = p^{\mathrm{ss}}\left(x, v - \frac{\tilde{J} - J^{\mathrm{ss}}}{L \int dv' p^{\mathrm{ss}}(x, v')}\right) \tag{6.4.2}$$

which coincides with the stationary distribution for $\tilde{J} = J^{\mathrm{ss}}$ as desired.

Such an ansatz that essentially shifts the stationary distribution in the velocity has the appropriate shift in the average observable that gives the stationary current in the denominator of the bound. Moreover, it is similar in spirit to the typical densities expected for free diffusion which consist of the shifted stationary distribution, see Sec. 5.1. Promising at first, the problem becomes apparent when the level 2 LDF is evaluated as it yields integrals with finite boundaries over the stationary distribution. As a result, the bound lacks a physical interpretation and requires knowledge of the complete stationary distribution.

A full proof of the bound (6.3.2) for underdamped dynamics would probably require large deviation techniques that go beyond the established methods. Insight might also come from martingale methods [23, 79], which at the current stage still requires the diffusion tensor to be invertible, which is not the case for underdamped diffusion in phase space. Nevertheless, the method follows a similar rationale as the free diffusion bound. In more detail, the bound follows by splitting the stochastic observable in an increasing process an a fluctuating martingale and estimating its statistics by the martingale subprocess. The free diffusion bound, on the other hand, can be interpreted as a splitting of reversible and irreversible contributions. Apparently, the reversible contributions increase the uncertainty product so that it is bound by the uncertainty product of the irreversible part.

Chapter 7

Beating the overdamped TUR limit

So far, we have focused on forces that do not depend on the velocity. In such systems, the numerical results presented so far suggest that the TUR holds regularly for large times. For underdamped dynamics, forces that depend on the velocity as well are, however, rather common. Most prominently, velocity-dependent forces appear in presence of a magnetic field in form of the Lorentz force that is proportional to the velocity. Other incidents include models for feedback cooling [80, 81, 82] where the friction coefficient is effectively reduced [83] or even of non-linear nature [84] and active matter [85, 86, 87].

For such generalized forces, a breakdown of the overdamped bound on the precision is not particularly surprising as such forces can be used to implement feedback mechanism that lower the uncertainty [88]. For instance in the case of feedback cooling, the particle is effectively subject to a lower temperature in comparison to the temperature reflected in the bound. Furthermore, more involved steering mechanisms can be implemented that limit the velocity fluctuations.

In a stochastic model of ballistic transport in multiterminal conductors, a violation of the TUR was, however, also observed in the presence of a magnetic field [60, 61]. This violation is less obvious, as the magnetic field does not break the fluctuation-dissipation theorem. Mathematically and rather abstract, the breakdown of the TUR in such models can be explained by the broken Onsager symmetry.

As an extension to the analysis in multiterminal conductor models, it is natural to investigate the effects of a magnetic field on the TUR in continuous underdamped Langevin systems [89]. To this end, we revisit the Brownian gyrator and indeed observe a violation of the TUR. In order to get an intuition on the effects contributing to an increase of precision, we introduce a more transparent model before we conclude the focus on generalized forces.

7.1 The Brownian gyrator in a magnetic field

The Brownian gyrator that has been introduced in Sec. 6.3.3 is a good starting point for the analysis. Due to its simplicity it is still solvable analytically. However, the dynamics showed to be more complex than free diffusion thus alowing for a more general perspective on the effect of magnetic forces. Finally, the model is also relevant from an experimental point of view as pointed out before.

7.1.1 The model

As an analytically traceable model, we revisit the underdamped Brownian gyrator in this section. In addition to the previously considered circular driving force κ and the harmonic force with constant k, a Lorentz force $\boldsymbol{F}_{\mathrm{L}}(\boldsymbol{v}) = qB(v_2, -v_1)^{\intercal}$ induced by a magnetic field of strength B that is perpendicular to the plane of the particle motion acts on the particle of charge q. In the following, we collect the charge and magnetic field in the product $b \equiv qB$.

The resulting dynamics is still linear and governed by the Langevin equation

$$\begin{aligned} \dot{\boldsymbol{x}} &= \boldsymbol{v} \\ m\dot{\boldsymbol{v}} &= \begin{pmatrix} -k & \kappa \\ -\kappa & -k \end{pmatrix} \boldsymbol{x} + \begin{pmatrix} -\gamma & b \\ -b & -\gamma \end{pmatrix} \boldsymbol{v} + \boldsymbol{\xi} \end{aligned} \tag{7.1.1}$$

which in addition to Eq. (6.3.14) contains the Lorentz force.

When the real parts of all eigenvalues of the dynamics are positive, the system is stable and the probability distribution eventually converges to a steady state. This stability condition of the system is given by

$$\gamma k + \kappa b - \kappa^2 m/\gamma > 0. \tag{7.1.2}$$

In other words, the particle can be confined by the potential if the strength of torque $|\kappa|$ is moderate enough to satisfy the stability condition, otherwise the particle escapes from the potential. A magnetic field can further stabilize the system if κ and b have the same sign. On the other side, different signs of κ and b reduces the stability.

This is due to the Lorentz force pushing the particle either inward or outward of the potential depending on the sign of κb. When $\kappa b < 0$, the magnetic field reinforces the tendency to increase the radial distance. When $\kappa b > 0$, however, the Lorentz force makes the particle prefer to head towards the center of the potential. The additional stabilization due to a magnetic field can be observed in the center column of Fig. 7.1.1. While a negative product κb increases the radius of typical trajectories in the $\boldsymbol{x}$-plane, the motion becomes more centered for higher magnetic fields. The localization effect only occurs in the presence of both the external torque and the magnetic field.

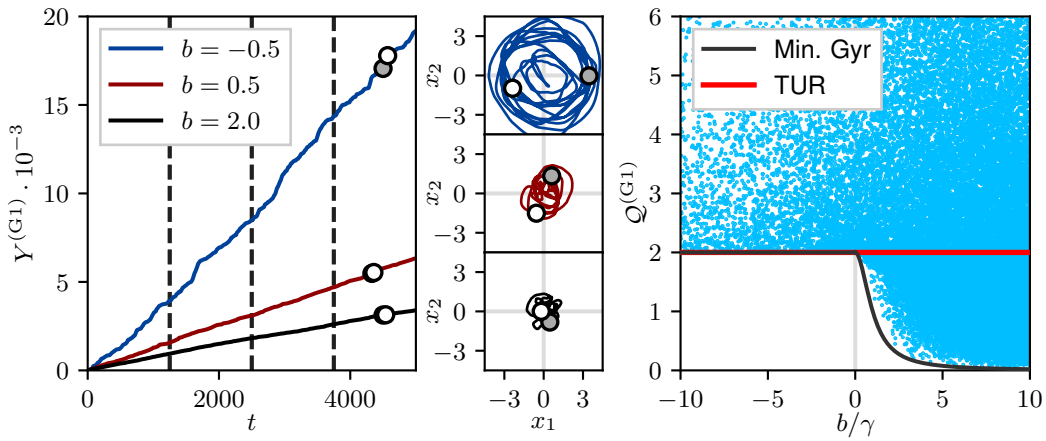

FIGURE 7.1.1: *Left* and *center column*: Sample trajectories of the integrated current $Y^{(G1)}(\mathcal{T})$ and corresponding motion in the x_1-x_2-plane. The shown $\boldsymbol{x}$-motion in the center column corresponds to the intervals that are marked with dots in the left axis. From top to bottom the magnetic field is increased with driving $\kappa = 1$.
Right column: Scatter plot of the uncertainty product for the Gyrator in presence of a magnetic field, Eq. (7.1.11), evaluated for different parameters. The solid black line corresponds to the minimal uncertainty product, Eq. (7.1.14) while the red line gives the bound expected from the overdamped TUR.

7.1.2 Exact expressions of mean value and diffusion coefficient

Due to the linear character of the dynamics, Eq. (7.1.1), the cumulants of motion can be calculated analytically for integrated currents that depend linear on $\boldsymbol{x}$ and $\boldsymbol{v}$, respectively, such as the particle current Eq. (6.3.17)

$$Y_1^{(G1)}(\mathcal{T}) = \int_0^{\mathcal{T}} dt\, [x_2(t)v_1(t) - x_1(t)v_2(t)] \tag{7.1.3}$$

or the accumulated work done against the driving torque κ. This can be done by calculating the largest eigenvalue of the tilted operator. In the shorthand notation $\boldsymbol{z} = (x_1, x_2, v_1, v_2)^\mathsf{T}$ the adjoint of the tilted operator for the current $Y_1^{(G1)}(\mathcal{T})/\mathcal{T}$ takes on the form

$$\mathcal{L}^\mathsf{T}(\lambda) = \boldsymbol{z} \cdot \mathsf{A}^\mathsf{T} \nabla_{\boldsymbol{z}} + \nabla_{\boldsymbol{z}} \cdot \mathsf{D} \nabla_{\boldsymbol{z}} + \lambda \boldsymbol{z} \cdot \mathsf{W} \boldsymbol{z} \tag{7.1.4}$$

with the matrices

$$\mathsf{A} \equiv \frac{1}{m} \begin{pmatrix} 0 & 0 & m & 0 \\ 0 & 0 & 0 & m \\ -k & \kappa & -\gamma & b \\ \kappa & k & -b & -\gamma \end{pmatrix} \qquad \mathsf{W} = \begin{pmatrix} 0 & 0 & 0 & -1 \\ 0 & 0 & 1 & 0 \\ 0 & 0 & 0 & 0 \\ 0 & 0 & 0 & 0 \end{pmatrix} \tag{7.1.5}$$

and the diagonal diffusion matrix $\mathsf{D} = \mathrm{diag}[0, 0, kT\gamma/m^2, kT\gamma/m^2]$.

To solve the eigenvalue problem for this adjoint tilted operator, we make a Gaussian ansatz

$$g(z, \lambda) = \exp\left(-\frac{1}{2} z \cdot \mathbb{C}(\lambda) z\right) \tag{7.1.6}$$

with a symmetric matrix $\mathbb{C}(\lambda)$. Since the untilted Fokker-Planck operator preserves probability, the left eigenfunction for $\lambda = 0$ is a constant and thus $\mathbb{C}(0) = 0$.

Applying $\mathcal{L}(\lambda)$ on the eigenvalue equation yields the condition

$$\frac{1}{2}\left[\mathsf{A}^\intercal \mathbb{C}(\lambda) + \mathbb{C}(\lambda)\mathsf{A} + \mathsf{W} + \mathsf{W}^\intercal\right] = \mathbb{C}(\lambda)\mathsf{D}\mathbb{C}(\lambda) \tag{7.1.7}$$

and an eigenvalue that is simply the trace

$$\alpha(\lambda) = -\mathrm{tr}\left[\mathsf{D}\mathbb{C}(\lambda)\right] \tag{7.1.8}$$

which indeed is the largest eigenvalue as it vanishes for $\lambda = 0$.

Since we are only interested in the first and second cumulant we can expand $\mathbb{C}(\lambda) = \lambda \mathbb{C}_1 + \lambda^2 \mathbb{C}_2$ in second order of λ around 0. This allows to solve Eq. (7.1.7) for each order individually. The cumulants turn out to be

$$\left\langle Y_1^{(\mathrm{G1})}(\mathcal{T})\right\rangle = \mathcal{T}\frac{2\kappa T}{b + k\gamma/\kappa - m\kappa/\gamma} \tag{7.1.9}$$

and

$$\mathrm{Var}\left[Y_1^{(\mathrm{G1})}(\mathcal{T})\right] = \mathcal{T}\frac{4\left(\gamma^2 k^2/\kappa + b\kappa^2 m/\gamma + \kappa\gamma^2 + 3m\kappa k\right)T^2}{\left(b + \gamma k/\kappa - m\kappa/\gamma\right)^3} \quad ; (\mathcal{T} \gg \frac{\gamma}{m}). \tag{7.1.10}$$

Employing the balance of work and heat in the steady state, the uncertainty product is given by

$$\mathcal{Q}^{(\mathrm{G1})}(\mathcal{T}) = \frac{2\left(\gamma^2 k^2/\kappa^2 + b\kappa m/\gamma + \gamma^2 + 3mk\right)}{\left(b + \gamma k/\kappa - m\kappa/\gamma\right)^2} \tag{7.1.11}$$

$$\geq 2\frac{\left(\gamma k + m\kappa^2/\gamma\right)^2 + \kappa^2\gamma^2}{\left(b\kappa + \gamma k - m\kappa^2/\gamma\right)^2} \tag{7.1.12}$$

for large times. Here, the last line follows by inserting the stability condition, Eq. (7.1.2).

7.1.3 Effect of a magnetic field on the TUR

After having obtained the analytice expression for the uncertainty product, we can now easily investigate different parameter regimes of the Brownian gyrator.

Upon looking at the expression, it is trivial that the uncertainty product is always larger than 2 for $b\kappa \leq 0$. Evaluating the uncertainty product for different parameters as shown in Fig. 7.1.1, however, shows that it can fall below 2 for $b\kappa > 0$ thus violating the TUR. Since the last in Eq. (7.1.12) is monotonic in m/γ, the overdamped inertia limit $m/\gamma \to 0$ produces the natural estimate

$$\lim_{\mathcal{T}\to\infty} \mathcal{Q}^{(\mathrm{G1})}(\mathcal{T}) \geq 2\frac{\gamma^2 k^2 + \kappa^2\gamma^2}{(b\kappa + \gamma k)^2} = 2\frac{1+\kappa^2/k^2}{(1+b\kappa/(\gamma k))^2} \geq \frac{2}{1+(b/\gamma)^2} \tag{7.1.13}$$

which in turn can be minimized for $b/\gamma = \kappa/k$, ultimately leading to the simple expression

$$\lim_{\mathcal{T}\to\infty} \mathcal{Q}^{(\mathrm{G1})}(\mathcal{T}) \geq \frac{2}{1+(b/\gamma)^2} \tag{7.1.14}$$

which is plotted in Fig. 7.1.1 as solid line.

For large magnetic fields, this bound and with it the uncertainty product can approach 0. However, this comes with the caveat of a decreasing current as Eq. (7.1.9) goes to 0 in the same limit. This decrease with increasing strength of the magnetic field is a result of a stronger localized motion of the particle.

The localization of motion also seems responsible for the breakdown of the TUR in the gyrator. Although both the mean rate and dispersion become smaller for large magnetic fields individually, the squared relative uncertainty ϵ^2 converges to a finite value. The dissipated heat, on the other hand, is proportional to the particle current and thus scales as b^{-1}, leading to the uncertainty product approaching 0 for large magnetic fields.

Nevertheless, the breakdown of the TUR cannot be solely ascribed to the decrease of the entropy production as a consequence of the localization. The validity of the TUR crucially depends on the chosen observable. To compare conceptually different currents we consider the class of winding number currents that basically counts the number of crossings of the positive x_1-axis with a weighting factor $\phi(z)$. Formally this current is given by

$$Y^{\phi}(\mathcal{T}) = \int_0^{\mathcal{T}} dt\, \phi(z(t))\delta(x_2(t))\mathrm{sign}\left[v_2(t)\right]\chi_{x_1} \tag{7.1.15}$$

where χ_{x_1} is an indicator that is 1 if $x_1 > 0$ and 0 otherwise. The uncertainty product associated with the current $Y^{\phi}(\mathcal{T})$ is given as

$$\mathcal{Q}^{\phi} \equiv \lim_{\mathcal{T}\to\infty} \frac{\mathrm{Var}\left[Y^{\phi}(\mathcal{T})\right]}{\langle Y^{\phi}(\mathcal{T})\rangle^2}\sigma\mathcal{T} \tag{7.1.16}$$

An advantage of such a winding number current is that it could be directly measured in experimental situations without tracing complete trajectories of the particle.

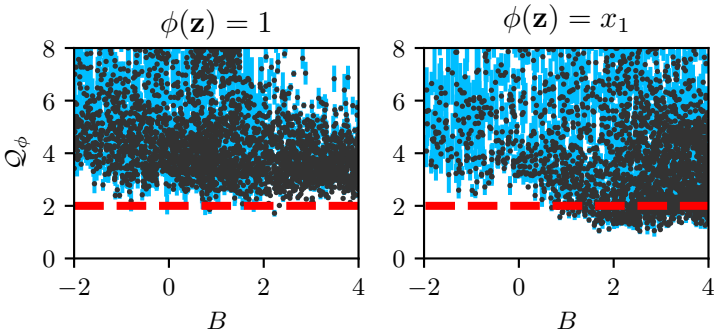

FIGURE 7.1.2: Numerical results for the uncertainty product $\mathcal{Q}_\phi$ for the winding number current (7.1.15) with two different weighting factors $\phi(z) = 1$ (left) and $\phi(z) = x_1$ (right). Each dot represents one stable parameter set with $B \in [-2, 4]$, $\kappa \in [0.05, 5]$, $k \in [0, 4]$, $\gamma \in [0.1, 10]$, $T \in [0.5, 1.5]$. The mass m is set to unity. The entropy production rate σ is calculated on base of the analytic expression, Eq. (7.1.9). The vertical blue lines are an estimator for the error. The error is estimated by calculating the 25 % percentile for the slope of the mean current and its variance on an ensemble of trajectories. The error of the uncertainty product then follows by propagation of error.

Since it is not possible to calculate the uncertainty product analytically, we numerically calculate the winding number current for two conceptually different weighting factors $\phi(z) = 1$ and $\phi(z) = x_1$. The gyrator with constant weight can be interpreted as a continuous Brownian clock. Such systems are of special interest in the context of biochemical oscillations [90, 91]. In contrast, the latter case of increasing weight is inspired by the particle current considered so far, Eq. (7.1.3). The uncertainty products for both weights are depicted in Fig. 7.1.2 for random parameters. The results show that the uncertainty product goes well below 1 for the increasing weight. The uncertainty product of the current with constant weight, however, seems to be bounded from below by 1 in the margin of error. In this special case the contribution to the current is independent from the radial distance and thus the localization of motion does not affect the current as strongly.

In principle, an inequality dubbed the "hysteretic thermodynamic uncertainty relation" [92], which takes into account both the original and a time-reversed dynamics, can be applied to models with broken time-reversal symmetry. In the case of the gyrator model, applying the relation is, however, only possible for a weak magnetic field. For strong magnetic fields the time-reversed dynamics can become unstable since the stability condition (7.1.2) is not symmetric with respect to b. Moreover, the activity bound that was derived in Sec. 6.1.1 can be generalized to include velocity dependent forces as

well [62]. In their respective range of validity both inequalities provide exponentially weaker lower bounds on the uncertainty product than the putative TUR, Eq. (3.45), does. Given these shortcommings, a theory that describes the breakdown of the TUR or the physical relevance behind the tight estimate Eq. (7.1.14) is still missing.

7.2 An illustrative model with magnetic field

In the previous section the Brownian gyrator was introduced as a physically feasible yet simple model. In this model, the TUR can be violated when a magnetic field reinforces the constraining character of the harmonic potential. However, this does not generalize to arbitrary currents. For instance, the uncertainty product of the winding number current that essentially counts the revolutions in the gyrator does not fall below the expected bound of 2. Unfortunately, studying different currents in the gyrator is troublesome since many currents vanish due to the symmetry in the system. In contrast, measuring more general currents, as the winding number current, requires numerical analysis that is prone to errors.

To further examine the effect of the current of choice on the uncertainty, we boil the gyrator down to a more illustrative and transparent model that shares some of its characteristics with the Brownian gyrator: Diffusion in a infinitely long harmonic channel with a magnetic field oriented perpendicular to the plane of motion.

7.2.1 Model and Cumulants

The motion is described by the two-dimensional underdamped Langevin equation

$$\dot{\boldsymbol{x}} = \boldsymbol{v} \qquad \dot{\boldsymbol{v}} = -\begin{pmatrix} 0 \\ k \end{pmatrix} \cdot \boldsymbol{x} + \begin{pmatrix} f \\ 0 \end{pmatrix} + \begin{pmatrix} -\gamma & b \\ -b & -\gamma \end{pmatrix} \cdot \boldsymbol{v} + \boldsymbol{\xi} \tag{7.2.1}$$

which is a channel that is confined harmonically in x_2 direction and driven by a force F in x_1 direction. As for the gyrator, a magnetic field of strength B is applied perpendicular to the $\boldsymbol{x}$-plane. As before, the strength of the induced Lorentz force is given by $b = Bq$.

The stationary distribution is a shifted Gaussian

$$p^{\mathrm{ss}}(\boldsymbol{x}, \boldsymbol{v}) \propto \exp\left[-\frac{k}{2T}\left(x_2 + \frac{b}{k}\frac{mf}{\gamma}\right)^2 - \frac{m}{2T}\left(v_1 - \frac{mf}{\gamma}\right)^2 - \frac{m}{2T}v_2^2\right] \tag{7.2.2}$$

where, logically, the mean of v_1 is shifted due to the external driving force. Furthermore, the mean displacement in direction x_2 is increased by the interaction of the magnetic field and the driving force. The Lorentz force pushes

the particle up the walls of the harmonic confinement due to the non-zero mean velocity in v_1 direction.

We are interested in the cumulants for an observable

$$Y^{(\mathrm{C})}_{(k1,k2)}(\mathcal{T}) = \int_0^{\mathcal{T}} dt (k_1 + k_2 x_2(t)) v_1(t) \tag{7.2.3}$$

that is the average velocity along the channel weighted by an factor that depends on the excursion. It is worth noting that the constant contribution k_1 can also be introduced by a force in x_2 direction that shifts the center of the channel or by an offset in the x_2 coordinate.

As outlined in the previous section, the cumulants can be calculated via the adjoint tilted operator

$$\mathcal{L}^{\mathsf{T}}(\lambda) = \boldsymbol{z} \cdot \mathsf{A}_{\mathrm{C}}^{\mathsf{T}} \nabla_{\boldsymbol{z}} + \nabla_{\boldsymbol{z}} \cdot \mathsf{D}_{\mathrm{C}} \nabla_{\boldsymbol{z}} + \lambda(\boldsymbol{w} + \boldsymbol{z} \cdot \mathsf{W}_{\mathrm{C}}) \cdot \boldsymbol{z} + v_1 \partial_{x1} + \boldsymbol{f} \nabla_{\boldsymbol{z}} \tag{7.2.4}$$

that acts on the vector $\boldsymbol{z} = (x_2, v_1, v_2)^{\mathsf{T}}$. Here, the matrices are

$$\mathsf{A}_{\mathrm{C}} \equiv \frac{1}{m} \begin{pmatrix} 0 & 0 & m \\ 0 & -\gamma & b \\ -k & -b & -\gamma \end{pmatrix} \qquad \boldsymbol{w} = \begin{pmatrix} 0 \\ k_1 \\ 0 \end{pmatrix} \qquad \mathsf{W}_{\mathrm{C}} \equiv \begin{pmatrix} 0 & k_2 & 0 \\ 0 & 0 & 0 \\ 0 & 0 & 0 \end{pmatrix} \tag{7.2.5}$$

and the diagonal diffusion matrix is given by $\mathsf{D}_{\mathrm{C}} = \mathrm{diag}[0, kT\gamma/m^2, kT\gamma/m^2]$.

Plugging the shifted Gaussian

$$g(\boldsymbol{z}) = \exp\left[-\boldsymbol{z} \cdot \mathbb{C}(\lambda) \boldsymbol{z} - \boldsymbol{a}(\lambda) \cdot \boldsymbol{z}\right] \tag{7.2.6}$$

with yet undetermined symmetric matrix $\mathbb{C}(\lambda)$ and vector $\boldsymbol{a}(\lambda)$ as an ansatz in the tilted operator yields the conditions

$$\frac{1}{2}\left(\mathbb{C}(\lambda)\mathsf{A}_{\mathrm{C}} + \mathsf{A}_{\mathrm{C}}^{\mathsf{T}}\mathbb{C}(\lambda)\right) = \mathbb{C}(\lambda)\mathsf{D}_{\mathrm{C}}\mathbb{C}(\lambda) + \frac{\lambda}{2}\left(\mathsf{W}_{\mathrm{C}} + \mathsf{W}_{\mathrm{C}}^{\mathsf{T}}\right) \tag{7.2.7}$$

$$\mathsf{A}_{\mathrm{C}}^{\mathsf{T}} \boldsymbol{a}(\lambda) + \mathbb{C}(\lambda)\boldsymbol{f} = 2\mathbb{C}(\lambda)\mathsf{D}_{\mathrm{C}}\boldsymbol{a}(\lambda) + \lambda \boldsymbol{w}, \tag{7.2.8}$$

where the two lines guarantee that the terms in second and first order in $\boldsymbol{z}$, respectively, vanish. From these, the elements of $\boldsymbol{a}$ and D_{C} can be obtained by expansion in λ which in term defines the eigenvalue

$$\alpha(\lambda) = -\mathrm{Tr}\left[\mathsf{D}_{\mathrm{C}}\mathbb{C}(\lambda)\right] + \boldsymbol{a}(\lambda) \cdot \mathsf{D}_{\mathrm{C}}\boldsymbol{a}(\lambda) - \boldsymbol{f} \cdot \boldsymbol{a}(\lambda). \tag{7.2.9}$$

As before the conditions Eqs. (7.2.7) and (7.2.8) can be expanded in orders of λ and the solution can subsequently be used to calculate the first and second derivative of the eigenvalue. While the mean of the observable takes on the compact form

$$\left\langle Y^{(\mathrm{C})}_{(k1,k2)}(\mathcal{T}) \right\rangle = \mathcal{T}\frac{f}{\gamma}\left(k_1 - k_2 \frac{bf}{k\gamma}\right), \tag{7.2.10}$$

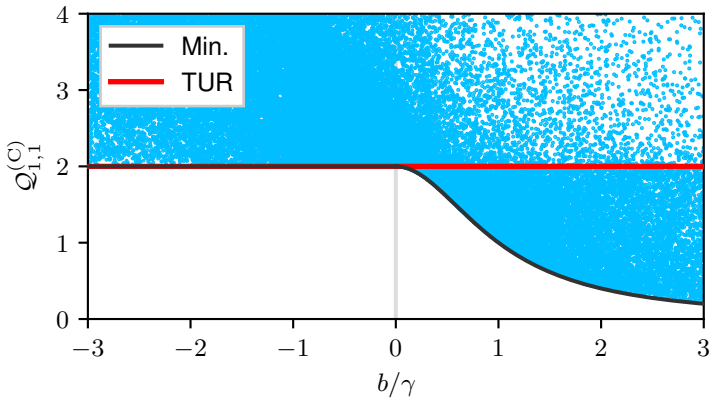

FIGURE 7.2.1: Scatter plot of the TUR, Eq. (7.2.12), in the channel for different parameters and positive force $f > 0$. The observable of choice is the current Eq. (7.2.3) with $k_1 = k_2 = 1$. The red line corresponds to the overdamped TUR. The black line depicts the minimum of the uncertainty product which coincides with the minimum of the gyrator, Eq. (7.1.14).

the variance is more complex and will not be given explicitly. The mean value has two contributions. First, the observable increases as a consequence of the regular current in 1-direction when $k_1 \neq 0$. Second, there is a contribution that is proportional to k_2 and involves the mean displacement from the center due to the Lorentz force and the mean velocity in v_1 direction. Both contributions can be interpreted in a static image by picturing a particle moving with mean speed $\langle v_1 \rangle = f/\gamma$ along $\langle x_2 \rangle = bf/(k\gamma)$.

Since a force is only applied in one direction, the entropy production is the same as for free diffusion in one dimension $\sigma = mf^2/(\gamma T)$. From this, we can calculate the associated uncertainty product

$$\mathcal{Q}^{(k_1,k_2)} = \frac{\mathrm{Var}\left[Y^{(C)}_{(k1,k2)}(\mathcal{T})\right]}{\left\langle Y^{(C)}_{(k1,k2)}(\mathcal{T})\right\rangle^2}\sigma\mathcal{T} \tag{7.2.11}$$

for any weighting in the observable (7.2.3) which yields the rather complex expression

$$\mathcal{Q}^{(k_1,k_2)} = 2 + 2\frac{\left[\frac{f^2}{k^2}\left(1+\frac{3b^2}{\gamma^2}\right) - 2\frac{bfk_1}{k\gamma k_2} + \frac{(b^2+\gamma^2)T}{k(b^2+\gamma^2+km/2)}\right]}{\left(\frac{k_1}{k_2} - \frac{bf}{k\gamma}\right)^2}. \tag{7.2.12}$$

This expression can be easily evaluated for arbitrary parameters as shown in Fig. 7.2.1.

7.2.2 Effect of the weight on the TUR

Now that we have described a method to calculate the uncertainty product for different weighting, we can analyze the effect of different forms of the weighting function on the uncertainty product.

First we consider the mean current in the channel without an x_2-dependence, e.g. $k_2 = 0$. For this choice, the first condition Eq. (7.2.7) does not show any λ-dependence and can thus be solved by $\mathbb{C}(\lambda) = \mathbf{0}$. As a result, the shift becomes

$$\boldsymbol{a}(\lambda) = \lambda k_1 \left(-\frac{b}{\gamma}, -\frac{m}{\gamma}, 0\right)^{\mathsf{T}}. \tag{7.2.13}$$

Inserting this expression in the expression for the eigenvalue and calculating the mean velocity and variance reveals that neither of both quantities is dependent on the magnetic field. In fact, the uncertainty product $\mathcal{Q}^{(k_1,0)}$ is 2 independently of the choice of the parameters.

In other words, the sole existence of a magnetic field does not break the TUR. This finding is also in line with the numerical indication for a TUR bounding the uncertainty of the winding number current in the gyrator and the ballistic transport in a multiterminal model, where the TUR can be recovered for two terminals [60].

If there is no contribution $k_1 = 0$ all terms in the uncertainty product, Eq. (7.2.12), are positive thus also preserving the lower bound of 2. Only in interaction with k_1, the TUR can become lower than this bound for specific parameter sets. As discussed, the TUR holds for a negative magnetic field and positive force. In contrast, when the sign of f and b is different, the TUR can be violated. Interestingly, the minimal uncertainty product coincides with the one from the gyrator, Eq. (7.1.14), but is attained for $m \to \infty$ and a different optimal force

$$f^* = \frac{b\gamma k}{2b^2 + \gamma^2} \frac{k_1}{k_2}. \tag{7.2.14}$$

7.3 Conclusion

In this chapter we have investigated the effect of a velocity-dependent force on the TUR, in particular of a magnetic field. To this end we first revisited the Brownian gyrator as a simple, yet relevant model consisting of a charged particle driven inside a two-dimensional harmonic confinement. Using the analytic results, we observe that the uncertainty product for the accumulated distance traveled in the gyrator can go below the bound implied by the TUR, if the Lorentz force typically pushes the particle inwards thus leading to a larger localization.

To pinpoint the reason for the breakdown of the TUR, we consider the winding number current that essentially counts the number of revolutions in

the gyrator irrespective of the distance to the center of symmetry. The TUR does hold for such an observable for arbitrary magnetic field in the margin of error.

In order to analyze the dependence on the choice of the current in more depth, we consider a more stripped down model consisting of a particle diffusing in a harmonic channel. We can analytically evaluate the uncertainty product for linear weighting that is applied perpendicular to the channel. The results underline the observations from the gyrator model. The TUR is recovered for a flat weighting that resembles the winding number current. For an increasing weight, in contrast, the TUR can be violated for a driven particle if a magnetic field is present.

Notably, the magnetic field neither causes a localization in the channel model nor causes an increase in the current due to circular trajectories. As a consequence, the violation can not be attributed to a localization that leads to less dissipation, as for the gyrator, or to a sole increase of the current due to circular paths.

Overall, the reason for the violation is not only due to the magnetic field but rather an interplay between the choice of observable, the driving force and the Lorentz force itself. The reduced uncertainty can be traced back to a term in the variance that can become negative. One interpretation is that the magnetic field allows a kind of feedback that actively steers the particle. If we consider a positive force and a negative magnetic field, the particle settles at at negative mean position. If the particle moves faster, the Lorentz force increases and the particle is pushed down against the harmonic potential. In the contrary case of a slower particle, the Lorentz force does not balance the harmonic potential and the particle falls down towards the center of the potential. This difference can be used to "control" the particle. If the absolute contribution to the observable, i.e. the weight, is typically larger for the slower particle and smaller for the faster ones, fluctuations in the rate of growth of the observable are smoothed out. This way, the weight compensates for the fluctuations in the velocity. In this sense, the magnetic field acts just like an additional velocity-dependent feedback $-\alpha v$ that is used in models for feedback cooling.

The same interpretation can be directly applied to the gyrator model. Only if the weighting increases with the radius, as for the distance traveled or the work current, the magnetic field can be used as a feedback mechanism. For the winding number current, such a feedback mechanism cannot be implemented and the TUR is recovered for arbitrary magnetic fields.

Chapter 8

Concluding Perspective

Although originally introduced as a conjecture for discrete Markov networks in 2015 [12], the thermodynamic uncertainty relation has proofed as a universal property of stochastic systems and sparked a number of related research. Using large deviation theory it was possible to proof the relation for discrete Markov jump processes [38] and continuous overdamped Langevin dynamics [39]. Utilizing the large deviation framework helped to reveal a large class of thermodynamic inequalities and to embed the TUR in this class of relations.

Modified versions for discrete time [93], high dimensional observables [67], arbitrary initial states [67, 94], periodically driven systems [95, 96] and quantum systems [97, 98, 99] have been presented subsequently. Despite the achievements in the respective fields, the putative generalization to underdamped dynamics still is pending. Although no definite proof was provided in this thesis, it shows many features that motivate further analysis and reveals challenges that have to be met.

The underdamped dynamics provide much more freedom in both the dynamics and the representable observables. A priori, time-symmetric observables can be treated in the underdamped regime. For such observables, a TUR involving only the irreversibility can never hold as it leads to a contradiction in the equilibrium limit where the latter vanishes. Furthermore, velocity dependent forces can be implemented.

In order to follow the original proof of the overdamped TUR, we introduced the large deviation framework for the underdamped regime in Chapter 3. Unfortunately, it cannot be generalized to underdamped motion straightforwardly. Under the premises of the overdamped contraction principle, one is free to chose an ansatz for the empirical density and, independently, for the empirical current [38, 39]. For underdamped dynamics, in contrast, the continuity equation connects the empirical current and density thus leaving only the latter as a free parameter.

Building on the framework we explored the properties of the underdamped large deviation function in Chapter 5. Overall, the function shares many features with the overdamped LDF. In particular, the numerical data suggests

that a parabolic bound that would imply the TUR holds just like in the overdamped case for large times. This is further substantiated by direct measurements of the uncertainty product.

While not directly applicable to underdamped dynamics, the rational behind the overdamped proof can be transferred to underdamped dynamics. Two different interpretations of the proof, namely a timescale ansatz and an amplification of the irreversible current have been discussed in Chapter 6. Both yield the same bound in the overdamped regime, however, they lead to two conceptually different bounds in the underdamped regime. On the one hand the timescale ansatz provides a typical weak bound and involves terms that characterize the activity. First introduced in Ref. [48], the ansatz has lead to a class of related bounds Refs. [45, 62, 100]. On the other hand, the bound that is based on the rescaling of irreversible contributions involves the entropy production as desired, but does not bound the uncertainty but the derivative of the mean velocity with respect to the friction coefficient. In practice this derivative is hard to obtain.

This ambiguity quite generally poses the question how to interpret the ansatz that yields the overdamped bound and ultimately reveals the physical mechanism that limits the uncertainty. Exploring the consequences for underdamped dynamics might give an indication if the interpretation is relevant. For instance the comparison of the two aforementioned bounds confirms that an important property of the ansatz in fact is that it adapts only the irreversible contribution. Such insights can proof useful in tightening the existing thermodynamic bounds [39], in bringing order in the increasing number of thermodynamic inequalities [101, 102], in exploring the limitations of the original TUR and ultimately in providing new bounds. Furthermore, the TUR could be generalized to a broader class of systems.

Another challenge is the finite-time generalization of the bound. So far, the proofs for the original TUR rely on either large deviation theory or an expansion of the cumulant generating function [69] that results in the Cramér-Rao bound. Since those two methods are essentially equivalent, it is not surprising that both involve a Kullback-Leibler divergence that gives a contribution whenever the empirical distribution does not coincide with the stationary one. While this can be circumvented in the overdamped regime, it is inevitable for underdamped dynamics where one is only allowed to vary this distribution. For small times any other contributions vanish and the Kullback-Leibler divergence becomes dominant. Numerically, an exponential dependence of the uncertainty product is observed for small times that behaves like a relaxation. To reconstruct this effect, the empirical distribution could be time-dependent and follow a relaxation from the original steady state in an empirical one. Such time-dependent ansatzes are also relevant for driven systems with time-depend driving [95] and systems that are not in a steady state [67, 94]. Developing concepts for such time-dependent

ansatzes could improve the quality of existing underdamped bounds in the small-time regime. Moreover, a focus on only this small time regime can also illuminate whether tight and insightful bounds can be derived along the lines of the discussed proofs or if a method that goes beyond the established frameworks has to be found.

More generally, underdamped systems offer a suitable environment to develop a unified and deep understanding. For instance, the analysis of free diffusion in Chapter 4 showed a difference between observables that are even or odd under time-reversal. A similar discrepancy has been observed for discrete dynamics where traffic observables [46] are bound by a different measure than current-like observables. Analysing the range of validity of the activity bound gives an indication that there might exist a bound in the spirit of the TUR that is valid and tight for current-like observables, and a bound for traffic-like, even observables. It would be interesting to further study the differences between these two types of observables and to understand how the precision is bounded.

Additional insight can also be gained from analyzing for which observable the tightest bound can be obtained. It would be of great interest to extend the work done for overdamped particles [103] to the underdamped domain where the velocity-dependence of the observable is an additional degree of freedom.

Another intriguing feature are velocity-dependent forces as discussed in Chapter 7, most notably magnetic fields. Such forces can, however, also be used to implement feedback mechanisms that break the fluctuation-dissipation relation and effectively reduce the temperature in the system [82]. In this thesis, the violations of the TUR in presence of a magnetic field were attributed to a similar effect that "steers" the particle depending on the velocity. Understanding such feedback mechanisms and how they differ from regular potential forces could answer general questions regarding systems under feedback such as active matter. It would be most interesting to see, if the precision can be bound by including additional quantities, i.e. information theoretical measures, as done for fluctuation theorems with feedback and measurement [104, 105, 106]. First advances in this direction have been made recently [88, 100, 94].

Beyond the scope of this thesis, it would be worthwhile to assess the validity of bounds in the case of a spatially varied temperature as well. Although, the dynamics of such systems can also be described in the overdamped regime, the entropy production does not carry over in this limit [17]. In more detail, it is possible that heat is exchanged despite the system reaching an apparent equlibirum state. As a consequence, the overdamped TUR can not be used to estimate the heat. An underdamped uncertainty relation based on observables that can also be measured in the position marginalized view, for instance a directional weight only measuring the current in

one specific direction, could be used to estimate the exchanged heat. Such observables are beyond the scope of the overdamped TUR.

A more universal issue that arose in this thesis is the role of free diffusion. Numerical data suggests that the uncertainty product can be bound for all times by using free diffusion as a reference (see Chapter 6). In fact, the overdamped TUR as well as the ansatzes that lead to its proof can be motivated by a comparison with free diffusion. The exceptional character of a driven process without potential barriars has recently been reported for Markovian jump processes. It was found that not only the second eigenvalue that captures the coherence of oscillations is bounded by the corresponding value for an asymmetric random walk [107], but its complete spectrum [108]. This poses the question, if the TUR is only one manifestation of free diffusion bounding diffusion processes on a more general basis.

Bibliography

[1]R. Brown, "XXVII. A brief account of microscopical observations made in the months of June, July and August 1827, on the particles contained in the pollen of plants; and on the general existence of active molecules in organic and inorganic bodies", Philosophical Magazine Series 2 **4**, 161–173 (1828).

[2]A. Einstein, "Über die von der molekularkinetischen Theorie der Wärme geforderte Bewegung von in ruhenden Flüssigkeiten suspendierten Teilchen", Ann. Phys. **17**, 549 (1905).

[3]M. von Smoluchowski, "Zur kinetischen Theorie der Brownschen Molekularbewegung und der Suspensionen", Ann. Phys. **326**, 756–780 (1906).

[4]M. P. Langevin, "Sur la théorie du mouvement brownien", Comptes Rend. Acad. Sci. (Paris) **146**, 530 (1908).

[5]D. S. Lemons and A. Gythiel, "Paul langevin's 1908 paper "on the theory of brownian motion" ["sur la théorie du mouvement brownien," c. r. acad. sci. (paris) 146, 530–533 (1908)]", American Journal of Physics **65**, 1079–1081 (1997).

[6]H. Kramers, "Brownian motion in a field of force and the diffusion model of chemical reactions", Physica **7**, 284–304 (1940).

[7]G. E. Uhlenbeck and L. S. Ornstein, "On the theory of the brownian motion", Phys. Rev. **36**, 823–841 (1930).

[8]M. Schliwa and G. Woehlke, "Molecular motors", en, Nature **422**, 759–765 (2003).

[9]K. Sekimoto, "Langevin equation and thermodynamics", Prog. Theor. Phys. Supp. **130**, 17 (1998).

[10]U. Seifert, "Entropy production along a stochastic trajectory and an integral fluctuation theorem", Phys. Rev. Lett. **95**, 040602 (2005).

[11]U. Seifert, "Stochastic thermodynamics, fluctuation theorems and molecular machines", Rep. Prog. Phys. **75**, 126001–126009 (2012).

[12]A. C. Barato and U. Seifert, "Thermodynamic uncertainty relation for biomolecular processes", Phys. Rev. Lett. **114**, 158101 (2015).

[13]P. Pietzonka, A. C. Barato, and U. Seifert, "Universal bound on the efficiency of molecular motors", J. Stat. Mech.: Theor. Exp. **2016**, 124004 (2016).

[14]J. Li, J. M. Horowitz, T. R. Gingrich, and N. Fakhri, "Quantifying dissipation using fluctuating currents", en, Nat Commun **10**, 1–9 (2019).

[15]Y. M. Blanter and M. Büttiker, "Rectification of fluctuations in an underdamped ratchet", Phys. Rev. Lett. **81**, 4040–4043 (1998).

[16]A. Dechant, N. Kiesel, and E. Lutz, "Underdamped stochastic heat engine at maximum efficiency", en, EPL **119**, 50003 (2017).

[17]A. Celani, S. Bo, R. Eichhorn, and E. Aurell, "Anomalous Thermodynamics at the Microscale", Phys. Rev. Lett. **109**, 260603 (2012).

[18]J. Gieseler, R. Quidant, C. Dellago, and L. Novotny, "Dynamic relaxation of a levitated nanoparticle from a non-equilibrium steady state", en, Nature Nanotech **9**, 358–364 (2014).

[19]J. Gieseler and J. Millen, "Levitated Nanoparticles for Microscopic Thermodynamics—A Review", en, Entropy **20**, 326 (2018).

[20]É. Fodor, C. Nardini, M. E. Cates, J. Tailleur, P. Visco, and F. van Wijland, "How far from equilibrium is active matter?", Phys. Rev. Lett. **117**, 038103 (2016).

[21]D. Mandal, K. Klymko, and M. R. DeWeese, "Entropy production and fluctuation theorems for active matter", Phys. Rev. Lett. **119**, 258001 (2017).

[22]J. M. Horowitz and T. R. Gingrich, "Proof of the finite-time thermodynamic uncertainty relation for steady-state currents", Phys. Rev. E **96**, 020103 (2017).

[23]S. Pigolotti, I. Neri, É. Roldán, and F. Jülicher, "Generic properties of stochastic entropy production", Phys. Rev. Lett. **119**, 140604 (2017).

[24]A. Dechant and S.-i. Sasa, "Current fluctuations and transport efficiency for general Langevin systems", en, J. Stat. Mech. **2018**, 063209 (2018).

[25]K. Sekimoto, *Stochastic Energetics*, en, Lecture Notes in Physics (Springer-Verlag, Berlin Heidelberg, 2010).

[26]H. Mori, "Transport, Collective Motion, and Brownian Motion*)", Progress of Theoretical Physics **33**, 423–455 (1965).

[27]R. Zwanzig, "Nonlinear generalized langevin equations", Journal of Statistical Physics **9**, 215–220 (1973).

[28]H. Risken, *The Fokker-Planck equation*, 2nd (Springer-Verlag, Berlin, 1989).

[29]W. Sutherland, "Lxxv. a dynamical theory of diffusion for non-electrolytes and the molecular mass of albumin", The London, Edinburgh, and Dublin Philosophical Magazine and Journal of Science **9**, 781–785 (1905).

[30]P. E. Kloeden and E. Platen, *Numerical Solution of Stochastic Differential Equations*, en, Stochastic Modelling and Applied Probability (Springer-Verlag, Berlin Heidelberg, 1992).

[31]H. Touchette, "Introduction to dynamical large deviations of markov processes", Physica A: Statistical Mechanics and its Applications **504**, Lecture Notes of the 14th International Summer School on Fundamental Problems in Statistical Physics, 5–19 (2018).

[32]A. Lazarescu, "The physicist's companion to current fluctuations: one-dimensional bulk-driven lattice gases", Journal of Physics A: Mathematical and Theoretical **48**, 503001 (2015).

[33]M. Chaichian and A. Demichev, *Path integrals in physics. volume i: stochastic processes and quantum mechanics* (Institute of Physics publishing, Bristol and Philadelphia, 2001).

[34]R. E. Spinney and I. J. Ford, "Entropy production in full phase space for continuous stochastic dynamics", Phys. Rev. E **85**, 051113 (2012).

[35]R. Spinney and I. Ford, "Fluctuation relations: a pedagogical overview", in *Nonequilibrium statistical physics of small systems* (John Wiley & Sons, Ltd, 2013) Chap. 1, pp. 3–56.

[36]H. Touchette, "The large deviation approach to statistical mechanics", Physics Reports **478**, 1–69 (2009).

[37]J. Hoppenau, D. Nickelsen, and A. Engel, "Level 2 and level 2.5 large deviation functionals for systems with and without detailed balance", New J. Phys. **18**, 083010 (2016).

[38]T. R. Gingrich, J. M. Horowitz, N. Perunov, and J. England, "Dissipation bounds all steady-state current fluctuations", Phys. Rev. Lett. **116**, 120601 (2016).

[39]M. Polettini, A. Lazarescu, and M. Esposito, "Tightening the uncertainty principle for stochastic currents", Phys. Rev. E **94**, 052104 (2016).

[40]C. Maes, K. Netocny, and B. Wynants, "Steady state statistics of driven diffusions", Physica A **387**, 2675–2689 (2008).

[41]R. L. Jack, M. Kaiser, and J. Zimmer, "Symmetries and Geometrical Properties of Dynamical Fluctuations in Molecular Dynamics", en, Entropy **19**, 562 (2017).

[42]T. R. Gingrich, G. M. Rotskoff, and J. M. Horowitz, "Inferring dissipation from current fluctuations", J. Phys. A **50**, 184004 (2017).

[43]P. Pietzonka, F. Ritort, and U. Seifert, "Finite-time generalization of the thermodynamic uncertainty relation", Phys. Rev. E **96**, 012101 (2017).

[44]B. Øksendal, *Stochastic differential equations: an introduction with applications, sixth edition*, en, Universitext (Springer, Berlin Heidelberg, 2003).

[45]T. Van Vu and Y. Hasegawa, "Uncertainty relations for underdamped langevin dynamics", Phys. Rev. E **100**, 032130 (2019).

[46]J. P. Garrahan, "Simple bounds on fluctuations and uncertainty relations for first-passage times of counting observables", Phys. Rev. E **95**, 032134 (2017).

[47]I. Di Terlizzi and M. Baiesi, "Kinetic uncertainty relation", J. Stat. Mech.: Theor. Exp. **52**, 02LT03 (2019).

[48]L. P. Fischer, P. Pietzonka, and U. Seifert, "Large deviation function for a driven underdamped particle in a periodic potential", Phys. Rev. E **97**, 022143 (2018).

[49]J. Kurchan, "Fluctuation theorem for stochastic dynamics", en, J. Phys. A: Math. Gen. **31**, 3719–3729 (1998).

[50]B. Lindner and I. M. Sokolov, "Giant diffusion of underdamped particles in a biased periodic potential", Phys. Rev. E **93**, 042106 (2016).

[51]M. Žonda, W. Belzig, and T. Novotný, "Voltage noise, multiple phase-slips, and switching rates in moderately damped josephson junctions", Phys. Rev. B **91**, 134305 (2015).

[52]P. Tsobgni Nyawo and H. Touchette, "Large deviations of the current for driven periodic diffusions", Phys. Rev. E **94**, 032101 (2016).

[53]J. Mehl, T. Speck, and U. Seifert, "Large deviation function for entropy production in driven one-dimensional systems", Phys. Rev. E **78**, 011123 (2008).

[54]D. Lacoste, A. W. C. Lau, and K. Mallick, "Fluctuation theorem and large deviation function for a solvable model of a molecular motor", Phys. Rev. E **78**, 011915 (2008).

[55]A. A. Budini, "Fluctuation relations with intermittent non-gaussian variables", Phys. Rev. E **84**, 061118 (2011).

[56]T. Speck, A. Engel, and U. Seifert, "The large deviation function for entropy production: the optimal trajectory and the role of fluctuations", J. Stat. Mech.: Theor. Exp., P12001 (2012).

[57]P. Reimann, C. van den Broeck, H. Linke, P. Hänggi, M. Rubi, and A. Pérez-Madrid, "Giant acceleration of free diffusion by use of tilted periodic potentials", Phys. Rev. Lett. **87**, 010602 (2001).

[58]P. Pietzonka, K. Kleinbeck, and U. Seifert, "Extreme fluctuations of active Brownian motion", New J. Phys. **18**, 052001 (2016).

[59]B. Nguyen, U. Seifert, and A. C. Barato, "Phase transition in thermodynamically consistent biochemical oscillators", J. Chem. Phys. **149**, 045101 (2018).

[60]K. Brandner, T. Hanazato, and K. Saito, "Thermodynamic Bounds on Precision in Ballistic Multiterminal Transport", Phys. Rev. Lett. **120**, 090601 (2018).

[61]K. Macieszczak, K. Brandner, and J. P. Garrahan, "Unified Thermodynamic Uncertainty Relations in Linear Response", J. Stat. Mech.: Theor. Exp. **121**, 130601 (2018).

[62]J. S. Lee, J.-M. Park, and H. Park, "Thermodynamic uncertainty relation for underdamped Langevin systems driven by a velocity-dependent force", arXiv (2019).

[63]C. Maes and M. H. van Wieren, "Time-symmetric fluctuations in nonequilibrium systems", Phys. Rev. Lett. **96**, 240601 (2006).

[64]V. Lecomte, C. Appert-Rolland, and F. van Wijland, "Thermodynamic formalism for systems with markov dynamics", Journal of Statistical Physics **127**, 51–106 (2007).

[65]M. Baiesi, C. Maes, and B. Wynants, "Nonequilibrium Linear Response for Markov Dynamics, I: Jump Processes and Overdamped Diffusions", en, J Stat Phys **137**, 1094 (2009).

[66]G. Falasco and M. Baiesi, "Nonequilibrium temperature response for stochastic overdamped systems", New Journal of Physics **18**, 043039 (2016).

[67]A. Dechant, "Multidimensional thermodynamic uncertainty relations", J. Phys. A: Math. Theor. **52**, 035001 (2019).

[68]M. Baiesi, U. Basu, and C. Maes, "Thermal response in driven diffusive systems", en, Eur. Phys. J. B **87**, 277 (2014).

[69]A. Dechant and S.-i. Sasa, "Fluctuation–response inequality out of equilibrium", Proceedings of the National Academy of Sciences **117**, 6430–6436 (2020).

[70]J. M. Horowitz and T. R. Gingrich, "Proof of the finite-time thermodynamic uncertainty relation for steady-state currents", Phys. Rev. E **96**, 020103 (2017).

[71]N. Grønbech-Jensen and O. Farago, "A simple and effective verlet-type algorithm for simulating langevin dynamics", Molecular Physics **111**, 983–991 (2013).

[72]Filliger, Roger and Reimann, Peter, "Brownian Gyrator: A Minimal Heat Engine on the Nanoscale", **99**, 230602 (2007).

[73]C. Kwon, J. D. Noh, and H. Park, "Nonequilibrium fluctuations for linear diffusion dynamics", Phys. Rev. E **83**, 061145 (2011).

[74]P. Pietzonka and U. Seifert, "Universal trade-off between power, efficiency, and constancy in steady-state heat engines", J. Stat. Mech.: Theor. Exp. **120**, 190602 (2018).

[75]K. H. Chiang, C. L. Lee, P. Y. Lai, and Y. F. Chen, "Electrical Autonomous Brownian Gyrator", Phys. Rev. Lett. **96**, 032123 (2017).

[76] A. Argun, J. Soni, L. Dabelow, S. Bo, G. Pesce, R. Eichhorn, and G. Volpe, "Experimental Realization of a Minimal Microscopic Heat Engine", Phys. Rev. E **96**, 052106 (2017).

[77] P. Pietzonka, "Thermodynamic bounds on current fluctuations", PhD thesis (Universität Stuttgart, 2018).

[78] Y. Hasegawa and T. Van Vu, "Fluctuation theorem uncertainty relation", Phys. Rev. Lett. **123**, 110602 (2019).

[79] I. Neri, É. Roldán, and F. Jülicher, "Statistics of infima and stopping times of entropy production and applications to active molecular processes", Phys. Rev. X **7**, 011019 (2017).

[80] J. Mertz, O. Marti, and J. Mlynek, "Regulation of a microcantilever response by force feedback", Applied Physics Letters **62**, 2344–2346 (1993).

[81] P. F. Cohadon, A. Heidmann, and M. Pinard, "Cooling of a mirror by radiation pressure", Phys. Rev. Lett. **83**, 3174–3177 (1999).

[82] P. Bushev, D. Rotter, A. Wilson, F. ç. Dubin, C. Becher, J. Eschner, R. Blatt, V. Steixner, P. Rabl, and P. Zoller, "Feedback cooling of a single trapped ion", Phys. Rev. Lett. **96**, 043003 (2006).

[83] K. H. Kim and H. Qian, "Entropy production of brownian macromolecules with inertia", Phys. Rev. Lett. **93**, 120602 (2004).

[84] A. Dechant, D. A. Kessler, and E. Barkai, "Deviations from boltzmann-gibbs statistics in confined optical lattices", Phys. Rev. Lett. **115**, 173006 (2015).

[85] F. Schweitzer, W. Ebeling, and B. Tilch, "Complex motion of brownian particles with energy depots", Phys. Rev. Lett. **80**, 5044–5047 (1998).

[86] L. Schimansky-Geier and T. Pöschel, eds., *Stochastic Dynamics*, en, Lecture Notes in Physics (Springer-Verlag, Berlin Heidelberg, 1997).

[87] U. Erdmann, W. Ebeling, L. Schimansky-Geier, and F. Schweitzer, "Brownian particles far from equilibrium", The European Physical Journal B - Condensed Matter and Complex Systems **15**, 105–113 (2000).

[88] P. P. Potts and P. Samuelsson, "Thermodynamic uncertainty relations including measurement and feedback", Phys. Rev. E **100**, 052137 (2019).

[89] H.-M. Chun, L. P. Fischer, and U. Seifert, "Effect of a magnetic field on the thermodynamic uncertainty relation", Phys. Rev. E **99**, 042128 (2019).

[90] A. C. Barato and U. Seifert, "Cost and precision of brownian clocks", Phys. Rev. X **6**, 041053 (2016).

[91] R. Marsland, W. Cui, and J. M. Horowitz, "The thermodynamic uncertainty relation in biochemical oscillations", Journal of The Royal Society Interface **16**, 20190098 (2019).

[92]K. Proesmans and J. M. Horowitz, "Hysteretic thermodynamic uncertainty relation for systems with broken time-reversal symmetry", Journal of Statistical Mechanics: Theory and Experiment **2019**, 054005 (2019).

[93]K. Proesmans and C. Van den Broeck, "Discrete-time thermodynamic uncertainty relation", Europhys. Lett. **119**, 20001 (2017).

[94]K. Liu, Z. Gong, and M. Ueda, "Thermodynamic Uncertainty Relation for Arbitrary Initial States", arXiv:1912.11797 [cond-mat], arXiv: 1912.11797 (2019).

[95]T. Koyuk, U. Seifert, and P. Pietzonka, "A generalization of the thermodynamic uncertainty relation to periodically driven systems", J. Phys. A: Math. Theor. **52**, 02LT02 (2019).

[96]T. Koyuk and U. Seifert, "Operationally accessible bounds on fluctuations and entropy production in periodically driven systems", Phys. Rev. Lett. **122**, 230601 (2019).

[97]B. K. Agarwalla and D. Segal, "Assessing the validity of the thermodynamic uncertainty relation in quantum systems", Phys. Rev. B **98**, 155438 (2018).

[98]K. Ptaszy ński, "Coherence-enhanced constancy of a quantum thermoelectric generator", Phys. Rev. B **98**, 085425 (2018).

[99]G. Guarnieri, G. T. Landi, S. R. Clark, and J. Goold, "Thermodynamics of precision in quantum nonequilibrium steady states", Phys. Rev. Research **1**, 033021 (2019).

[100]T. Van Vu and Y. Hasegawa, "Thermodynamic uncertainty relations under arbitrary control protocols", Phys. Rev. Research **2**, 013060 (2020).

[101]A. C. Barato, R. Chetrite, A. Faggionato, and D. Gabrielli, "A unifying picture of generalized thermodynamic uncertainty relations", en, J. Stat. Mech. **2019**, 084017 (2019).

[102]J. M. Horowitz and T. R. Gingrich, "Thermodynamic uncertainty relations constrain non-equilibrium fluctuations", en, Nat. Phys. **16**, 15–20 (2019).

[103]D. M. Busiello and S. Pigolotti, "Hyperaccurate currents in stochastic thermodynamics", Phys. Rev. E **100**, 060102 (2019).

[104]T. Sagawa and M. Ueda, "Fluctuation theorem with information exchange: role of correlations in stochastic thermodynamics", Phys. Rev. Lett. **109**, 180602 (2012).

[105]A. C. Barato and U. Seifert, "Unifying three perspectives on information processing in stochastic thermodynamics", Phys. Rev. Lett. **112**, 090601 (2014).

[106]J. M. R. Parrondo, J. M. Horowitz, and T. Sagawa, "Thermodynamics of information", Nat. Phys. **11**, 131–139 (2015).

[107] A. C. Barato and U. Seifert, "Coherence of biochemical oscillations is bounded by driving force and network topology", Phys. Rev. E **95**, 062409 (2017).

[108] M. Uhl and U. Seifert, "Affinity-dependent bound on the spectrum of stochastic matrices", Journal of Physics A: Mathematical and Theoretical (2019).

Danksagung

Der Weg zur Promotion gleicht in manchen Teilen einer Odyssee an deren Ende all die Erfolge in Form dieser Abhandlung präsentiert werden. Doch wäre auch Homers Epos bei weitem weniger heldenhaft ohne die Unterstützung die er erfährt. Darum ist es mir ein besonderes Anliegen solchen Personen am Ende meinen persönlichen Dank auszusprechen.

An erster Stelle gilt mein Dank Herrn Prof. Dr. Udo Seifert, der diese Arbeit wissenschaftlich und persönlich begleitete, durch die richtigen Fragen stets neue Impulse setzte und dessen physikalische Neugier nicht nur im Rahmen dieser Arbeit sondern auch persönlich eine Bereicherung war. Die Jahre am II. Institut für theoretische Physik haben damit tiefe Spuren hinterlassen.

Ich danke Herr Prof. Dr. Eric Lutz für die freundliche Bereitschaft als Mitberichter zu fungieren. Weiterhin danke ich Herr Prof. Dr. Sebastian Loth für die Übernahme des Vorsitzes. Auch für die freundliche und konstruktive Atmosphäre in der mündlichen Prüfung danke ich vielmals.

Dr. Patrick Pietzonka danke ich für die vielen lehrreichen und inspirierenden Gespräche im Rahmen der Masterarbeit und der Anfangsphase der Promotion sowie den Austausch darüber hinaus. Durch viele Diskussionen ergaben sich stets neue Fragestellungen und Erkenntnisse die auch im Rahmen dieser Arbeit dokumentiert sind.

I thank Dr. Hyun-Myung Chun for his impulses during his year as a postdoc at the institute. His presence, perspective and background allowed me to take on a different perspective and tackle the problem from a different point of view.

Ich danke Frau Anja Steinhauser für Ihre freundliche Art, stets mitdenkende Arbeitsweise und die vielen Entlastungen und aufmunternden Abwechslungen im Alltag sowie die Einblicke in die Historie des II. Instituts.

Ich danke meinen IT-Administrationskollegen Matthias Uhl und Timur Koyuk für die spannenden Arbeiten an Servern, Protokollen und Systemen sowie den Einsatz auch schwierige Probleme zusammen zu lösen. Matthias Uhl gebührt als langjährigem Zimmernachbar mit seinem offenen Ohr für Problem die teils mehr und teils weniger mit der Welt der Physik zu tun hatten ein besonderer Dank.

Ich danke all den Kollegen die meine Zeit am II. Institut für theoretische Physik auch jenseits der Arbeitszeiten bereichert haben. In dieser freundlichen und freundschaftlichen Atmosphäre konnten Erfolge und Rückschläge gleichermaßen abgefangen werden. Unterhaltsame Diskussionen boten stets die Möglichkeit den Kopf frei zu bekommen und den eigenen Horizont zu erweitern. Im besonderen möchte ich mich hier bei den langjährigen Kollegen Matthias Uhl, Basile Nguyen, Dr. Patrick Pietzonka, Dr. Sebastian Goldt, Steven Siegel, und Timur Koyuk bedanken.

Während meiner Promotionsphase durfte ich auch spannende und lehrreiche Abschlussarbeiten betreuen. Ich danke Carl Biermann, Steven Siegel und Finn Schmolke für ihren Einsatz bei diesen Projekten und den persönlichen und wissenschaftlichen Erfahrungen die ich in diesen Phasen sammeln durfte.

Zuletzt gilt mein Dank all denen Freunden die mich privat während dieser Phase begleitet haben. Ich danke Freunden und Bekannten aus Orchestern, Ensembles, Studium und Schule die mich mit Ratschlägen, Ablenkung und offenen Ohren an der Universität und darüber hinaus stets unterstützt haben. Ein besonderer Dank gilt meiner Familie und meiner Partnerin die mir das Studium und die Promotion ermöglicht haben indem sie mir den Rücken frei hielten und mich gestärkt haben wenn es nötig war.